

PDF hosted at the Radboud Repository of the Radboud University Nijmegen

The following full text is a publisher's version.

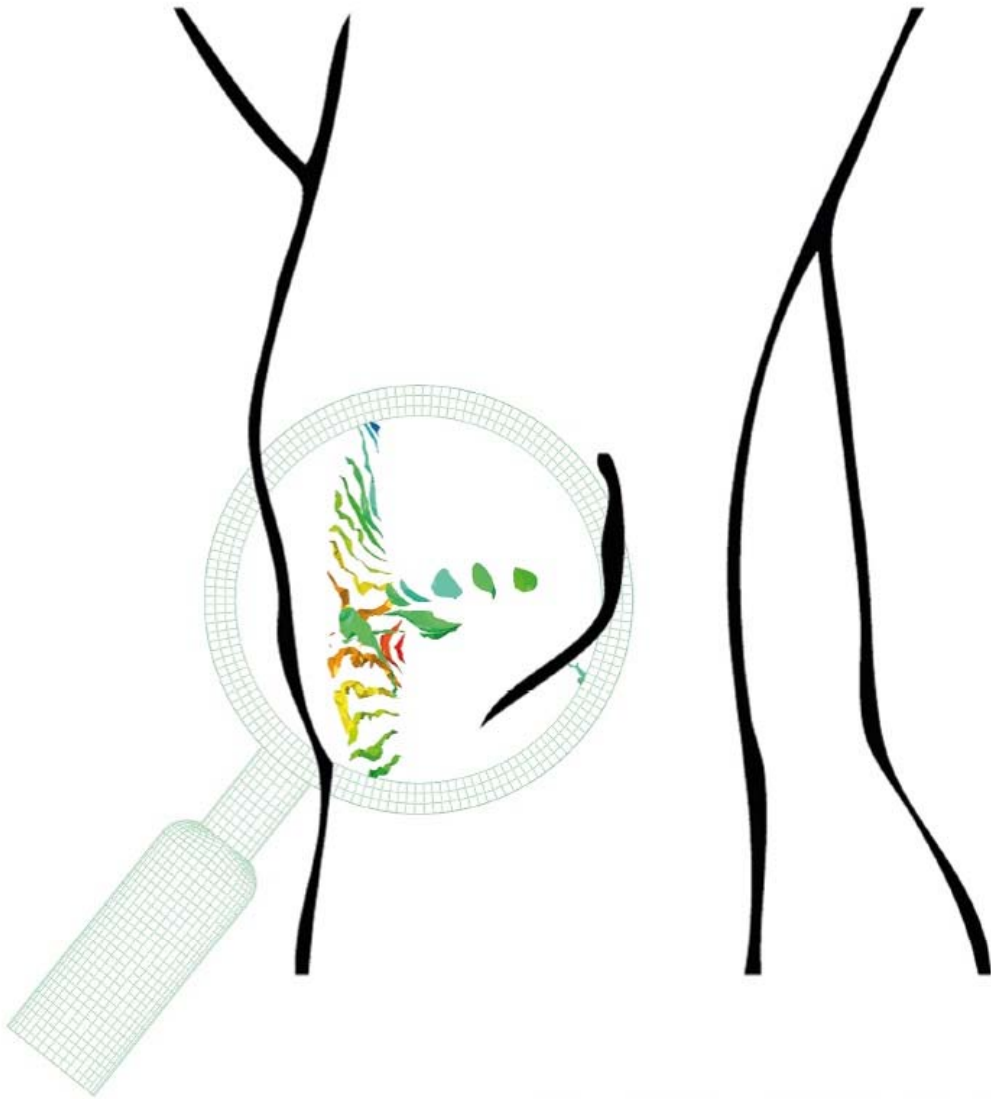
For additional information about this publication click this link.

<http://hdl.handle.net/2066/196839>

Please be advised that this information was generated on 2019-06-02 and may be subject to change.

Personalized Finite Element Models of The Knee Joint

A Platform for Optimal Orthopedic Surgery Pre-planning



Hamid Naghibi Beidokhti

Personalized finite element models of the
knee joint: a platform for optimal
orthopedic surgery pre-planning

Hamid Naghibi Beidokhti

© **Hamid Naghibi Beidokhti, 2018.**

All rights reserved. No part of this thesis may be reproduced in any form without written permission of the author.

Cover design:

Zahra Khorami

Layout:

Hamid Naghibi Beidokhti

Printing:

IPSKAMP printing, Enschede

ISBN:

978-94-028-1253-4

The work presented in this thesis was carried out within the Radboud Institute for Health Sciences.

Subject-specifieke eindige element modellen van de knie: een methode voor geoptimaliseerde pre-operatieve planning

Proefschrift

ter verkrijging van de graad van doctor

aan de Radboud Universiteit Nijmegen

op gezag van de rector magnificus prof. dr. J.H.J.M. van Krieken,

volgens besluit van het college van decanen

in het openbaar te verdedigen op dinsdag 19 november 2018

om 10.30 uur precies

door

Hamid Naghibi Beidokhti

geboren op 21 maart 1986

Gonabad, Iran

Promotoren:

prof. dr. ir. N.J.J. Verdonschot

prof. dr. ir. A.H. van den Boogaard (Universiteit Twente)

Copromotor:

dr. ir. D.W. Janssen

Manuscriptcommissie:

prof. dr. ir. N. Karssemeijer

prof. dr. ir. H.F.J.M. Koopman (Universiteit Twente)

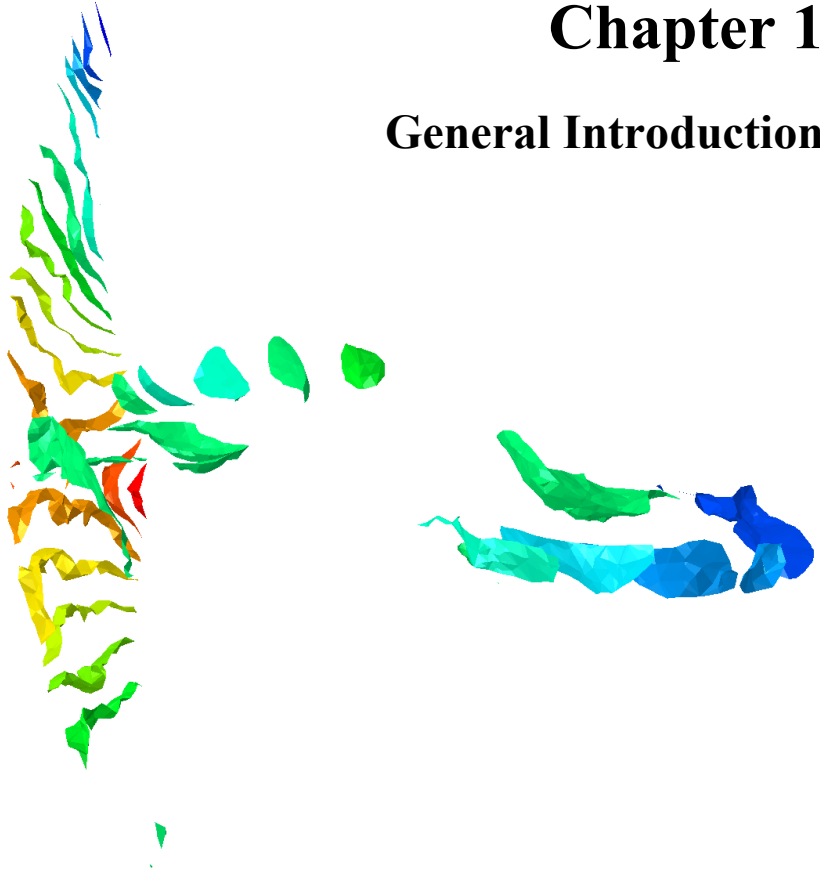
prof. dr. P. Vena (Politecnico di Milano, Italië)

Table of contents

		Page
Chapter 1	Introduction	7
Chapter 2	A Comparison between Dynamic Implicit and Explicit Finite Element Simulations of the Native Knee Joint	17
Chapter 3	The Influence of ligament Modelling Strategies on the Predictive Capability of Finite Element Models of the Human Knee Joint	37
Chapter 4	The peripheral soft tissues should not be ignored in the finite element models of the human knee joint	63
Chapter 5	A Noninvasive MRI Based Approach to Estimate the Mechanical properties of Human Knee Ligaments	83
Chapter 6	Optimal Graft Positioning and Tensioning in ACL Reconstructive Surgery Using Novel Finite Element Modeling Techniques	105
Chapter 7	The Implications of Non-Anatomical Positioning of a Meniscus Prosthesis for Human Knee Joint Biomechanics	131
Chapter 8	Summary, Discussion and Future Perspectives	157
Chapter 9	Nederlandse samenvatting	173
Appendixes		179
Acknowledgments		197
PhD portfolio		201
List of publications		203
Curriculum Vitae		207

Chapter 1

General Introduction



1. Introduction

The knee is a synovial joint formed by articulations between three main components: the distal part of the femur, the proximal part of the tibia, and the patella (Figure 1). The knee joint is one of the most complex joints in the human body, undergoing very large forces under complex articulation conditions, making it vulnerable to a variety of injuries.

The tibial plateau, femoral condyles and posterior surface of the patella are covered with articular cartilage to facilitate smooth articulations. The primary function of cartilage is to maintain a smooth surface allowing lubricated, near-frictionless movement and to help transmit articular forces in the joint [1]. Passive stabilization of the knee joint is provided by the ligaments, which restrain joint motion. The main tibiofemoral ligaments are the medial (MCL) and lateral collateral ligaments (LCL), and the anterior (ACL) and posterior cruciate ligaments (PCL) in the center of the knee joint. These structures are responsible for stabilizing the joint in the anterior-posterior (AP), medial-lateral (ML) and proximal-distal (PD) directions, but also constrain internal-external (IE) and valgus-varus (VV) rotations, while the knee can rotate around flexion-extension (FE) axis in different daily activities. The menisci are fibrocartilaginous structures that sit on the medial and lateral tibial plateau, deepening the tibiofemoral articulating surfaces. The menisci improve stability, shock absorption and smoothed load transmission within the knee.

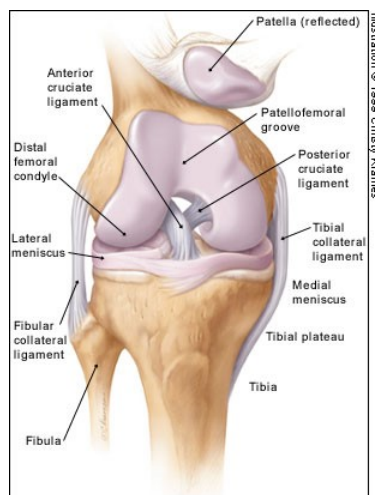


Figure 1: Anterior view of the osseous, ligamentous and fibrocartilaginous structures of the knee.

The knee joint is susceptible to many injuries. The tibiofemoral articular cartilage is of great interest, as osteoarthritis (OA) has a significant impact on quality of life. Injuries involving knee ligaments (i.e. ACL rupture) can cause joint instability, which may eventually lead to degenerative damage to other soft tissues. Trauma and unusual loading mechanism are known as the causes for meniscal injury, which is a common source of pain and functional impairment of the knee joint [2]. These types of injuries may induce OA which has large consequences for the individual and for the healthcare on a macro economical level.

Computational biomechanics is a widely used tool to assess complex orthopedic problems that remain elusive or difficult to understand. A common tool in numerical simulation is the finite element method (FEM), which can provide highly detailed information on the biomechanical response of knee structures. The first application of FEM in biomechanics goes back to 1972 [3]. Only a decade later, the first review on the application of FEM in orthopedic biomechanics was published by Huiskes and Chao [4]. With the evolution of computational power, a more complex representation of physiological tissues and their interactions has been introduced in order to gain more realistic biomechanical models and subsequent predictions.

Obviously, every FE model suffers from considerable simplifications that may narrow its potential area of application. These simplifications are mostly due to a number of physical and numerical constraints, such as lack of experimental data, limitations in characterization of knee structures, numerical convergence problems, and computationally expensive simulations, which can force FE modelers to simplify their knee models. These simplifications include omission of certain structures in the model (e.g. absence of menisci or ligaments), limited detail in the representation of tissue (e.g. modeling ligaments as one dimensional springs rather than with three dimensional continuum elements), simplified boundary conditions (e.g. modeling simple axial loading versus a gait cycle), incorporation of time (static or dynamic simulation), mathematical description of material properties (e.g. cartilage as linear elastic, nonlinear hyperelastic, or biphasic) and inclusion of time-dependent behavior (e.g. viscoelasticity, remodeling, etc.).

Due to the large variation in the anatomy and mechanical properties of knee joint structures between subjects, efforts are being made to model the knee joint in a more patient-specific manner. For developing patient-specific FE models, while the geometries can be segmented from imaging data (i.e. MRI and CT), the characterization of patient-specific properties in a non- or minimally invasive manner remains a big challenge.

2. Thesis outline:

The aim of this thesis is to develop subject-specific finite element modeling of human knee joint as a clinical surgery pre-planning tool. The dissertation is divided into three main parts, as summarized in the following.

In the first part (Part I), fundamental aspects of an FE model of the human knee joint with personalized ligamentous structures are assessed. Consequently, the solution strategies and crucial considerations in enhancing the predictions of a knee FE model are evaluated.

In the second part (Part II), two subject-specific clinical interventions are evaluated using subject-specific FE modeling techniques. As a result, FE models are implemented as surgical pre-planning tools to improve the outcomes of ACL-reconstruction and meniscal implantation surgeries outcomes.

In the third part (Part III), novel methods to non-invasively characterize the knee ligament properties are investigated, in order to practically be implemented in in-vivo FE modeling. A laxity-based approach, and an MRI-based technique are introduced to estimate the mechanical properties of knee ligaments.

Finally, the separate studies in this thesis are summarized and the current state, achieved improvements and future perspectives in knee FE modeling as a clinical surgery pre-planning tool are discussed in the last chapter.

2.1. Part 1: FE Model Development

A comparison between dynamic implicit and explicit finite element simulations of the native knee joint

Time integration algorithms for dynamic problems in FE analysis can be classified as either Implicit or Explicit. Although previously both static/dynamic implicit and dynamic explicit methods have been used, a comparative study on the outcomes of both methods is of high interest for the knee modeling community. In chapter 2, the aim was to compare static, dynamic implicit and dynamic explicit solutions in the analysis of a knee joint to assess the prediction of dynamic effects, potential convergence problems, the accuracy and stability of the calculations, the difference in computational time, and the influence of mass-scaling in the explicit formulation. The heel-strike phase of fast, normal and slow gait was simulated for two different body masses in a model of human native knee joint.

The influence of ligament modelling strategies on the predictive capability of finite element models of the human knee joint

In finite element models knee ligaments can be represented either by a group of one-dimensional springs, or by three-dimensional continuum elements based on segmentations. Continuum models closer approximate the anatomy, and facilitate ligament wrapping, while spring models are computationally less expensive. In addition, the mechanical properties of ligaments can be based on literature, or can be adjusted specifically for the subject. In chapter 3, the effect of ligament modelling strategy on the predictive capability of FE models of the human knee joint was investigated. The effect of literature-based versus specimen-specific optimized material parameters was evaluated. Experiments were performed on three human cadaver knees, which were simulated in FE models with ligaments modeled either using springs, or using continuum representations. In the spring representation, the collateral ligaments were each modelled with three springs, and the cruciate ligaments with two single-element bundles. Stiffness parameters and pre-strains were optimized based on laxity tests for both approaches. Validation experiments were conducted to evaluate the outcomes of the FE models.

The mechanical effects of ignoring the peripheral soft tissues in the finite element models of the human knee joint

FE models of the knee joint generally incorporate soft tissue structures like the tibiofemoral ligaments, but typically neglect tissues like skin, the peripheral knee soft tissues, and the posterior capsule. It is, however, unknown how these peripheral structures influence the biomechanical response of the knee. In chapter 4, the aim was to assess the significance of the peripheral soft tissues and posterior capsule on the kinematics and laxities of human knee joint, based on experimental tests on three human cadaveric specimens. Subsequently, a computational approach to model the target tissues in FE modeling was developed.

2.2. Part 2: Ligament Properties Characterization for FE Models

As a part of model development, a laxity-based technique was introduced and implemented in chapter 3 to characterize the knee ligament properties. Using cadaveric testing, a series of in-vitro laxity tests were performed, and accordingly, the ligament parameters were calculated following optimization routines. The experiments were designed in a way that they could be implemented under in-vivo conditions.

Noninvasive ligament properties estimation from MRI

The laxity-based method introduced for characterization of the knee ligaments properties, may not always be suitable or proof to be accurate for clinical implementation. As an innovative alternative and/or additional assessment, an MRI-based approach for the estimation of ligament properties was proposed in chapter 5. In this chapter, the aim was to assess if mechanical properties of the knee ligaments are correlated with their structural specifications (e.g. volume cross-sectional area, etc.) and with MRI parameters.

2.3. Part 3: Towards clinical Applications

A novel subject-specific ACL reconstruction workflow to optimize surgical parameters: demonstration in a cadaveric setting

As a novel clinical application of the developed validated FE models of knee joints, ACL-reconstruction treatments were targeted. According to the literature, in many cases ACL reconstruction surgery does not reduce the OA risk [5]–[13]. A major reason is believed to be that the overall biomechanical behavior of the knee is not restored contributing in OA progression. A non-optimal reconstruction, as a result of improper graft positioning with a non-optimal fixation force, can fail to restore the native knee biomechanics. In chapter 6, a workflow based on the developed FE model of the cadaveric knee joint was proposed and studied to minimize the variations between the biomechanical outcomes of the reconstructed and the intact joint.

The Implications of Non-Anatomical Meniscus Implantations for Human Knee Joint Biomechanics

A second clinical application of the FE models of the knee joint focused on meniscus replacement surgery for patients with medial meniscus injury. At the Orthopedic Research Lab of Radboudumc a meniscus implant was developed, which has been studied extensively to optimize the geometry, material properties and fixation of the implant [14]–[16]. One remaining issue, however, was the positioning of the implant in the knee joint. In chapter 7, the aim was therefore to assess the implications of non-anatomical positioning of the medial meniscus implant. The outcomes of this study may provide insight into the possible consequences of meniscus implant positioning errors for the biomechanical behavior of the knee and implant.

2.4. Summary, Discussion and Future perspectives

In chapter 8, a summary of the main findings of the studies described in this thesis is presented. This chapter also reflects on the strengths and limitations of the developed FE models of the knee joints as clinical pre-planning tools. A discussion on the results of each study is presented, which is followed by future

perspectives in developing FE models of the knee joint for optimal patient-specific treatment and surgery pre-planning.

References

- [1] A. E. Peters, R. Akhtar, E. J. Comerford, and K. T. Bates, “Tissue material properties and computational modelling of the human knee: A critical review,” *PeerJ*, pp. 1–48, 2018.
- [2] G. I. Drosos and J. L. Pozo, “The causes and mechanisms of meniscal injuries in the sporting and non-sporting environment in an unselected population,” *Knee*, vol. 11, pp. 143–149, 2004.
- [3] W. A. M. Brekelmans, H. W. Poort, and T. J. J. H. Slooff, “A new method to analyse the mechanical behaviour of skeletal parts,” *Acta Orthop. Scand.*, vol. 43, pp. 301–317, 1972.
- [4] R. Huiskes and E. Y. S. Chao, “A SURVEY OF FINITE ELEMENT ANALYSIS IN ORTHOPEDIC BIOMECHANICS : THE FIRST DECADE,” *J. Biomchanics*, vol. 16, no. 6, pp. 385–409, 1983.
- [5] I. Holm, B. E. Øiestad, M. A. Risberg, and A. K. Aune, “No Difference in Knee Function or Prevalence of Osteoarthritis After Reconstruction of the Anterior Cruciate Ligament With 4-Strand Hamstring Autograft Versus Patellar Tendon – Bone Autograft,” pp. 448–454, 2010.
- [6] C. Hui *et al.*, “Fifteen-Year Outcome of Endoscopic Anterior Cruciate Ligament Reconstruction With Patellar Tendon Autograft for “Isolated ” Anterior Cruciate Ligament Tear,” *Am. J. Sports Med.*, no. C, pp. 89–98, 1994.
- [7] A. R. Æ. M. S. Kuster, “Function , osteoarthritis and activity after ACL-rupture: 11 years follow-up results of conservative versus reconstructive treatment,” pp. 442–448, 2008.
- [8] H. Louboutin *et al.*, “Osteoarthritis in patients with anterior

cruciate ligament rupture : A review of risk factors,” *Knee*, vol. 16, no. 4, pp. 239–244, 2009.

[9] S. L. Keays, P. A. Newcombe, J. E. Bullock-saxton, M. I. Bullock, and A. C. Keays, “Factors Involved in the Development of Osteoarthritis After Anterior Cruciate Ligament Surgery,” pp. 455–463.

[10] A. Manuscript, “NIH Public Access,” vol. 22, no. 4, pp. 347–357, 2013.

[11] R. Mihelic, H. Jurdana, Z. Jotanovic, T. Madjarevic, and A. Tudor, “Long-term results of anterior cruciate ligament reconstruction : a comparison with non-operative treatment with a follow-up of 17 – 20 years,” pp. 1093–1097, 2011.

[12] A. P. C. Study, “Prevalence of Tibiofemoral Osteoarthritis 15 Years After Nonoperative Treatment of Anterior Cruciate Ligament Injury,” pp. 1717–1725, 2008.

[13] J. Struwer and T. M. Frangen, “Knee function and prevalence of osteoarthritis after isolated anterior cruciate ligament reconstruction using bone-patellar tendon-bone graft : long-term follow-up,” pp. 171–177, 2012.

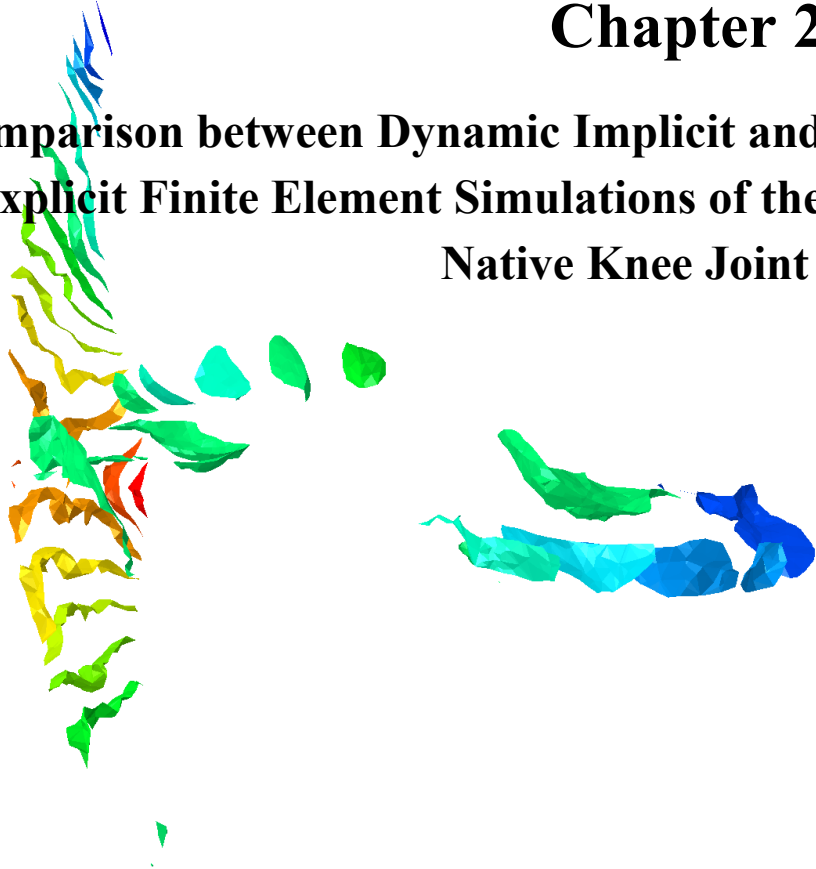
[14] M. Khoshgoftar, A. C. T. Vrancken, T. G. van Tienen, P. Buma, D. Janssen, and N. Verdonshot, “The sensitivity of cartilage contact pressures in the knee joint to the size and shape of an anatomically shaped meniscal implant,” *J. Biomech.*, vol. 48, no. 8, pp. 1427–1435, 2015.

[15] A. C. T. Vrancken *et al.*, “3D geometry analysis of the medial meniscus – a statistical shape modeling approach,” *J. Anat.*, vol. 225, no. 4, pp. 395–402, 2014.

[16] A. C. T. Vrancken, W. Madej, G. Hannink, N. Verdonshot, T. G. Van Tienen, and P. Puma, “Short Term Evaluation of an Anatomically Shaped Polycarbonate Urethane Total Meniscus Replacement in a Goat Model,” *PLoS One*, vol. 10, no. 7, pp. 1–16, 2015.

Chapter 2

A Comparison between Dynamic Implicit and Explicit Finite Element Simulations of the Native Knee Joint



Naghbi Beidokhti, H., Janssen, D., Khoshgoftar, M., Sprengers, A., Perdahcioglu, E.S., Van den Boogaard, T., Verdonschot, N., 2016. Medical Engineering and Physics. 38, 1123–1130.

1. Introduction

The finite element (FE) method has been widely used to investigate knee biomechanics [1]. The general trend over the last decades is to develop more realistic, reliable, accurate, and computationally effective models. As a result, many sensitivity studies have been performed to identify the essential parameters. Subsequently, these data can be used to generate a model that has adequate detail, while avoiding unnecessary long calculation times. An important aspect in many analyses of the knee joint is the omission of dynamic effects, due to the difficulties and complexities involved with dynamic simulations (Table1).

Time integration algorithms for dynamic problems in finite element analysis can be classified as either Implicit or Explicit. In general, the implicit method defines the state of the model at each time increment based on the information of that same time increment and the previous time increment, while the explicit method uses the data of the previous time increment to solve the motion equations during the new time increment. The implicit algorithm requires iterative solutions for each time increment, and the accuracy of the solution is dictated by the convergence criterion, thereby ensuring that the errors of the updated results are lower than a tolerance value. Finite element equations in the explicit algorithm are formulated as being dynamic, and in this method they can be solved directly without requiring iteration [2]. The explicit method is conditionally stable, and the critical time step for the operator (without damping) is a function of the material specification and the smallest element size in the system. In the explicit method, the time increment must always be less than the critical time step. Otherwise, the solution will be unstable and oscillations will occur in the model's response, what can lead to excessively distorted elements. To increase the critical time step, and consequently decrease the computational time, a mass-scaling option is available. In mass-scaling, the density of the system is increased artificially to allow the solver to use larger time increments. However, it is important to ensure that the added mass does not change the physics of the problem. Some studies assessed the influence of mass-scaling option on the outcomes of their models, and suggested a priori comparison of simulations with and without mass scaling to confirm that the kinetic energy is insignificant compared to the strain energy absorbed by the model [3]–[5].

Table 1: The finite element studies targeted the knee joint.

Solution Strategy			Joint type	
Static	Dynamic		Intact Knee	Implanted Knee
	Implicit	Explicit		
[6]–[9]	[7], [10]–[14]	[15]–[22]	[6]–[9], [11], [13]–[15], [20], [21]	[10], [16]–[20], [22]

The selection between implicit and explicit methods has been the subject of many studies. Several studies have compared implicit and explicit finite element simulations of sheet metal forming [23]–[30]. Some of them have utilized the implicit algorithm to analyze the process quasi-statically, particularly for slower dynamic problems with less nonlinearity (e.g. [26]), and some others have suggested using the explicit method due to the high nonlinear contact conditions [23], [28], [31]. Moreover, a few combined algorithms of implicit and explicit time integration have been proposed [32], [33].

In the field of bioengineering, with a specific focus on knee joint simulations, some dynamic explicit and dynamic implicit simulations have been reported, on both intact and implanted knees (Table 1). Furthermore, a large number of implicit (quasi-) static studies have been reported. However, a comparative study on the outcomes of dynamic implicit and explicit methods to calculate outcome parameters such as cartilage stress and meniscus deformation has not been reported previously, yet is of high interest for the knee modeling community.

The aim of this study is therefore to compare static, dynamic implicit and dynamic explicit solutions in the analysis of the knee joint in a case study. More specifically, we compared the prediction of dynamic effects, potential convergence problems, the accuracy and stability of the calculations, the computational time between the two methods and furthermore assessed the influence of mass-scaling in the explicit formulation.

2. Materials and Methods

To compare static, implicit dynamic and explicit dynamic analyses more efficiently, a case study based on the Open-knee model [34] was performed simulating heel strike of the stance phase. In this model, three different walking speeds were analyzed: fast, normal and slow walking.

The tibiofemoral joint of the left knee of a 77 kg-weight female cadaver was segmented, including the tibia (proximal), femur (distal), cruciate ligaments (ACL and PCL), collateral ligaments (MCL and LCL), femoral and tibial cartilage, and the lateral and medial menisci (Figure 1).

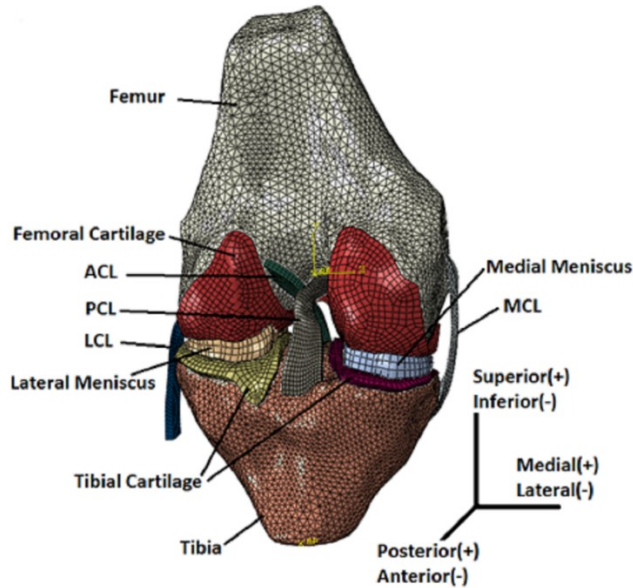


Figure 1: Finite element model of the tibiofemoral joint.

Bones were considered to behave as rigid bodies due to the high difference in elasticity modulus with their surrounding soft tissues. Previously, it has been shown in finite element solutions for rigid versus deformable bones that contact variables such as maximum pressure, mean pressure, contact area, total contact force and coordinates of the center of pressure did not change by more than 2% [35]. The mass of the tibia and femur were represented by a concentrated mass point at its center of rotation at full extension [8]. A previous study by Armstrong et al. [36] indicated that for short-term responses the femoral and tibial cartilage behaves in an elastic isotropic manner, with a Young's modulus of 5 MPa and a Poisson ratio of 0.46 [37], which were adopted for the current study. For the same reason, the menisci were modeled as elastic isotropic with a Young's modulus and Poisson ratio of 59 MPa and 0.49, respectively [8]. The collateral and cruciate ligaments were modeled as Neo-Hookean hyperelastic isotropic, in which the strain energy function ψ is described as a function of the first

invariant of the left Cauchy-Green deformation tensor (I_1) and the elastic volume ratio (J):

$$\psi = C_{10}(I_1 - 3) + \frac{1}{2D}(J - 1)^2 \quad (1)$$

Where C_{10} and D are the Neo-Hookean constant and the inverse of the bulk modulus, respectively. The parameters for the different ligaments are given in Table 2.

Table 2: Selected material parameters for ligaments [8].

	C_{10}	D
ACL	1.95	0.00683
PCL	3.25	0.0041
MCL	1.44	0.00126
LCL	1.44	0.00126

The tibia was constrained in all rotational and translational directions, while the femur was completely unconstrained except for the flexion angle, which was fixed in full extension. The load magnitude was based on Wang et al. [38], whereas the time period was selected from Kito et al. [39]. From these data we simulated an axial load of 1560N, which was applied in a ramp pattern at three different loading times of 0.02, 0.1 and 1.0 seconds, representing fast, normal and slow gait, respectively. With the assumption of no mal-alignment in the joint in the frontal plane (valgus/varus conformity), the axial load was applied along the mechanical axis of the femur [40]. Two different weights of 70 and 100 kg were considered as the weight of the upper parts of the body located along the mechanical axis of the femur.

All soft tissues in the model were meshed with 8-node three-dimensional solid (continuum) elements (C3D8, Abaqus 6.13, Dassault Systemes). Based on a mesh convergence study, an approximate element size of 0.5mm was chosen, with the whole model containing about 64,000 nodes and 48,000 elements.

Although the Lagrangian multiplier method is available for implicit solution to enforce the exact sticking conditions on contact surfaces, it may not be suitable for high dynamic simulations as it may result in small time increments and convergence problems [31]. In an exploratory study, the outcomes of analyses with the penalty and lagrangian methods were compared. Both methods resulted

in very comparable initial outcomes, although with the Lagrangian method the simulation could not be fully completed due to the convergence errors. Consequently, contact between the articular surfaces (femur, menisci and tibia) was modeled by the penalty method in both solution strategies, with a friction coefficient of 0.01 [41].

The standard and explicit solvers of Abaqus software v6.13 (Pawtucket, RI, USA) were utilized in this study. In the explicit solver a bulk viscosity parameter is available, which introduces damping associated with the volumetric straining to improve the high speed simulations. The bulk viscosity parameter was set to 0.03 in this study, but for a single case (fast gait, mass: 70kg) we also assessed its sensitivity by varying the bulk viscosity from 0.06 (default value) to 0.03 and 0.0.

To investigate the accuracy of the explicit with respect to the implicit method, first, in the explicit solutions mass-scaling was disabled, and automatic incrementation was used in both implicit and explicit solutions. To assess the effect of mass-scaling in the explicit solutions, the simulations of slow, normal and fast gaits were repeated, with scaled mass where the concentrated masses were not scaled.

3. Results

3.1. Fast gait:

During fast gait the reaction force acting on the tibia reached about 2300N with a mass of 70 kg, and 2500N with a mass of 100 kg (Figure 2). As expected, the quasi-static case followed the applied load pattern, with a reaction force increasing from zero to 1560N, and subsequently remaining constant.

For both masses, in the dynamic implicit and dynamic explicit solutions the reaction force fluctuated around the quasi-static response in a damped manner caused by the energy loss due to friction. More damping was seen in the explicit simulation due to the viscosity parameter, which resulted in a lower peak value as compared to the implicit solution. The explicit solution with scaled mass, however, resulted in a less-oscillating tibial reaction force than non-scaled mass explicit solution, due to the additional damping.

While the reaction force response was quite similar for both formulations, in the dynamic implicit analyses the femur experienced more posterior motion than in the quasi-static analyses (Figure 2). The same trend was seen in femoral internal rotation, for both masses.

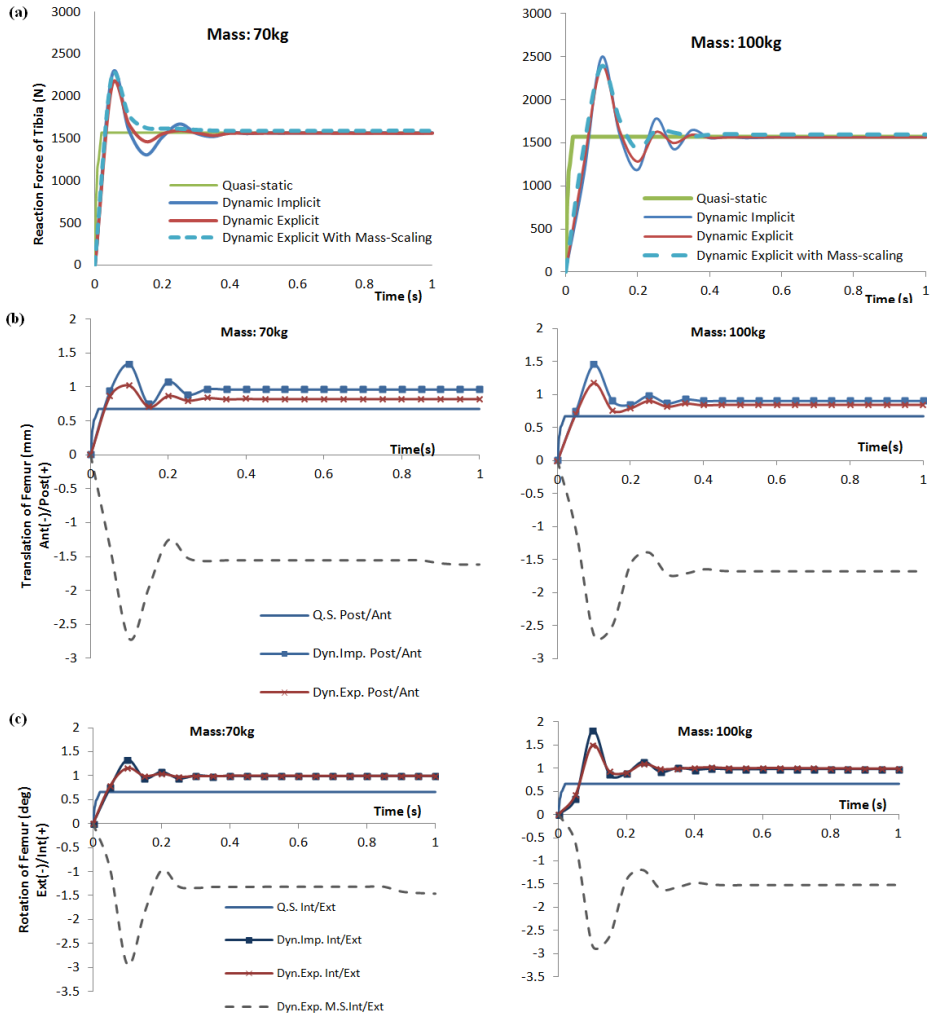


Figure 2: comparison between quasi-static, dynamic implicit and dynamic explicit with and without mass-scaling outcomes in the fast gait case for both masses of 70kg and 100kg; (a) the reaction force of tibia, (b) Anterior/posterior translational motion of femur and (c) Internal/external rotational motion of femur.

Although the translations in the explicit and implicit analyses were comparable in the medial and inferior direction, in the posterior direction the explicit analyses resulted in less translation.

The largest differences were seen in the explicit analysis with mass scaling, resulting even in anterior displacements and internal rotations, which were opposite to those predicted by the quasi-static and dynamic implicit and explicit analyses without mass-scaling.

The analyses of the tibial contact pressure at the end of the simulation demonstrated that the contact pressures in the dynamic analyses were higher than the quasi-static simulations, in particular in the medial cartilage. In turn, the meniscus strain was similar in dynamic and quasi-static analyses, except for small differences in the posterior horn attachments (Figure 3). The same trend, but with larger differences, was seen at the point in time when the peak responses took place.

In both mass cases, the explicit solution resulted in the same tibial contact pressure and menisci strain as the implicit solution, in both distribution and value, where it was more discrete in the explicit solution.

The meniscus displacement contours demonstrated higher displacement in the posterior side of the medial and lateral menisci, confirming the higher posterior translation and valgus rotation of the femur in dynamic simulations. However, the explicit analysis resulted in the same menisci displacement as the implicit solution.

The explicit simulations with mass-scaling, with both masses (70kg (Figure 3) and 100kg), showed different tibial contact pressures, menisci strain and menisci displacement, in which the anterior sides of the tibial cartilage and the menisci experienced higher stresses and displacements.

In all outcomes, the distributions at the time of peak region (first peak) were comparable with those at the end of simulation time, but with larger differences in magnitude.

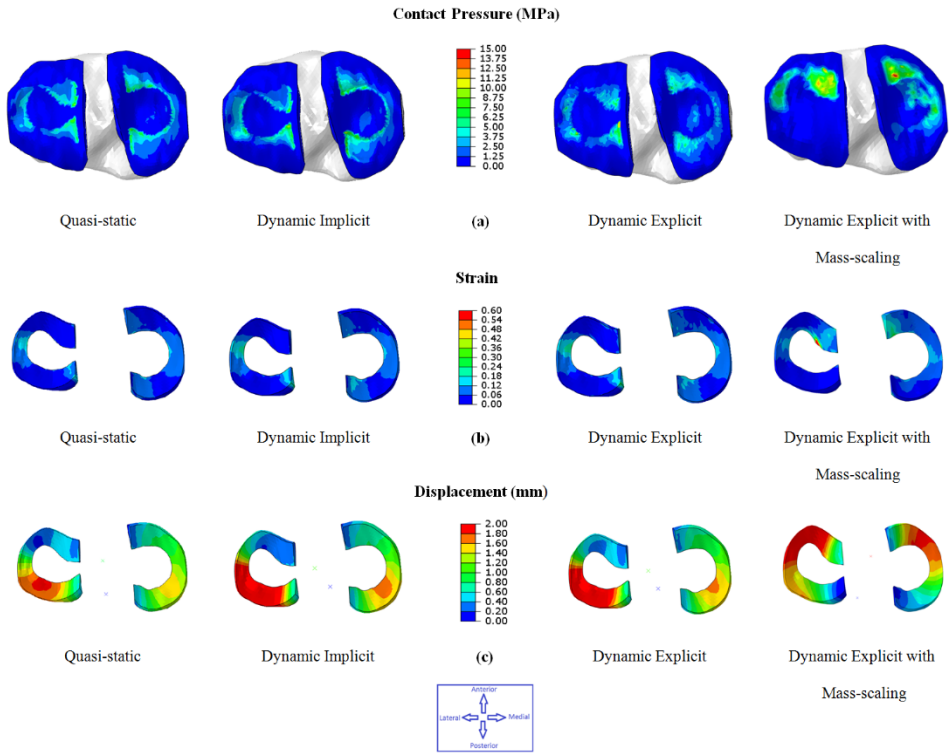


Figure 3: comparison between the outcomes of quasi-static, dynamic implicit, dynamic explicit and dynamic explicit with mass-scaling analyses in fast gait case with the mass of 70kg at the end of simulation time; (a) contact pressure at tibial cartilages, (b) strain at menisci and (c) displacement of menisci.

3.2. Normal gait:

In normal gait, with a loading time of 0.1 second, the reaction force of the tibia in the dynamic simulations showed small differences with quasi-static analyses, where with the mass of 100kg small initial fluctuations around the quasi-static solution were seen (Figure 4). The dynamic (implicit) and quasi-static analyses resulted in the same femoral translations, except in posterior direction, where the dynamic effect caused more posterior motion. The internal rotation was also higher in the dynamic analyses.

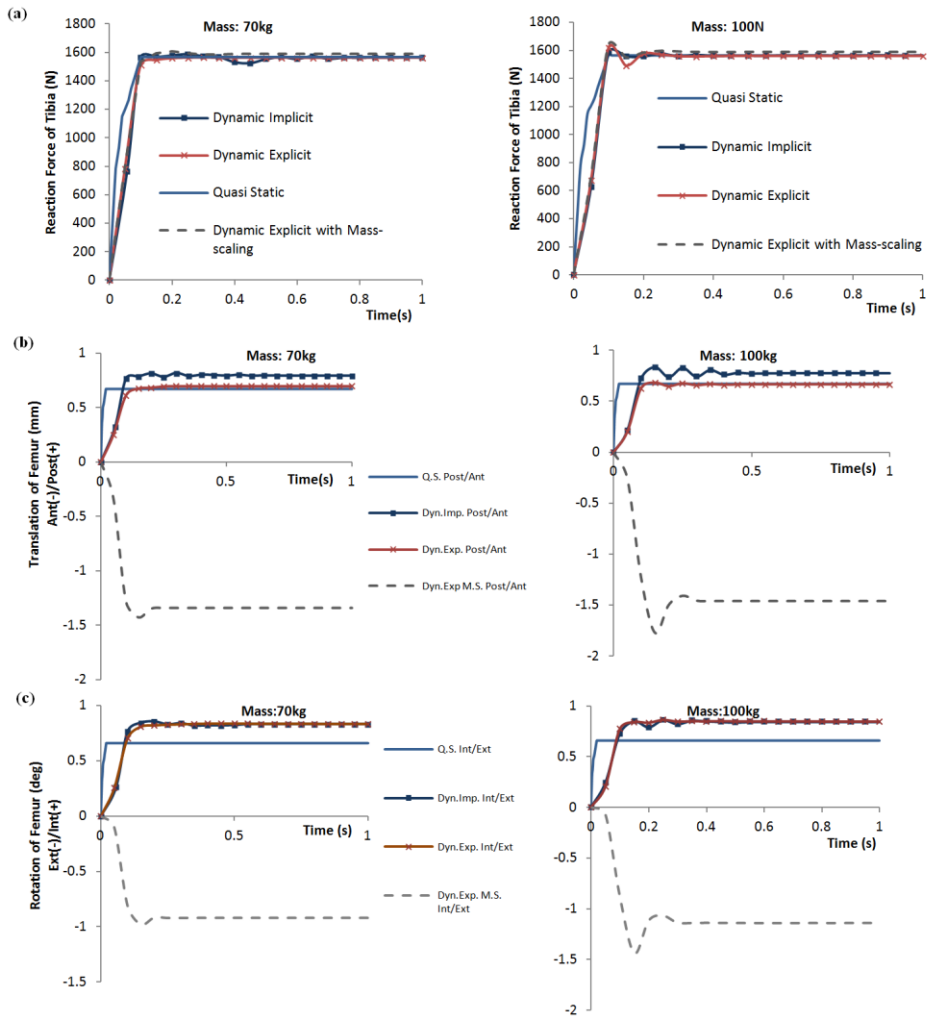


Figure 4: comparison between quasi-static, dynamic implicit and dynamic explicit with and without mass-scaling outcomes in the normal gait case for both masses of 70kg and 100kg; (a) the reaction force of tibia, (b) translational anterior-posterior motion of femur and (c) internal-external rotational motion of femur.

In normal gait, the implicit and explicit solutions resulted in a similar tibial reaction force (Figure 4). Although the explicit solution resulted in the same femoral rotations as the implicit analyses, the femoral posterior translations in explicit analyses were similar to the quasi-static solution. Applying mass scaling in the dynamic solution resulted in a slightly higher tibial reaction force. Moreover, when using mass scaling, the femoral translations in anterior-posterior direction and femoral internal-external rotations increased oppositely to the

translations and rotations predicted by quasi-static, dynamic implicit and dynamic explicit solutions (Figure 4). Contact pressure on the tibial cartilage and the meniscus strains were similar in the dynamic implicit and dynamic explicit solutions. The posterior displacement of the menisci, however, was higher in the implicit simulation.

3.3. Slow gait:

In the slow gait case, as expected, in both mass cases, the dynamic solutions resulted in the same outcomes as the quasi-static simulation. A small initial deviation in reaction force from quasi-static analyses was seen in the dynamic implicit analyses (Figure 5-a). However, the femoral translation and rotation, tibial cartilage contact pressure, meniscus strains and displacement as simulated in the dynamic implicit analyses were more similar to the quasi-static analyses.

For both masses, the implicit and explicit simulations demonstrated similar cartilage pressure distributions, and meniscus displacements and deformations, with a negligible effect of mass scaling (Figure 5-b).

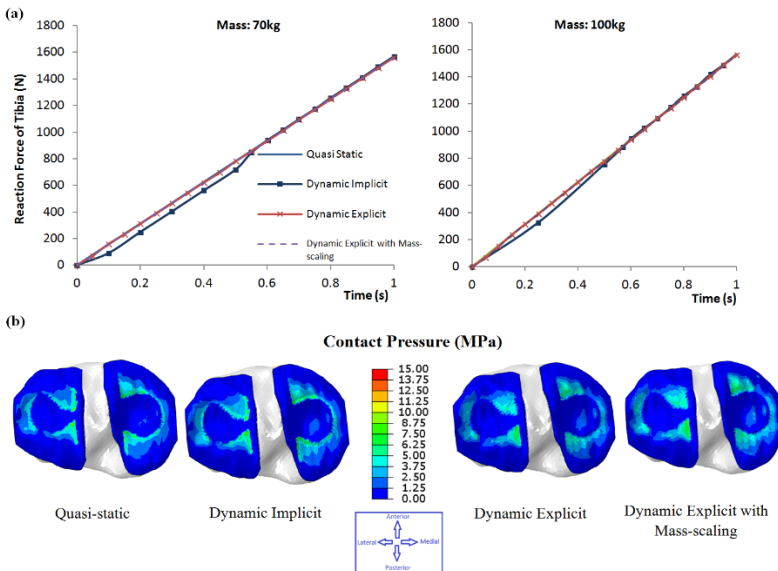


Figure 5: comparison between the reaction force of tibia in quasi-static, dynamic implicit and dynamic explicit with and without mass-scaling analyses in the slow gait case for both masses of 70kg and 100kg (a); comparison between the contact pressure at tibial cartilages of quasi-static, dynamic implicit, dynamic explicit and dynamic explicit with mass-scaling analyses in slow gait case with the mass of 70kg (b).

Loading time had a significant effect on the computational time for the implicit dynamic simulations, whereas this effect was much lower for the explicit analyses (Table 3). In the fast gait case (loading time of 0.02s) the dynamic implicit analyses took almost two times the dynamic explicit analyses. Mass-scaling in the explicit simulations reduced the computational time by 11 hours for mass of 70kg and 13 hours for mass of 100 kg.

Table 3: Computational time in different dynamic solutions in this study (in hours).

Studied Case Solution Type	Mass: 70kg			Mass: 100kg		
	Fast Gait (h)	Normal Gait (h)	Slow Gait (h)	Fast Gait (h)	Normal Gait (h)	Slow Gait (h)
Dynamic Implicit	87	54	33	94	56	35
Dynamic Explicit	49	52	48	51	51	53
Dynamic Explicit with Mass-scaling	38	42	44	38	42	50

The explicit method was stable when a bulk viscosity parameter of 0.03 was used, which introduced some damping associated with the volumetric straining to improve the high speed simulations. Without this parameter the damping in explicit was less, and the results were more similar to the implicit results, but at high speeds the simulations were stopped due to instability errors. In the specific case of fast gait, the bulk viscosity parameter was varied from 0.0 to 0.06. The results of these analyses indicated that increasing the bulk viscosity parameter caused a reduction in the tibial reaction force, and an increase in the difference with the implicit solutions (Table 4).

Table 4: Tibial reaction force in fast gait case at first peak region and end of simulation for three different bulk viscosity parameters in explicit solutions (mass: 70kg).

Bulk Viscosity Parameter	Tibial Reaction Force (N)		Difference with Dynamic Implicit (%)	
	1 st peak	t=1	1 st Peak	t=1
0	2240	N/A	1.8	N/A
0.03	2190	1561	3.9	0.0
0.06	2130	1557	6.6	0.3

4. Discussion

The aim of this study was to compare static, dynamic implicit and dynamic explicit solutions for simulating the knee joint. In general, the implicit method is more reliable for dynamic analysis due to its iterative approach, but obtaining convergence remains an issue, in some cases forcing the user to apply unrealistic simplifications in boundary and loading conditions, contact formulations, material properties and geometries. Our results indicate that ignoring the dynamic effect by analyzing the problem in a quasi-static manner, for walking, can result in differences of up to 52% in joint forces, and altered joint motion. The tibial reaction forces predicted in the current simulations (ranging from 2130 to 2240 N for a bodyweight of 70 kg in explicit solution) were also in good agreement with the ground reaction force measured during the impact phase hopping (2400N for a bodyweight of 80 kg) [42]. Although there is a difference in activity (hopping vs. gait), the loading rate and joint position were very similar (loading time $t=0.02s$).

Comparison between the outcomes of the mathematically reliable implicit and the explicit methods in the three different cases revealed an acceptable agreement, at the end of simulation time periods, in relative tibiofemoral translational and rotational motions with the maximum deviations (from implicit outcomes) of 0.15mm in translations and 0.17deg. In rotations as well as contact pressure at tibial cartilages, menisci displacement and strain at menisci. The differences between the explicit and implicit solutions were mostly caused by the viscosity parameter in explicit simulations.

Particularly for the fast gait case, the computational time was much less in the explicit analysis than in the implicit analysis. The computational time in explicit analyses remained constant, while in implicit analyses, it dropped substantially with expanding the loading time and, consequently, with a reduced dynamic effect. As a result, from a calculation time and accuracy perspective, the implicit method seems to be more appropriate at lower speeds.

In explicit analyses, however, to reduce the computational time, the mass-scaling option is available, which increases the stable time increment by artificially adding mass to the system. Although in this study mass-scaling could decrease the mean computational time, it resulted in unacceptable outcomes at higher speeds, whereas in the slow gait in which the kinetic energy of the whole system

was less than 4% of the strain energy, the outcomes were negligibly affected. This is in agreement with Prior's study [43], in which mass-scaling was suggested when the proportion of kinetic energy to strain energy is less than 5%. In this case the dynamic effect is negligible and problems can be solved with quasi-static solution.

In this study, a relatively simple loading configuration was used to compare the results of quasi-static, implicit and explicit dynamic simulations of the knee joint. As a boundary condition, we chose the heel-strike phase of the gait cycle, since this is the instance during which the largest change in axial load takes place. Second, the viscoelastic properties of menisci, cartilages and ligaments were not considered. These viscoelastic properties may provide additional damping of the knee joint, which in turn may decrease the stable time increment in the dynamic explicit analyses. Third, the menisci and cartilage were modeled as elastic isotropic, where for menisci the higher elastic modulus in circumferential direction could decrease the transverse translations of femur in this study. Moreover, the nonhomogeneous bone properties, beside the nonlinearities involved in cartilage modeling, can guide the modeler to a more realistic outcome on both bone-cartilage and cartilage-cartilage articular surfaces, particularly at activities with lower loading rates.

In conclusion, the current study illustrates that explicit analyses are suitable to simulate dynamic loading of the knee joint. In high-speed simulations, explicit analyses offer a substantial reduction of the required computational time with similar cartilage stresses and meniscus strains. Hence, the computationally less expensive explicit analyses can be used as a diagnostic tool to investigate the effect of various orthopedic interventions in the knee joint. Although mass-scaling can provide even more gain in computational time, it is not recommended for high-speed activities, in which inertial forces play a significant role.

Acknowledgments

This study was a part of BioMechTools project (ERC-2012-ADG LS7), received funding from the European Research Council under the European Union's Seventh Framework Program (FP/2007-2013) / ERC Grant Agreement n. 323091.

References

- [1] M. Kazemi, Y. Dabiri, and L. P. Li, “Recent advances in computational mechanics of the human knee joint,” *Comput. Math. Methods Med.*, vol. 2013, 2013.
- [2] F. J. Harewood and P. E. McHugh, “Comparison of the implicit and explicit finite element methods using crystal plasticity,” *Comput. Mater. Sci.*, vol. 39, no. 2, pp. 481–494, 2007.
- [3] M. Langseth, O. S. Hopperstad, and T. Berstad, “Crashworthiness of aluminium extrusions: validation of numerical simulation, effect of mass ratio and impact velocity,” *Int. J. Impact Eng.*, vol. 22, no. 9–10, pp. 829–854, 1999.
- [4] A. T. Akarca, S.S., Altenhof, W.J., Alpas, “Finite element analysis of sliding contact between a circular asperity and an elastic surface in plane strain condition,” in *International LS-DYNA Users Conference*, 2006.
- [5] T. a. Burkhart, D. M. Andrews, and C. E. Dunning, “Finite element modeling mesh quality, energy balance and validation methods: A review with recommendations associated with the modeling of bone tissue,” *J. Biomech.*, vol. 46, no. 9, pp. 1477–1488, 2013.
- [6] Y. Wang, Y. Fan, and M. Zhang, “Comparison of stress on knee cartilage during kneeling and standing using finite element models,” *Med. Eng. Phys.*, vol. 36, no. 4, pp. 439–447, 2014.
- [7] K. S. Halonen, M. E. Mononen, J. S. Jurvelin, J. Töyräs, and R. K. Korhonen, “Importance of depth-wise distribution of collagen and proteoglycans in articular cartilage-A 3D finite element study of stresses and strains in human knee joint,” *J. Biomech.*, vol. 46, no. 6, pp. 1184–1192, 2013.
- [8] E. Peña, B. Calvo, M. a. Martínez, and M. Doblaré, “A three-dimensional finite element analysis of the combined behavior of ligaments and menisci in the healthy human knee joint,” *J. Biomech.*, vol. 39, no. 9, pp. 1686–1701, 2006.
- [9] R. Mootanah, C. W. Imhauser, F. Reisse, D. Carpanen, R. W. Walker, M. F. Koff, M. W. Lenhoff, R. Rozbruch, a T. Fragomen, Y. M.

Kirane, S. R. Rozbruch, Z. Dewan, K. Cheah, J. K. Dowell, and H. J. Hillstrom, "Development and Verification of a Computational Model of the Knee Joint for the Evaluation of Surgical Treatments for Osteoarthritis," *Computer methods in biomechanics and biomedical engineering*, vol. 17, no. 13. Taylor & Francis, pp. 1502–17, 2014.

[10] L. Zach, L. Kunčická, P. Růžička, and R. Kocich, "Design, analysis and verification of a knee joint oncological prosthesis finite element model," *Comput. Biol. Med.*, vol. 54, pp. 53–60, 2014.

[11] M. Kazemi and L. P. Li, "A viscoelastic poromechanical model of the knee joint in large compression," *Med. Eng. Phys.*, vol. 36, no. 8, pp. 998–1006, 2014.

[12] M. Kazemi, L. P. Li, P. Savard, and M. D. Buschmann, "Creep behavior of the intact and meniscectomy knee joints," *J. Mech. Behav. Biomed. Mater.*, vol. 4, no. 7, pp. 1351–1358, 2011.

[13] G. Papaioannou, C. K. Demetropoulos, and Y. H. King, "Predicting the effects of knee focal articular surface injury with a patient-specific finite element model," *Knee*, vol. 17, no. 1, pp. 61–68, 2010.

[14] G. Papaioannou, G. Nianios, C. Mitrogiannis, D. Fyhrie, S. Tashman, and K. H. Yang, "Patient-specific knee joint finite element model validation with high-accuracy kinematics from biplane dynamic Roentgen stereogrammetric analysis," *J. Biomech.*, vol. 41, no. 12, pp. 2633–2638, 2008.

[15] P. Beillas, G. Papaioannou, S. Tashman, and K. H. Yang, "A new method to investigate in-vivo knee behavior using a finite element model of the lower limb," *J. Biomech.*, vol. 37, no. 7, pp. 1019–1030, 2004.

[16] a. C. Godest, M. Beaugonin, E. Haug, M. Taylor, and P. J. Gregson, "Simulation of a knee joint replacement during a gait cycle using explicit finite element analysis," *J. Biomech.*, vol. 35, no. 2, pp. 267–275, 2002.

[17] J. P. Halloran, A. J. Petrella, and P. J. Rullkoetter, "Explicit finite element modeling of total knee replacement mechanics," *J. Biomech.*, vol. 38, no. 2, pp. 323–331, 2005.

[18] M. a. Baldwin, C. W. Clary, C. K. Fitzpatrick, J. S. Deacy, L. P.

Maletsky, and P. J. Rullkoetter, “Dynamic finite element knee simulation for evaluation of knee replacement mechanics,” *J. Biomech.*, vol. 45, no. 3, pp. 474–483, 2012.

[19] D. Kluess, W. Mittelmeier, and R. Bader, “Intraoperative impaction of total knee replacements: An explicit finite-element-analysis of principal stresses in ceramic vs. cobalt-chromium femoral components,” *Clin. Biomech.*, vol. 25, no. 10, pp. 1018–1024, 2010.

[20] M. a. Baldwin, C. Clary, L. P. Maletsky, and P. J. Rullkoetter, “Verification of predicted specimen-specific natural and implanted patellofemoral kinematics during simulated deep knee bend,” *J. Biomech.*, vol. 42, no. 14, pp. 2341–2348, 2009.

[21] D. S. Liu, Z. W. Zhuang, and S. R. Lyu, “Relationship between medial plica and medial femoral condyle - A three-dimensional dynamic finite element model,” *Clin. Biomech.*, vol. 28, no. 9–10, pp. 1000–1005, 2013.

[22] M. M. Ardestani, M. Moazen, and Z. Jin, “Gait modification and optimization using neural network-genetic algorithm approach: Application to knee rehabilitation,” *Expert Syst. Appl.*, vol. 41, no. 16, pp. 7466–7477, 2014.

[23] H. H. Choi, S. M. Hwang, Y. H. Kang, J. Kim, and B. S. Kang, “Comparison of implicit and explicit finite-element methods for the hydroforming process of an automobile lower arm,” *Int. J. Adv. Manuf. Technol.*, vol. 20, no. 6, pp. 407–413, 2002.

[24] S. Kugener, “Simulation of the Crimping Process by Implicit and Explicit Finite Element Methods,” *Technology*, vol. 4, pp. 8–15, 1995.

[25] L. M. Kutts, A. B. Pifko, J. a Nardiello, and J. M. Papazian, “Slow-dynamic finite element simulation processes,” *Comput. Struct.*, vol. 66, no. 1, pp. 1–17, 1998.

[26] R. P. N. Rebelo, J. C. Nagtegaal, L. M. Taylor, “Comparison of implicit and explicit finite element methods in the simulation of metal forming processes,” in *International Conference on Numerical Methods in Industrial Forming Processes NUMIFORM 92*, 1992, pp. 99–108.

[27] W. Rust and K. Schweizerhof, “Finite element limit load analysis

of thin-walled structures by ANSYS (implicit), LS-DYNA (explicit) and in combination,” *Thin-Walled Struct.*, vol. 41, no. 2–3, pp. 227–244, 2003.

[28] J. S. Sun, K. H. Lee, and H. P. Lee, “Comparison of implicit and explicit finite element methods for dynamic problems,” *J. Mater. Process. Technol.*, vol. 105, no. 1–2, pp. 110–118, 2000.

[29] L. Taylor, J. Cao, A. P. Karafillis, and M. C. Boyce, “Numerical simulations of sheet-metal forming,” *J. Mater. Process. Technol.*, vol. 50, no. 1–4, pp. 168–179, 1995.

[30] T. B. Wang, S.P., Choudhry, S., and Wertheimer, “Comparison between the static implicit and dynamic explicit methods for FEM simulation of sheet forming processes,” in *NUMIFORM 98*, 1997.

[31] S. Hibbitt, Karlsson, “ABAQUS Theory Manual.” Pawtucket, RI, USA, 1997.

[32] L. Noels, L. Stainier, and J. P. Ponthot, “Combined implicit/explicit time-integration algorithms for the numerical simulation of sheet metal forming,” *J. Comput. Appl. Math.*, vol. 168, no. 1–2, pp. 331–339, 2004.

[33] L. Noels, L. Stainier, and J. P. Ponthot, “Energy conserving balance of explicit time steps to combine implicit and explicit algorithms in structural dynamics,” *Comput. Methods Appl. Mech. Eng.*, vol. 195, no. 19–22, pp. 2169–2192, 2006.

[34] S. Sibole, C. Bennetts, B. Borotikar, S. Maas, and A. J. Van Den Bogert, “OpenKnee: A 3D finite element representation of the knee joint,” 2010.

[35] T. L. H. Donahue, M. L. Hull, M. M. Rashid, and C. R. Jacobs, “A finite element model of the human knee joint for the study of tibio-femoral contact,” *J. Biomech. Eng.*, vol. 124, no. 3, pp. 273–280, 2002.

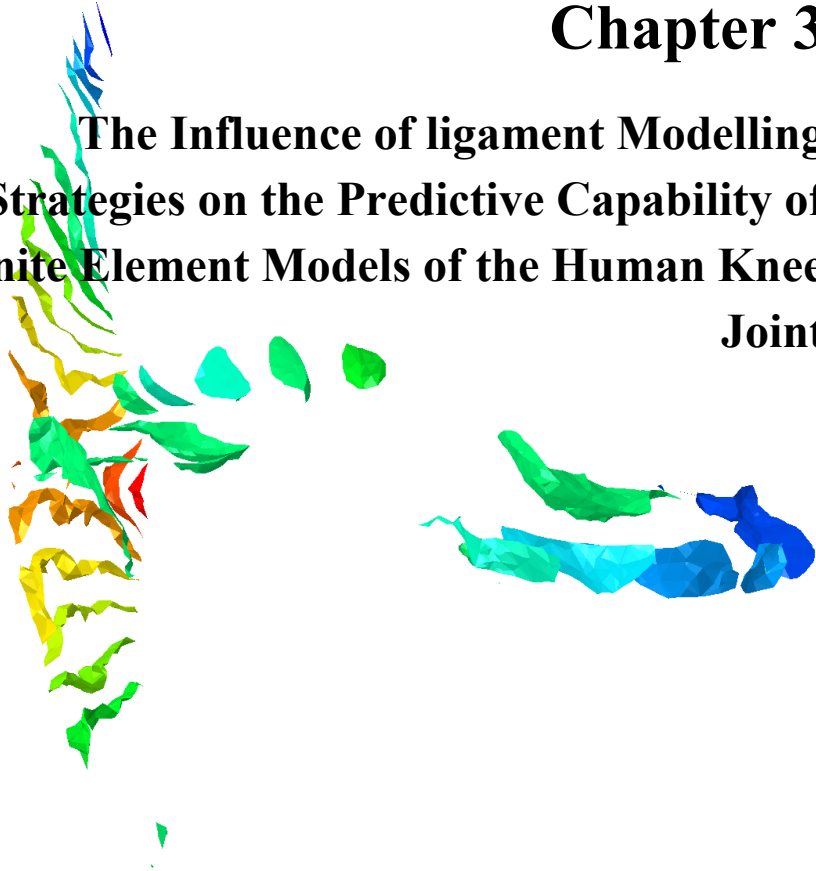
[36] C. G. Armstrong, W. M. Lai, and V. C. Mow, “An analysis of the unconfined compression of articular cartilage,” *J. Biomech. Eng.*, vol. 106, no. 2, pp. 165–173, 1984.

[37] D. E. Shepherd and B. B. Seedhom, “Thickness of human articular cartilage in joints of the lower limb,” *Ann. Rheum. Dis.*, vol. 58, no. 1, pp. 27–34, 1999.

- [38] H. Wang, T. Chen, P. Torzilli, R. Warren, and S. Maher, “Dynamic contact stress patterns on the tibial plateaus during simulated gait: A novel application of normalized cross correlation,” *J. Biomech.*, vol. 47, no. 2, pp. 568–574, 2014.
- [39] T. Kito and T. Yoneda, “Dominance of gait cycle duration in casual walking,” *Hum. Mov. Sci.*, vol. 25, no. 3, pp. 383–392, 2006.
- [40] J. R. Moreland, L. W. Bassett, and G. J. Hanker, “Radiographic analysis of the axial alignment of the lower extremity,” *J Bone Jt. Surg Am*, vol. 69, no. 5, pp. 745–749, 1987.
- [41] V. W. A. Unsworth, D. Dowson, “The Frictional Behavior of Human Synovial Joint-Part1: Natural Joint,” *J. Tribol.*, vol. 97, no. 3, pp. 369–376, 1974.
- [42] P. Beillas, G. Papaioannou, S. Tashman, and K. . Yang, “A new method to investigate in-vivo knee behavior using a finite element model of the lower limb,” *J. Biomech.*, vol. 37, no. 7, pp. 1019–1030, 2004.
- [43] a. M. Prior, “Applications of implicit and explicit finite element techniques to metal forming,” *J. Mater. Process. Technol.*, vol. 45, no. 1–4, pp. 649–656, 1994.

Chapter 3

The Influence of ligament Modelling Strategies on the Predictive Capability of Finite Element Models of the Human Knee Joint



Naghibi Beidokhti, H., Janssen, D., Van de Groes, S., Hazrati, J., Van den Boogaard, T., Verdonschot, N., 2017. Journal of Biomechanics. 65, 1-11.

1. Introduction

Ligaments have a large effect on knee joint kinematics and biomechanics, and are therefore of interest in computational models. Ligaments are commonly modelled as one-dimensional (1D) spring elements, or as three-dimensional (3D) constitutive elements [1]. Springs are widely used in finite element (FE) models [2]–[13]. The mechanical response of the ligaments is usually described by three distinct regions, with zero compression during ligament shortening, and a tensile response with an initial toe region and a final linear region. Blankevoort and Huiskes (1991) developed a model based on tensile tests of Butler et al. (1986), which is one the most often used models. Although a few studies implemented wrapping of springs (i.e. [16]–[18]) in most spring models this phenomenon is neglected [1]. An advantage of using springs is that they are computationally inexpensive.

Alternatively, ligament geometries are modelled as 3D structures assigned with constitutive material properties. Such an approach enables ligament wrapping, and allows analysis of the regional biomechanical response, but is computationally more expensive. The mathematical description of the material properties in continuum models remains challenging [9]. Ligaments are composed of a ground matrix (elastin), combined with fibres (collagen type I and III) that are active in tension, making it a highly anisotropic material [19]. The ground matrix is usually modelled as a hyperelastic material, while various models are used to model the fibres [20], [21].

Beside the manner of implementation, there is also a spread in the reported mechanical properties. Particularly experimental data from Butler et al. (1986) and Blankevoort and Huiskes (1991) have often been used in computational models [22]. Conversely, it is also possible to adjust the material properties specifically for the subject [2], [23], [24], as literature values may not always be appropriate for each specific case.

Although there are several options available for ligament modelling, the implications of modelling strategies on joint biomechanics are unknown. The aim of this study was therefore to evaluate the effects of:

a) The ligament modelling approach (non-linear springs (1D) vs. transversely isotropic continuum (3D) models); and,

b) The selection of the data used to describe the behaviour of ligaments (based either on the literature, or on subject-specific optimization),

on the predictive abilities of FE models of human native knee joints, based on cadaveric experiments. The outcome of this study can provide insight into knee ligament modelling in FE simulations to achieve more realistic knee models for clinical implementation.

2. Materials and Methods

The overall workflow of the study is schematically illustrated in Figure 1.

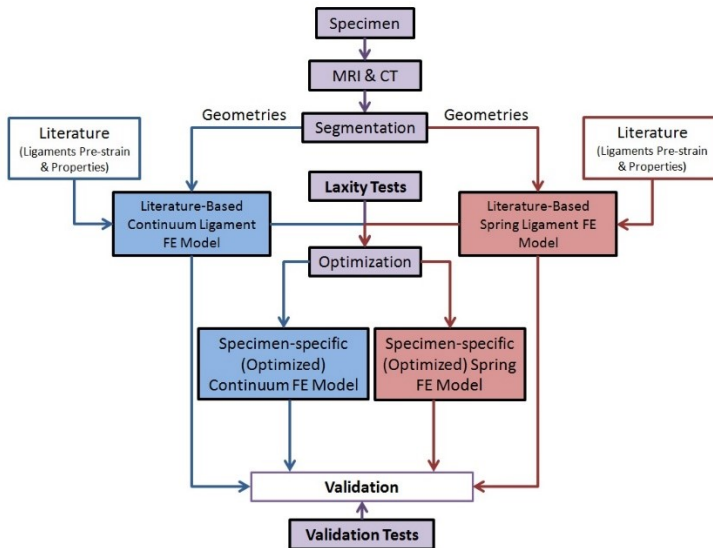


Figure 1: Schematic illustration of the current study methodology.

2.1. Experimental tests:

Three fresh-frozen cadavers with no signs of injuries or surgery were scanned in a 3T Philips Ingenia MRI scanner (Philips Healthcare, Best, The Netherlands), with two proton density and proton density SPAIR sequences with a slice thickness of 0.5mm.

After preparation the knees were positioned in a six-degree-of-freedom knee testing apparatus, in which the femur was unconstrained only in flexion-extension, and the tibia was unconstrained in all other translational and rotational

directions (Figure 2-a). The knee testing apparatus was schematically described in detail in Appendix A. Three groups of muscles were separated and subjected to constant forces: rectus femoris (20N), vastus medialis (10N), and vastus lateralis and vastus intermedius combined (10N) [25]–[27]. These loads were applied via ropes to stabilize the patella, and were not meant to be representative of quadriceps loads during in-vivo tasks.

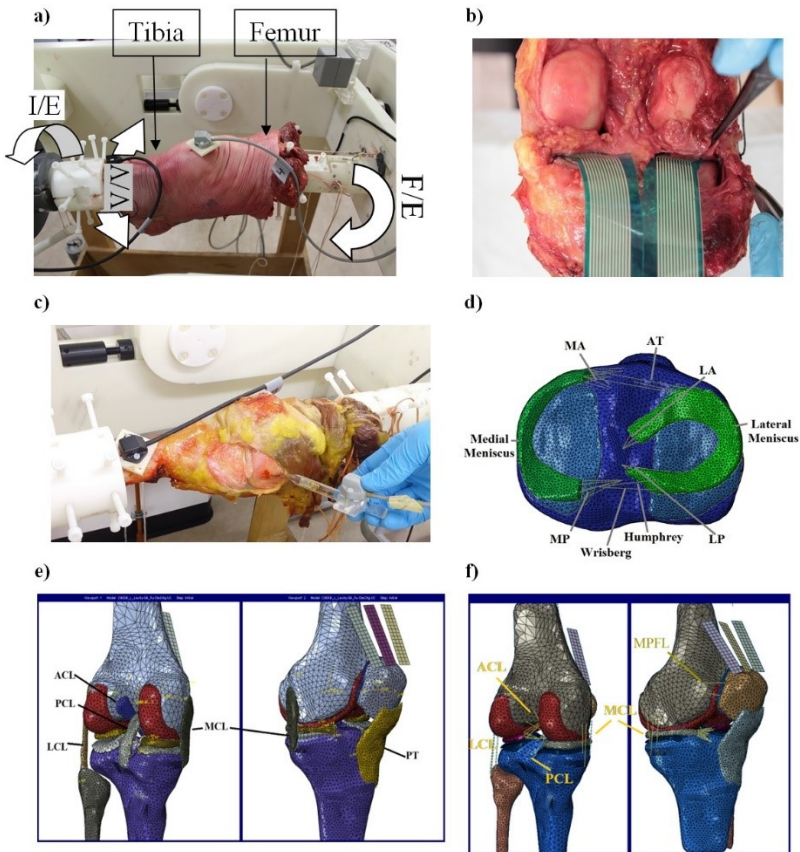


Figure 2: The experimental set-up, knee testing apparatus and Fastrak sensors (a); the pressure sensor film inserted in the knee joint (b); digitization of ligament insertions using a calibrated pen-stylus (c); modelled menisci attachments in FE model (d); a single specimen FE model with ligament continuum representations (e) and spring representations (f).

2.1.1. Laxity Tests:

The knees were subjected to a series of laxity tests, including internal-external torque (0 to ± 5.2 Nm) and valgus-varus moments (0 to ± 12 Nm) in five and four equally spaced steps, respectively, based on previous studies [28]–[30] which were used by Baldwin et al. (2012). The loads were applied to the tibia in 0° , 30° , 60° and 90° of flexion. Some laxity tests were randomly repeated to check reproducibility and repeatability. An electromagnetic tracking system (3Space Fastrak, Polhemus Incorporated, VT, USA) was used to track the position and orientation of the femur, tibia and patella (Figure 2-a). In-house developed scripts (MATLAB R2013a, Natick, MA) were used to convert the raw tracking data to kinematics in the knee joint coordinate system [31].

2.1.2. Validation Tests:

After the laxity tests, three different loading regimes were applied: 1) unloaded full extension to deep flexion (110°), 2) unloaded full extension to deep flexion (110°) with a 106N axial load acting on the tibia, and 3) full extension to 90° of flexion with a 100N anterior load applied to the tibia (~ 5 cm below the plateau). These loads were selected based on intended applications of the FE models in a later stage (e.g. analysis of ACL reconstructions), and observed the force magnitude limitations of the knee testing apparatus. Each loading condition was repeated twice to check repeatability.

Contact pressure measurements were performed using pressure sensors (Type 4011, Tekscan Inc., Boston, MA, USA). Each sensor was calibrated using a materials testing system (MMED, Materials Technology Corporation, La Canada, CA, USA) and a custom calibration tool consisting of two Teflon plates. The pressure sensor was inserted underneath the menisci from posteriorly, and sutured anteriorly and posteriorly (Figure 2-b). Due to the small width of the tibial plateau of the first cadaveric knee, the medial and lateral collateral ligaments had to be excised before sensor insertion in this specimen. The pressure measurements were repeated three times to check repeatability.

After the ligaments were excised, their insertion sites were digitized using an electromagnetic stylus (Figure 2-c).

2.2. Finite Element Model:

Mimics v18.0 (Materialise, Leuven, Belgium) was used to segment the bones (femur, tibia and patella), cartilage (tibial, femoral and patellar), menisci, cruciate ligaments (ACL and PCL), collateral ligaments (MCL and LCL), patellar tendon (PT), and the insertion sites of the medial and lateral patellofemoral ligaments (MPFL and LPFL) and the patellar tendon from the MRI scans. Each segmentation was performed by three different individuals to minimize variability. The bones segmented from MRI were furthermore compared with those segmented from CT to correct the interface between bone and cartilage. The tibiofemoral ligament insertion sites were estimated from segmentation (intersection of segmented ligament and cortical bone), and corrected using registered digitized points recorded during the experiment.

All soft tissues were meshed using 10-node modified quadratic tetrahedron (C3D10M) elements. Based on a mesh convergence study, an approximate element size of ~ 1.0 mm was chosen (see Appendix A for the number of elements in each segment). General contact with a frictionless penalty solution strategy was implemented [32]. The explicit solver of Abaqus software v6.13 (Pawtucket, RI, USA) was used. Based on a series of sensitivity analyses, a mass-scaling factor (average: 70) and solver viscosity parameter (0.03) were selected, consistent with an earlier study [32].

Bones were considered as rigid bodies. Cartilage was modelled as nonlinear Neo-Hookean hyperelastic isotropic, in which the strain energy function ψ is described as a function of the first invariant of the left Cauchy-Green deformation tensor (I_1) and the elastic volume ratio (J):

$$\psi = C_{10}(I_1 - 3) + \frac{1}{2D}(J - 1)^2 \quad (1)$$

C_{10} and D are the Neo-Hookean constant and the inverse of the bulk modulus, which were based on experimental compressive tests [33] ($C_{10}=0.86$ MPa; $D=0.048$ MPa $^{-1}$).

Menisci were modelled as transversely isotropic implementing the Holzapfel-Gesser-Ogden (HGO) hyperelastic model [20]. The strain energy function ψ is described as a function of Neo-Hookean terms, representing the non-collagenous

matrix, and $\bar{I}_{4(\alpha\alpha)}$, pseudo-invariants of $\bar{\mathbf{C}}$ and \mathbf{A}_α (directions of the fibres in the reference configuration):

$$\psi = C_{10}(\bar{I}_1 - 3) + \frac{1}{2D} \left(\frac{(J)^2 - 1}{2} - \ln(J) \right) + \frac{k_1}{2k_2} \{ \exp[k_2 \langle \bar{E}_\alpha \rangle^2] - 1 \} \quad (2)$$

With:

$$\bar{E}_\alpha = \kappa(\bar{I}_1 - 3) + (1 - 3\kappa)(\bar{I}_{4(\alpha\alpha)} - 1) \quad (3)$$

Constants k_1 and k_2 are material parameters and κ ($0 \leq \kappa \leq \frac{1}{3}$) describes the level of dispersion in the fibre directions. When $\kappa=0$, all fibres are perfectly aligned, and $\kappa = \frac{1}{3}$ describes an isotropic material [34].

Fibres were oriented in circumferential direction ($\kappa=0$), similar to [35]. Using curve fitting techniques, the HGO coefficients (k_1 and k_2) for the menisci were based on [36]. The Neo-Hookean parameters were estimated based on [37] and were assumed to equal for the medial and lateral menisci (Table 1).

Table 1: the HGO coefficients calculated for medial and lateral menisci based on the experimental data in the literature (Tissakht and Ahmed, 1995).

	C_{10} (MPa)	D (MPa ⁻¹)	k_1	k_2	κ
Medial Meniscus	1	0.005	5.04	0.889	0
Lateral Meniscus	1	0.005	8.48	1.559	0

Meniscus attachments were modelled as bundles of nonlinear no-compression springs (Figure 2-d). The horn attachments were represented by four springs ($k=400\text{N/mm}$), while the anterior transverse ligament was represented by three springs, in accordance with Haut Donahue et al. (2003) and in the range reported by Abraham et al. (2011). The anterior and posterior meniscofemoral ligaments were modelled using a single spring, based on Kusayama et al. (1994) ($k=49\text{N/mm}$).

Lateral and medial patellofemoral ligaments were modelled as two no-compression springs, based on Merican et al. (2009) (LPFL) and Kim et al. (2014) (MPFL), in accordance with Criscenti et al. (2016).

The rectus femoris, vastus medialis and grouped vastus lateralis and intermedius were modelled as membrane elements with passive properties from Robleto Jr (1997). These elements were proximally subjected to constant line loads of 20, 10 and 10 N, respectively, consistent with the experiments.

For each cadaveric knee, two separate FE models were developed:

1) *Ligament continuum model*: In this model the ligaments were represented as constitutive transversely isotropic materials (Figure 2-e). The HGO model was implemented to model ligaments, as described previously. The orientation of the fibres was modeled along with the ligament geometry in MCL, LCL, PCL and PT. The ACL was split with two different fibre orientations assigned to the anterior (aACL) and posterior ACL (pACL), estimated from ACL anatomy [45],[46] and the segmented geometry. The coefficients were calculated based on the experimental tensile tests [15] using curve fitting techniques. The initial strain for the ACL, MCL and LCL was based on Blankevoort and Huiskes (1991), similar to previous studies [47], [48]. The curved profile of the segmented PCL was assumed to correspond to the ligament pre-slackness [49], [50]. Thermal loading was applied to model the initial strain, with a negative expansion coefficient assigned to the ligament.

2) *Ligament spring model*: In this model the tibiofemoral ligaments were modelled using nonlinear no-compression springs (Figure 2-f). The ACL and PCL were modelled with two springs, while the LCL and MCL were modelled using three springs [14], estimating the insertion sites from the segmented model and anatomy textbooks. The initial springs parameters and reference lengths were based on Blankevoort and Huiskes (1991).

2.2.1. FE model optimization (FE fit to experimental laxity tests):

Besides using literature-based parameters, the spring (1D) and continuum (3D) models were also separately optimized to tune the ligament material parameters and initial strains, based on the experimental laxity tests. In the continuum

models, the following parameters were optimized: the model coefficients (k_1 and k_2) for all tibiofemoral ligaments, initial strain of the collateral ligaments and ACL, and the fibre distribution in ACL(κ). In the spring-based models, for each single spring, the spring coefficient and reference length (initial spring strain) were optimized.

Since the knees were scanned in extended position, the curved PCL was assumed to be representative for the initial slackness in the continuum model. The initial PCL strain was therefore not included in the optimization process. In the spring model, however, the initial slackness of the PCL was included in optimization.

In order to reduce the computational costs in the optimization procedure, motion-controlled laxity simulations were performed in which all rotations were prescribed, and reaction torques were calculated. The Nelder-Mead Downhill Simplex optimization method [51] was applied using Isight (Simulia, Providence, RI) to minimize the difference between the FE model calculated reaction torques and the experimental values.

2.2.2. Validation (FE compared to validation tests):

The three validation experiments (see above) were simulated with the 1D (spring) and 3D (continuum) ligament modelling approaches, with optimized values and with the literature-based values.

In all three loading cases the translational (anterior-posterior, medial-lateral and superior-inferior) and rotational (valgus-varus and internal-external) kinematics of the joint were extracted, after which the root mean square (RMS) differences with the experimental kinematics were calculated based on the values at 0, 30, 60, 90 and 110° (five points) in unloaded and axially loaded flexion, and at 0, 30, 60 and 90° (four points) in the anteriorly loaded flexion case. Eventually, for each loading case, orientation, and direction the RMS difference with experimental data was averaged for the three specimens. In the axially loaded case the contact area and peak contact pressure at the medial and lateral tibial cartilage was assessed. For the first cadaveric knee model (both continuum and spring models), the collateral ligaments were removed before contact pressure and area assessments, in order to replicate the experimental conditions for this specific specimen. The average RMS differences between the model predictions and in-

in vitro Tekscan measurements for five different flexion angles (0, 30, 60, 90 and 110°) were calculated.

3. Results

3.1. Optimization using laxity tests:

For each FE model, on average 2,800 and 3,500 simulations were completed for the spring and continuum model optimizations, respectively. The optimized ligament material property coefficients and reference strains are presented in Table 2 (spring model), and Table 3 (continuum model). As expected, optimization of the spring and continuum models resulted in an acceptable approximation of the experimental laxity (Figure 3).

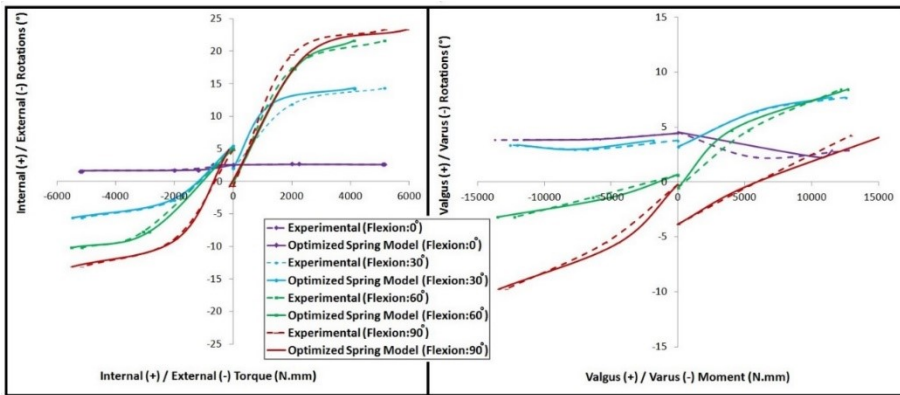


Figure 3: Single knee internal/external and varus/valgus experimental and optimized spring model laxity data at four different flexion angles of 0, 30, 60 and 90°.

Table 2: Literature-based and optimized ligament stiffness and reference strain in the spring (1D) FE model.

		aPCL	pPCL	aACL	pACL	aMCL	iMCL	pMCL	aLCL	sLCL	pLCL
Ligament stiffness (N)	Initial value	9000	9000	5000	5000	2750	2750	2750	2000	2000	2000
	Knee1	10879	9855	7354	5041	2101	2540	2764	1486	1621	1449
	Knee2	8990	1938	5457	5071	1476	944	2648	2349	2105	2309
	Knee3	3988	3792	4493	4657	2121	2300	2415	1916	1809	1822
Reference strain	Initial value	-0.24	-0.03	0.06	0.10	0.04	0.04	0.03	-0.25	-0.05	0.08
	Knee1	-0.35	-0.18	-0.32	0.02	0.11	-0.02	-0.12	-0.32	-0.19	0.00
	Knee2	-0.34	-0.23	-0.01	0.09	-0.03	0.26	-0.07	-0.23	-0.11	0.00
	Knee3	-0.24	-0.12	0.06	0.08	0.02	0.04	0.03	-0.14	0.00	0.05

3.2. Validation:

3.2.1. Kinematics validation:

The kinematics recorded in the three knees were quite repeatable, with maximum deviations of 6% and 8% for translational and rotational kinematics, respectively.

Table 4 sums up the RMS differences between the experimental measurements and the FE models. For unloaded and axially loaded deep flexion, the optimized spring and continuum models improved the kinematics predictions. The optimized continuum model resulted in the lowest valgus-varus (unloaded: $2.9 \pm 0.9^\circ$ and axially loaded: $2.7 \pm 1.0^\circ$) and internal-external (unloaded: $1.8 \pm 0.2^\circ$ and axially loaded: $2.2 \pm 1.2^\circ$) rotational errors, while the optimized spring model produced, in average, the best translations with a maximum translational error of $3.1 \pm 1.7\text{mm}$ (medial-lateral translation). Similar trends were observed for the individual flexion angles (see Appendix A).

Table 3: Literature-based and optimized ligament HGO coefficients and reference strain (ϵ_0) in the continuum (3D) FE models.

	ACL (aACL&pACL)				PCL		MCL			LCL			
	K1	K2	k	ϵ_0 (%)	K1	K2	K1	K2	ϵ_0 (%)	K1	K2	ϵ_0 (%)	
Initial value	52.27	5.789	0	8.0	46.18	2.758	41.21	5.351	4.0	41.21	5.351	3.0	
Optimized value	Knee1	52.52	5.86	0.005	8.1	46.42	2.73	41.01	5.07	3.9	14.57	5.26	3.3
	Knee2	39.41	3.14	0.000	3.0	16.11	1.703	26.02	3.502	1.0	38.10	4.098	2.0
	Knee3	47.9	3.075	0.003	3.1	14.8	1.814	31.74	1.491	1.6	31.33	1.418	1.5

In the anteriorly loaded tibia, compared with literature-based continuum model, no improvement was seen in varus-valgus rotations and medial-lateral translations in the optimized continuum model, while internal-external rotations ($3.8 \pm 0.8^\circ$) and anterior-posterior translations ($2.6 \pm 1.6\text{mm}$) improved. In the spring model, relative to the literature-based model, optimization resulted in a decrease in rotational and translational errors, although the superior-inferior translation error increased from $1.1 \pm 0.4\text{mm}$ to $1.9 \pm 1.1\text{mm}$. Compared to the optimized continuum model, the optimized spring model more closely resembled the experimental rotational laxity, as well as anterior-posterior translations.

Table 4: average RMS difference between experimental validation tests kinematics and two spring and continuum ligament FE models with literature-based and optimized ligament parameters for three specimens; the best predictions at each validation loading case were marked in bold.

	Average RMS difference ± standard deviation											
	Unloaded deep flexion				Tibia axially loaded deep flexion				Tibia anteriorly loaded flexion			
	Literature-based spring model	Optimized spring model	Literature-based continuum model	Optimized continuum model	Literature-based spring model	Optimized spring model	Literature-based continuum model	Optimized continuum model	Literature-based spring model	Optimized spring model	Literature-based continuum model	Optimized continuum model
Superior/Inferior translations (mm)	2.5±2.0	2.3±1.2	2.8±1.3	2.6±0.6	2.2±2.0	2.0±1.2	2.6±1.1	2.9±1.3	1.1±0.4	1.9±1.1	1.4±0.8	1.4±0.9
Lateral/Medial translations (mm)	2.5±2.0	1.6±1.7	2.1±1.1	1.9±1.2	3.4±1.4	3.1±1.7	3.4±2.5	2.4±1.6	3.1±1.4	2.8±0.8	2.7±1.1	2.8±1.1
Anterior/Posterior translations (mm)	5.8±2.1	3.0±2.2	7.4±2.2	3.8±1.5	5.8±2.3	2.9±2.2	7.4±2.8	4.1±1.4	3.1±1.3	2.2±0.4	2.9±1.3	2.6±1.6
Varus/Valgus rotations in °	5.6±2.0	3.5±0.3	5.0±2.6	2.9±0.9	5.7±1.8	3.8±0.6	3.9±1.4	2.7±1.0	4.1±2.4	3.2±1.7	4.1±0.5	4.3±1.3
Internal/External rotations in °	5.7±2.1	2.8±1.1	2.5±1.2	1.8±0.2	5.6±2.7	3.0±0.4	3.1±1.0	2.2±1.2	6.7±3.4	2.6±1.1	4.1±1.1	3.8±0.8

3.2.2. Contact variables validation:

Table 5 shows the average RMS differences of the tibiofemoral peak contact pressure and contact area between the experimental measurements and FE models. Due to a technical problem, no signal was recorded for the medial tibia plateau of the first cadaveric knee, and as a result, the RMS could not be calculated for this site.

Except for the lateral tibial cartilage of the second cadaveric knee spring model, both the optimized spring and continuum models improved the peak contact pressure with respect to the literature-based models. The optimized continuum models more closely resembled the experimental measurements at the medial tibial cartilage of the second and third specimens, and the lateral cartilage of the first specimen. In two other cases (lateral cartilage of the second and third knee), the optimized spring ligament models resulted in smaller peak contact pressure errors (0.20 ± 0.16 and 0.13 ± 0.41 MPa, respectively) than the continuum model (0.39 ± 0.29 and 0.19 ± 0.25 MPa, respectively).

Table 5: Average RMS difference between experimentally measured contact variables and two spring and continuum ligament FE models with literature-based and optimized ligament parameters for three specimens, during tibia axially loaded high flexion at 0, 30, 60, 90 and 110°; for each specimen; the best predictions were marked in bold.

		RMS±Standard Deviation							
		Peak Contact Pressure (MPa)				Contact Area (mm ²)			
		Literature-based spring model	Optimized spring model	Literature-based continuum model	Optimized continuum model	Literature-based spring model	Optimized spring model	Literature-based continuum model	Optimized continuum model
Knee1	Lateral	2.56±2.08	0.47±1.13	0.51±1.16	0.46±1.17	89±173	163±223	141±263	132±255
	Medial	N/A*	N/A*	N/A*	N/A*	N/A*	N/A*	N/A*	N/A*
Knee2	Lateral	0.19±0.19	0.20±0.16	1.13±0.50	0.39±0.29	279±243	307±290	131±217	102±172
	Medial	1.12±0.67	0.50±0.46	0.96±0.66	0.34±0.42	107±280	126±201	78±306	58±242
Knee3	Lateral	0.33±0.44	0.13±0.41	0.20±0.33	0.19±0.25	163±190	121±97	150±70	143±66
	Medial	0.74±0.41	0.37±0.38	0.51±0.43	0.36±0.35	284±302	175±266	106±277	90±233

*Due to a technical problem in sensor reader, the medial plateau pressure of the first knee was not recorded.

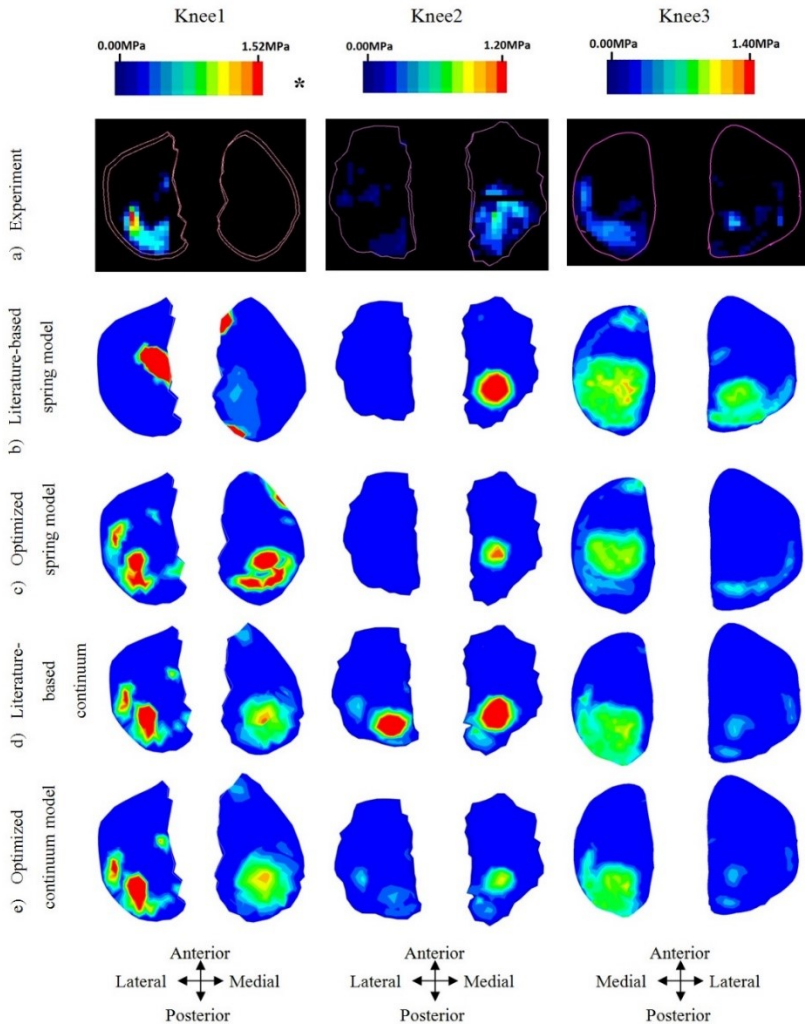


Figure 4. Contact pressure at medial and lateral tibial cartilages at a single flexion angle (90°) in tibia axially loaded high flexion case, for all three specimens, in: a) experiment, b) literature-based spring model, c) optimized spring model, d) literature-based continuum model, and e) optimized continuum model. (* Due to a technical problem in sensor reader, pressure map on medial plateau of the first knee was not recorded)

While the optimized continuum model decreased the contact area error, in two knees the optimized spring models actually led to larger RMS values (first and second knee). In one case only (lateral cartilage of the third knee), the optimized spring ligament gave a better prediction of the contact area (RMS $121 \pm 97 \text{ mm}^2$) than the continuum ligament model (RMS $143 \pm 66 \text{ mm}^2$).

Figure 4 shows the experimental contact pressure maps at 90°, and those simulated with the spring model with literature-based and optimized parameters, and with the continuum model with literature-based and optimized coefficients. The continuum models more closely approximated the experimental contact pressure pattern than the spring models (see also Appendix A).

4. Discussion

In the current study we investigated the effect of modelling choices on the predictive capability of FE models of the human knee joint. Knee ligaments were represented either by using springs, or by using continuum models based on ligament segmentations. Moreover, the effect of assigning material parameters based either on literature, or based on specimen-specific optimization was evaluated. Optimized material properties improved the kinematics and contact parameters for both approaches. Literature-based parameters, particularly for the spring models, led to relatively high errors in kinematics and contact pressures, mainly for larger flexion angles (90 and 110°).

The sensitivity of literature-based spring models may be attributed to the concentration of the actual ligament insertion area to a single point, or a few points in some ligaments. Mommersteeg et al. (1996) found that models with three or less line elements for knee ligaments can be very sensitive to geometrical variations. The optimized spring and continuum models were generally comparable in terms of joint kinematics, although the continuum and spring models showed slightly better rotational and translational predictions, respectively.

In the optimization process of both the spring and continuum ligament representations, for some ligaments the parameters varied noticeably within the defined bounds. The most notable differences between the three knees were seen in the PCL stiffness, where the optimized stiffness parameters in the first knee were consistently high, while in the third knee they were low. The optimized parameters, however, were within the physiological range reported in the literature [53]–[58]. On average, for a single knee model the optimization process took approximately 400 and 600 hours for spring and continuum ligament representations, respectively.

Although the subject-specific models improved the kinematics compared with the literature-based models, even these did not produce perfect predictions due to the assumptions and inaccuracies involved (i.e. ligament fibre alignment, insertion sites, segmentation errors, etc.). The implications of these errors should be evaluated depending on the objectives through sensitivity analyses. For instance, valgus-varus or internal-external rotation variations can lead to unacceptable errors in contact pressure predictions [59][60][61]. In the current study, the subject-specific spring and continuum models comparably predicted peak contact pressures and contact areas, with an acceptable agreement with the experimental measurements. However, based on the comparison of contact pressure patterns for all three specimens models (presented in Appendix A), the continuum model appears to provide slightly better predictions.

On average, the optimized spring model of the third knee showed the smallest difference in ligament parameters (except for PCL) compared to the literature-based spring model, which may explain the quite acceptable contact pressure prediction of the literature-based spring model. However, in high flexion (110°), where the maximum PCL tension occurs [50], the predictions of the literature-based model diverged from the experimental outcome. Despite these differences, in some cases the use of a spring model may be preferred, as this modelling approach resulted in a $\sim 30\%$ reduction of the computational time as compared to the continuum model.

It is worth mentioning that due to the discretization of the pressure distribution, and due to its physical stiffness, the use of Tekscan film sensors can result in an error of 1-4% for the peak pressure, and 3-9% for the contact area [62]–[64]. Nonetheless, the contact patterns measured in the experiments agreed well with the study of Yao et al. (2008), in which tibiofemoral contact during high flexion was estimated from MRI data. Despite the different loading conditions, the total contact area measured in this study showed a similar pattern with those calculated by Mesfar and Shirazi-Adl, (2006). The insertion of the Tekscan film may also alter the joint behaviour, which could further enlarge the differences between the physical measurements and FE predictions. However, comparison of the kinematics before and after insertion of the pressure sensors was recorded, as for instance shown in Figure 5 for a single case, which indicated the kinematic behaviour was not considerably affected by the pressure sensor (differences in translations and rotations were $\pm 2.0\text{mm}$ and $\pm 3^\circ$, respectively).

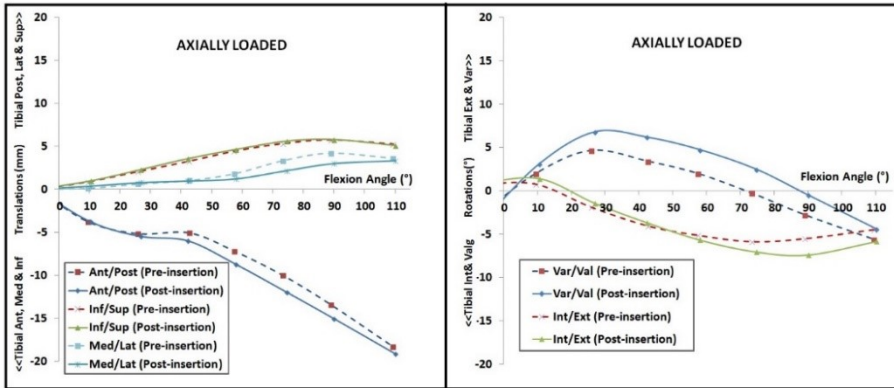


Figure 5: translational (left) and rotational (right) kinematics pre- and post-pressure sensor insertion during axially loaded high flexion for a single specimen.

In this study there were several limitations. First, comparing with physiological loads, the loads applied during the validation experiments were reduced due to structural limitations of the testing apparatus. Higher axial loads are expected during daily activities, and more rigorous testing data is required to evaluate the model representation in these ranges. However, for the current study we focused on comparing two different ligament modelling approaches in FE. Second, the depth-dependent material properties and inhomogeneity of the cartilage were not included, which may play a role in the mechanical response of the cartilage [67], [68]. Investigation of progression of osteoarthritis therefore probably requires a more detailed description of the cartilage mechanics. However, using a simplified material model, with a loading rate similar to this study ($\sim 0.5\text{Hz}$) [69], may have a less significant effect on the contact pressure, as shown by Mononen et al. (2012) and Mootanah et al. (2012). The hyperelastic parameters of the cartilage surfaces were based on experimental tests in the literature. Adopting the cartilage coefficients in a subject-specific manner might improve the predictions, although varying the cartilage stiffness by $\pm 10\%$, within the range reported by Shepherd and Seedhom (1999), caused a change of less than 4% and 7% in contact pressure and contact area, respectively. A homogenous circumferentially fibric hyperelastic definition was utilized to model menisci. Including inhomogeneity and radial fibres of the menisci may increase the validity of the contact variables, particularly when the absolute contact outcomes (i.e. contact stress) are of interest. Bones were modelled as rigid body, which according to Donahue et al. (2002) is a valid assumption under simple loads, but Venäläinen et al. (2016) showed that a non-rigid definition may be more realistic for more complex

loading conditions. Only three knee specimens were used, due to the substantial amount of time required for the experimental tests, model development, and optimization analyses. Despite this restriction, the current results unanimously showed the effect of the studied ligament modelling approaches. Finally, cruciate ligaments were modelled each with two bundles based on Blankevoort et al. (1991), which is a common approach [1]. As shown by Mommersteeg et al. (1996), increasing the number of cruciate ligaments spring bundles, i.e. as by Moglo and Shirazi-Adl (2003) and Baldwin et al. (2009), may improve the accuracy of the model outcomes.

In summary, when modelling the native knee joint in FE, adopting subject-specific material parameters affects and improves the quality of the model predictions. Comparing with the ligament spring representations used in this study, using a continuum modelling approach results in more accurate contact outcome variables. However, when mainly the prediction of joint kinematics is of interest, the spring ligament models provide a faster option. In this case, and particularly in high flexion, representing the ligaments with multiple spring elements covering the ligament insertion sites is recommended.

The method implemented in this study can be adapted to in-vivo patient-specific FE modelling to assess biomechanical behaviour of the joint, as all the main tibiofemoral ligament material properties were calculated based on the tests which can be performed non-invasively. Future work could involve only crucial (laxity) tests in order to reduce the required time for FE model creation, to be more practically implementable in clinical applications.

Acknowledgments

This study was a part of BioMechTools project (ERC-2012-ADG LS7), received funding from the European Research Council under the European Union's Seventh Framework Program (FP/2007-2013) / ERC Grant Agreement n. 323091.

Reference

- [1] F. Galbusera *et al.*, “Material models and properties in the finite element analysis of knee ligaments: a literature review.,” *Front. Bioeng. Biotechnol.*, vol. 2, no. November, p. 54, 2014.
- [2] M. a. Baldwin, C. W. Clary, C. K. Fitzpatrick, J. S. Deacy, L. P. Maletsky, and P. J. Rullkoetter, “Dynamic finite element knee simulation for evaluation of knee replacement mechanics,” *J. Biomech.*, vol. 45, no. 3, pp. 474–483, 2012.
- [3] M. Adouni and A. Shirazi-Adl, “Consideration of equilibrium equations at the hip joint alongside those at the knee and ankle joints has mixed effects on knee joint response during gait,” *J. Biomech.*, vol. 46, no. 3, pp. 619–624, 2013.
- [4] M. Adouni and A. Shirazi-Adl, “Partitioning of knee joint internal forces in gait is dictated by the knee adduction angle and not by the knee adduction moment,” *J. Biomech.*, vol. 47, no. 7, pp. 1696–1703, 2014.
- [5] B. Innocenti, S. Pianigiani, L. Labey, J. Victor, and J. Bellemans, “Contact forces in several TKA designs during squatting: A numerical sensitivity analysis,” *J. Biomech.*, vol. 44, no. 8, pp. 1573–1581, 2011.
- [6] H. Marouane, A. Shirazi-Adl, M. Adouni, and J. Hashemi, “Steeper posterior tibial slope markedly increases ACL force in both active gait and passive knee joint under compression,” *J. Biomech.*, vol. 47, no. 6, pp. 1353–1359, 2014.
- [7] S. Pianigiani, Y. Chevalier, L. Labey, V. Pascale, and B. Innocenti, “Tibio-femoral kinematics in different total knee arthroplasty designs during a loaded squat: A numerical sensitivity study,” *J. Biomech.*, vol. 45, no. 13, pp. 2315–2323, 2012.
- [8] A. P. Stylianou, T. M. Guess, and M. Kia, “Multibody muscle driven model of an instrumented prosthetic knee during squat and toe rise motions,” *J. Biomech. Eng.*, vol. 135, no. 4, p. 41008, 2013.
- [9] M. Freutel, H. Schmidt, L. Dürselen, A. Ignatius, and F. Galbusera, “Finite element modeling of soft tissues: Material models, tissue interaction and challenges,” *Clin. Biomech.*, vol. 29, no. 4, pp. 363–372, 2014.

- [10] H. Guo *et al.*, “A statistically-augmented computational platform for evaluating meniscal function,” *J. Biomech.*, vol. 48, no. 8, pp. 1444–1453, 2015.
- [11] P. Tanska, M. E. Mononen, and R. K. Korhonen, “A multi-scale finite element model for investigation of chondrocyte mechanics in normal and medial meniscectomy human knee joint during walking,” *J. Biomech.*, vol. 48, no. 8, pp. 1397–1406, 2015.
- [12] A. Imran, “Anterior Cruciate Ligament Fibres – Effects of Tibial Translation During Flexion at the Knee,” vol. III, pp. 4–7, 2012.
- [13] M. Adouni, a. Shirazi-Adl, and R. Shirazi, “Computational biodynamics of human knee joint in gait: From muscle forces to cartilage stresses,” *J. Biomech.*, vol. 45, no. 12, pp. 2149–2156, 2012.
- [14] L. Blankevoort and R. Huiskes, “Ligament-bone interaction in a three-dimensional model of the knee.,” *J. Biomech. Eng.*, vol. 113, no. 3, pp. 263–269, 1991.
- [15] D. L. Butler, M. D. Kay, and D. C. Stouffer, “Comparison of material properties in fascicle-bone units from human patellar tendon and knee ligaments.,” *J. Biomech.*, vol. 19, no. 6, pp. 425–432, 1986.
- [16] M. Bendjaballah, a Shirazi-Adl, and D. Zukor, “Finite element analysis of human knee joint in varus-valgus,” *Clin. Biomech.*, vol. 12, no. 3, pp. 139–148, 1997.
- [17] M. S. Hefzy and E. S. Grood, “An Analytical Technique for Modeling Knee Joint Stiffness—Part II: Ligamentous Geometric Nonlinearities,” *J. Biomech. Eng.*, vol. 105, no. 2, pp. 145–153, 1983.
- [18] M. Z. Bendjaballah, A. Shirazi-Adl, and D. J. Zukor, “Biomechanical response of the passive human knee joint under anterior-posterior forces,” *Clin. Biomech.*, vol. 13, pp. 625–633, 1998.
- [19] T. Ushiki, “Collagen fibers, reticular fibers and elastic fibers. A comprehensive understanding from a morphological viewpoint,” *Arch. Histol. Cytol.*, vol. 65, no. 2, pp. 109–126, 2002.
- [20] G. A. Holzapfel, T. C. Gasser, and R. W. Ogden, “A new constitutive framework for arterial wall mechanics and a comparative study of material models,” *J. Elast.*, vol. 61, no. 1–3, pp. 1–48, 2000.
- [21] J. a. Weiss, B. N. Maker, and S. Govindjee, “Finite element implementation of incompressible, transversely isotropic hyperelasticity,” *Comput. Methods Appl. Mech. Eng.*, vol. 135, no. 1–2, pp. 107–128, 1996.

- [22] F. Galbusera *et al.*, “Material Models and Properties in the Finite Element Analysis of Knee Ligaments: A Literature Review,” *Front. Bioeng. Biotechnol.*, vol. 2, no. November, pp. 1–11, 2014.
- [23] J. C. Gardiner and J. a Weiss, “Subject-specific finite element analysis of the human medial collateral ligament during valgus knee loading,” *J. Orthop. Res.*, vol. 21, no. 6, pp. 1098–1106, 2003.
- [24] C. Wan, Z. Hao, L. Tong, J. Lin, Z. Li, and S. Wen, “An update on the constitutive relation of ligament tissues with the effects of collagen types,” *J. Mech. Behav. Biomed. Mater.*, vol. 50, pp. 255–267, 2015.
- [25] F. Farahmand, W. Senavongse, and A. A. Amis, “Quantitative study of the quadriceps muscles and trochlear groove geometry related to instability of the patellofemoral joint,” *J. Orthop. Res.*, vol. 16, no. 1, pp. 136–143, 1998.
- [26] A. Rood *et al.*, “Patellofemoral Pressure Changes After Static and Dynamic Medial Patellofemoral Ligament Reconstructions,” *Am. J. Sports Med.*, vol. 43, no. 10, pp. 2538–2544, 2015.
- [27] F. Farahmand, M. N. Tahmasbi, and A. Amis, “The contribution of the medial retinaculum and quadriceps muscles to patellar lateral stability - An in-vitro study,” *Knee*, vol. 11, no. 2, pp. 89–94, 2004.
- [28] W. P. Seering, R. L. Piziali, D. A. Nagel, and D. J. Schurman, “The function of the primary ligaments of the knee in varus-valgus and axial rotation,” *J. Biomech.*, vol. 13, no. 9, pp. 785–794, 1980.
- [29] Keith L. Markolf, J. S. Mensch, and Harlan C. Amstutz, “Stiffness and laxity of the knee - the contributions of the supporting structures,” *J. bone Jt. Surg.*, vol. 58, no. 5, 1976.
- [30] D. L. Gollehon, P. A. Torzilli, and R. F. Warren, “The role of the posterolateral and cruciate ligaments in the stability of the human knee. A biomechanical study.,” *J. Bone Joint Surg. Am.*, vol. 69, no. 2, pp. 233–42, 1987.
- [31] W. J. Grood, E.S.; Suntay, “A joint coordinate system for the clinical description of three-dimensional motions applications to the knee,” *J. Biomech. Eng.*, vol. 105, no. 2, pp. 136–144, 1983.
- [32] H. Naghibi Beidokhti *et al.*, “A comparison between dynamic implicit and explicit finite element simulations of the native knee joint,” *Med. Eng. Phys.*, vol. 38, no. 2016, pp. 1123–1130, 2016.
- [33] D. E. Shepherd and B. B. Seedhom, “The ‘instantaneous’

compressive modulus of human articular cartilage in joints of the lower limb.," *Rheumatology (Oxford)*, vol. 38, no. 1, pp. 124–132, 1999.

[34] A. Abaqus and Simulia, "ABAQUS 6.11 Documentation," *Dassault Syst. Simulia*, p. 1100, 2011.

[35] M. Freutel, F. Galbusera, A. Ignatius, and L. Dürselen, "Material properties of individual menisci and their attachments obtained through inverse FE-analysis," *J. Biomech.*, vol. 48, no. 8, pp. 1343–9, 2015.

[36] M. Tissakht and a M. Ahmed, "Tensile Stress-Strain Characteristics of the Human Meniscal Material," *J. Biomech.*, vol. 28, no. 4, pp. 411–422, 1995.

[37] E. K. Danso *et al.*, "Characterization of site-specific biomechanical properties of human meniscus—Importance of collagen and fluid on mechanical nonlinearities," *J. Biomech.*, vol. 48, no. 8, pp. 1499–1507, 2015.

[38] T. L. Haut Donahue, M. L. Hull, M. M. Rashid, and C. R. Jacobs, "How the stiffness of meniscal attachments and meniscal material properties affect tibio-femoral contact pressure computed using a validated finite element model of the human knee joint," *J. Biomech.*, vol. 36, no. 1, pp. 19–34, 2003.

[39] A. C. Abraham, J. T. Moyer, D. F. Villegas, G. M. Odegard, and T. L. Haut Donahue, "Hyperelastic properties of human meniscal attachments," *J. Biomech.*, vol. 44, no. 3, pp. 413–418, 2011.

[40] T. Kusayama, C. D. Harner, G. J. Carlin, J. W. Xerogeanes, and B. A. Smith, "Anatomical and biomechanical characteristics of human meniscofemoral ligaments," *Knee Surgery, Sport. Traumatol. Arthrosc.*, vol. 2, no. 4, pp. 234–237, 1994.

[41] A. M. Merican, S. Sanghavi, F. Iranpour, and A. a. Amis, "The structural properties of the lateral retinaculum and capsular complex of the knee," *J. Biomech.*, vol. 42, no. 14, pp. 2323–2329, 2009.

[42] K. E. Kim, S. L. Hsu, and S. L. Woo, "Tensile properties of the medial patellofemoral ligament: the effect of specimen orientation," *J. Biomech.*, vol. 47, no. 2, pp. 592–595, 2014.

[43] G. Criscenti *et al.*, "Material and structural tensile properties of the human medial patello-femoral ligament," *J. Mech. Behav. Biomed. Mater.*, vol. 54, pp. 141–148, 2016.

[44] R. A. Robleto Jr, "An analysis of the musculotendon dynamics

of Hill-based models,” Texas Tech University, 1997.

[45] E. Stieven-Filho, E. T. Garschagen, M. Namba, J. L. V. da Silva, O. Malafaia, and L. A. M. da Cunha, “Anatomic study of the double-bundle of the anterior cruciate ligament with the knee in 90° flexion,” *Rev. Col. Bras. Cir.*, vol. 38, no. 5, pp. 338–42, 2011.

[46] L. Blankevoort, R. Huijskes, and a de Lange, “Recruitment of knee joint ligaments,” *J. Biomech. Eng.*, vol. 113, no. 1, pp. 94–103, 1991.

[47] E. Peña, B. Calvo, M. a. Martínez, and M. Doblaré, “A three-dimensional finite element analysis of the combined behavior of ligaments and menisci in the healthy human knee joint,” *J. Biomech.*, vol. 39, no. 9, pp. 1686–1701, 2006.

[48] Y. Song, R. E. Debski, V. Musahl, M. Thomas, and S. L. Y. Woo, “A three-dimensional finite element model of the human anterior cruciate ligament: A computational analysis with experimental validation,” *J. Biomech.*, vol. 37, no. 3, pp. 383–390, 2004.

[49] A. A. Amis, C. M. Gupte, A. M. J. Bull, and A. Edwards, “Anatomy of the posterior cruciate ligament and the menisiofemoral ligaments,” *Knee Surg. Sport. Traumatol. Arthrosc.*, vol. 14, pp. 257–263, 2006.

[50] S. Nakagawa *et al.*, “The posterior cruciate ligament during flexion of the normal knee,” *J. Bone Joint Surg. Br.*, vol. 86, no. 3, pp. 450–456, 2004.

[51] J. A. Nelder, R. Mead, B. J. A. Nelder, and R. Mead, “A Simplex Method for Function Minimization,” *Comput. J.*, vol. 7, no. 4, pp. 308–313, 1965.

[52] T. J. Mommersteeg, L. Blankevoort, R. Huijskes, J. G. Kooloos, and J. M. Kauer, “Characterization of the mechanical behavior of human knee ligaments: a numerical-experimental approach,” *J. Biomech.*, vol. 29, no. 2, pp. 151–160, 1996.

[53] P. S. Trent, P. S. Walker, and B. Wolf, “Ligament length patterns, strength, and rotational axes of the knee joint,” *Clinical orthopaedics and related research*. pp. 263–270, 1976.

[54] J. Wismans, F. Veldpaus, J. Janssen, A. Huson, and P. Struben, “A three-dimensional mathematical model of the knee-joint,” *J. Biomech.*, vol. 13, no. 8, 1980.

- [55] T. P. Andriacchi, R. P. Mikosz, S. J. Hampton, and J. O. Galante, "Model studies of the stiffness characteristics of the human knee joint," *J. Biomech.*, vol. 16, no. 1, pp. 23–29, 1983.
- [56] J. R. Robinson, A. M. J. Bull, and A. a. Amis, "Structural properties of the medial collateral ligament complex of the human knee," *J. Biomech.*, vol. 38, no. 5, pp. 1067–1074, 2005.
- [57] R. Jones *et al.*, "Mechanical properties of the human anterior cruciate ligament," *Clin. Biomech.*, vol. 10, no. 7, pp. 339–344, 1995.
- [58] S. L. Woo, J. M. Hollis, D. J. Adams, R. M. Lyon, and S. Takai, "Tensile properties of the human femur-anterior cruciate ligament-tibia complex. The effects of specimen age and orientation.," *Am. J. Sports Med.*, vol. 19, no. 3, pp. 217–225, 1991.
- [59] A. E. Engin and M. S. Korde, "Biomechanics of normal and abnormal knee joint," *J. Biomech.*, vol. 7, no. 4, 1974.
- [60] J. H. Heegaard, P. F. Leyvraz, and C. B. Hovey, "A computer model to simulate patellar biomechanics following total knee replacement: The effects of femoral component alignment," *Clin. Biomech.*, vol. 16, no. 5, pp. 415–423, 2001.
- [61] F. W. Werner, D. C. Ayers, L. P. Maletsky, and P. J. Rullkoetter, "The effect of valgus/varus malalignment on load distribution in total knee replacements," *J. Biomech.*, vol. 38, no. 2, pp. 349–355, 2005.
- [62] B. J. Fregly and W. G. Sawyer, "Estimation of discretization errors in contact pressure measurements.," *J. Biomech.*, vol. 36, no. 4, pp. 609–13, 2003.
- [63] K. N. Bachus, A. L. DeMarco, K. T. Judd, D. S. Horwitz, and D. S. Brodke, "Measuring contact area, force, and pressure for bioengineering applications: Using Fuji Film and TekScan systems," *Med. Eng. Phys.*, vol. 28, no. 5, pp. 483–488, 2006.
- [64] E. I. Drewniak, J. J. Crisco, D. B. Spenciner, and B. C. Fleming, "Accuracy of circular contact area measurements with thin-film pressure sensors," *J. Biomech.*, vol. 40, no. 11, pp. 2569–2572, 2007.
- [65] J. Yao, S. L. Lancianese, K. R. Hovinga, J. Lee, and A. L. Lerner, "Magnetic resonance image analysis of meniscal translation and tibio-menisco-femoral contact in deep knee flexion," *J. Orthop. Res.*, vol. 26, no. 5, pp. 673–684, 2008.
- [66] W. Mesfar and A. Shirazi-Adl, "Biomechanics of changes in

ACL and PCL material properties or prestrains in flexion under muscle force-implications in ligament reconstruction,” *Comput. Methods Biomech. Biomed. Engin.*, vol. 9, no. 4, pp. 201–209, 2006.

[67] R. Shirazi, A. Shirazi-Adl, and M. Hurtig, “Role of cartilage collagen fibrils networks in knee joint biomechanics under compression,” *J. Biomech.*, vol. 41, no. 16, pp. 3340–3348, 2008.

[68] M. E. Mononen *et al.*, “Effect of superficial collagen patterns and fibrillation of femoral articular cartilage on knee joint mechanics—A 3D finite element analysis,” *J. Biomech.*, vol. 45, no. 3, pp. 579–587, 2012.

[69] G. A. Ateshian, B. J. Ellis, and J. a Weiss, “EQUIVALENCE BETWEEN SHORT-TIME BIPHASIC AND INCOMPRESSIBLE ELASTIC MATERIAL RESPONSES,” *J. Biomech. Eng.*, vol. 129, no. 3, pp. 405–412, 2012.

[70] R. Mootanah, F. Risse, D. Carpanen, R. Walker, and H. J. Hillstrom, “The effects of the material properties of bones and soft tissues on knee joint contact stress,” in *10th international symposium on Biomechanics and Biomedical Engineering*, 2012.

[71] T. L. H. Donahue, M. L. Hull, M. M. Rashid, and C. R. Jacobs, “A finite element model of the human knee joint for the study of tibio-femoral contact,” *J. Biomech. Eng.*, vol. 124, no. 3, pp. 273–280, 2002.

[72] M. S. Venäläinen *et al.*, “Effect of bone inhomogeneity on tibiofemoral contact mechanics during physiological loading,” *J. Biomech.*, vol. 49, no. 7, pp. 1111–1120, 2016.

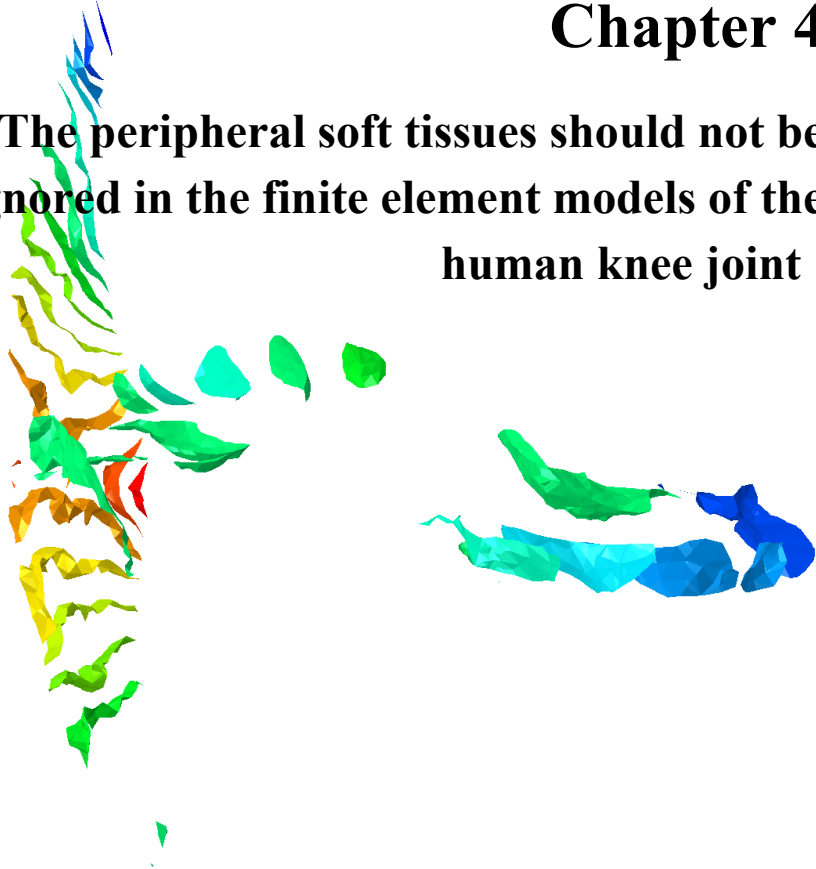
[73] L. Blankevoort, J. H. Kuiper, R. Huiskes, and H. J. Grootenboer, “Articular contact in a three-dimensional model of the knee,” *J. Biomech.*, vol. 24, no. 11, pp. 1019–1031, 1991.

[74] K. E. Moglo and a. Shirazi-Adl, “On the coupling between anterior and posterior cruciate ligaments, and knee joint response under anterior femoral drawer in flexion: A finite element study,” *Clin. Biomech.*, vol. 18, no. 8, pp. 751–759, 2003.

[75] M. A. Baldwin, P. J. Laz, J. Q. Stowe, and P. J. Rullkoetter, “Efficient probabilistic representation of tibiofemoral soft tissue constraint,” *Comput. Methods Biomech. Biomed. Engin.*, vol. 12, no. 6, pp. 651–659, 2009.

Chapter 4

The peripheral soft tissues should not be ignored in the finite element models of the human knee joint



Naghbi Beidokhti, H., Janssen, D., Van de Groes, S., Verdonchot, N., 2018. Medical and Biological Engineering and Computing. 56, 1189-1199.

1. Introduction

The finite element (FE) method is being widely utilized as a research tool to investigate knee biomechanics [1]. However, every FE model of either native or implanted knees suffers from limitations and simplifications [2]. In even the most comprehensive FE model of the knee, soft tissue structures like tendons and ligaments are being incorporated, but usually skin, peripheral soft tissues and the posterior capsule are ignored, mostly due to the lack of experimental data on their influence on the joint kinematics and laxity [3, 4] (Figure 1). On the other hand, only a few studies modeled posterior capsule in either native (i.e. Shin et al. [5]) or implanted (i.e. Baldwin et al. [6]) knee models, roughly approximating the properties based on the limited experimental data of Brantigan and Voshell [7] (Figure 1-c). The influence of these peripheral structures on the biomechanical behavior of the knee joint is largely unknown, and usually assumed to be of minor influence on the overall kinematics of the knee joint.

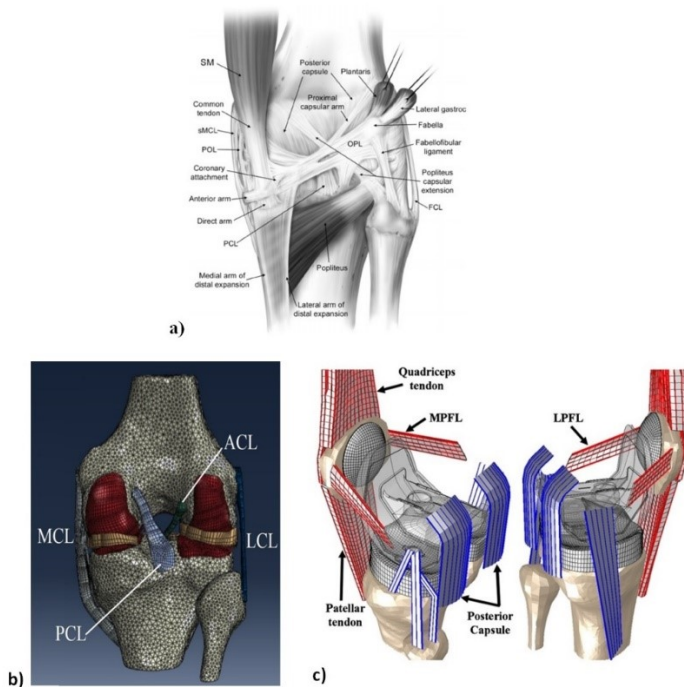


Figure 1: a posterior view of a schematic human knee joint (reproduced from [8] Elsevier license permission 3932521102554) (a); a typical FE model of a native knee joint (reused from [39], the original image was horizontally flipped and labeled) (b); and an FE model with posterior capsule inclusion (reproduced from [6] Elsevier license permission 3981261251500) (c).

Geiger et al. reviewed the posterolateral and posteromedial soft tissue structures [8]. LaPrade et al. verified the quantitative anatomy of medial structures of the knee joint including the posterior oblique ligament [9]. None of them, however, assessed the properties of their target tissues. A few studies investigated the effect of the lateral soft tissues, and more importantly of the popliteofibular ligament and popliteal tendon, on varus and external rotational laxities under limited loading conditions [10-13]. Their results indicated that the popliteofibular ligament contributes to posterolateral stability [12] and prevents excessive posterior translation and varus angulation [11], especially when the knee is flexed [13]. Sugita et al. indicated that the popliteal tendon and popliteofibular ligaments are equally important in posterolateral stability of the knee [10]. Griffith et al. measured the oblique popliteal ligament (OPL) force at different loading conditions and indicated that it takes part in the internal and valgus rotational stiffness at low flexions [14]. Rachmat et al. estimated the mechanical properties of posterior capsule based on isolated ex-situ uniaxial tensile tests [15]. Their results showed asymmetrical mechanical properties in the medial, central and lateral regions. However, the outcome based on the isolated ex-situ testing condition could only be correlated to a limited knee gesture (hyper-extension).

The influence of the peripheral structures and posterior capsule on knee joint laxity has not been completely described in the literature, but is of interest for computational modelers. The aim of this study, therefore, was to assess the significance of the peripheral soft tissues and posterior capsule on the kinematics and laxity of the human knee joint. Accordingly, a computational approach to model the target tissues in FE was sought.

2. Materials and Methods

2.1. Experimental Testing:

Three fresh-frozen cadavers with a mean age of 79 ± 21 years, with no signs of hard and soft tissues injuries and no history of surgery were selected for the current study. The specimens were received from the Anatomy Department of Radboud University Medical Center with a permission statement for experimental use. The knees were prepared following a standard protocol and positioned in a knee testing apparatus that allows for six degree of freedom

motions (Figure 2-a) [16-18]. Flexion-extension was applied to the femur, whereas the valgus-varus and internal-external rotations and anterior-posterior and medial-lateral translations were applied to the tibia.

The quadriceps muscles were subjected to constant forces provided by torsional springs representing the vastus lateralis (20 N), rectus femoris (20 N), and the grouped vastus medialis and intermedius (10 N) [16, 19, 20]. These loads were selected based on the force magnitude limitations of the knee testing apparatus, and applied in order to stabilize the patella, and as a result, were not meant to be representative of quadriceps loads during in-vivo tasks.

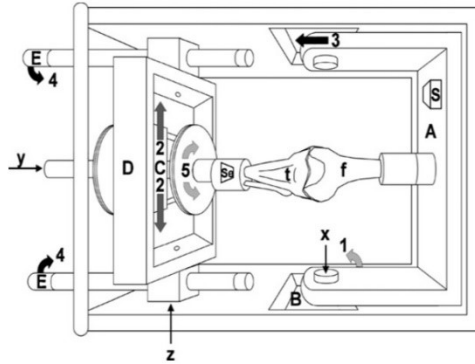
An electromagnetic tracking system (3Space Fastrak, Polhemus Incorporated, VT, USA) was used to track sensors that were rigidly attached to the femur, tibia, and patella, using base-plates screwed onto the bone. Subsequently, the knees with the base-plates in situ were CT-scanned (Toshiba Aquilion ONE, Otawara, Japan) with a slice thickness of 0.5 mm and segmented using Mimics v18.0 (Materialise, Leuven, Belgium). The segmented three-dimensional models were used to determine the relative position and orientation of sensors with respect to the joint. In-house developed scripts (MATLAB R2013a, Natick, MA) were used to calculate the knee joint centre (similar to [21]), and to convert the raw tracking data to kinematics in the knee joint coordinate system [22], as described by Grood and Suntay [23].

Six different loading conditions were applied to the intact knees (Figure 2-b) at four different flexion angles (0, 30, 60 and 90°): internal and external torque of 5.16 Nm, a varus and valgus moment of 12 Nm, and an anterior and posterior load of 100 N. These loads were based on the literature values and can provide sufficient laxity motion to characterize the knee ligamentous structures without damaging the cadaveric specimens [6, 23–25]. The loads were applied within the physiological loading range (~1 second). The measurements were performed after ~3 seconds of external loading, after which the biomechanical response of the ligamentous structures of the knee joint would not considerably be influenced by the tissue viscoelasticity [27].

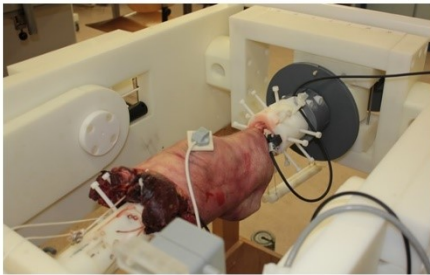
Subsequently, the knee joints were dissected by an experienced knee surgeon to remove the skin, peripheral soft tissues and posterior capsule, while preserving the salient tibiofemoral ligaments such as the anterior and posterior cruciate

ligaments, and the medial and lateral collateral ligaments (Figure 2-c). Subsequently, the loading conditions as described above were repeated to determine the effect of the dissection of the peripheral soft tissue structures. Each of the loading conditions was repeated three times to check the repeatability of the measurements, and their mean and standard deviation was calculated.

a)



b)



c)

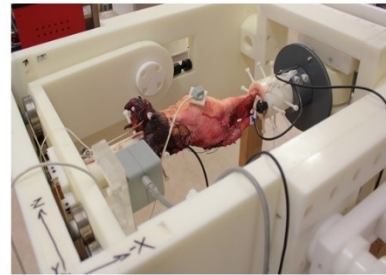


Figure 2: The six-DOF knee testing apparatus (a); a single knee joint positioned in the testing apparatus with the tracking sensors attached to bony segments: pre-dissection joint (b), and post-dissection joint (c).

2.2. Finite Element Modeling

Three validated subject-specific FE models of the three dissected knees were developed in our earlier study [28]. Five structures were added to each FE model, including oblique popliteal ligament (OPL), arcuate popliteal ligament (APL), medial capsule (M_{Cap}), lateral capsule (L_{Cap}) and anterolateral ligament (ALL) (Figure 3). The insertion sites were estimated from the segmented model and anatomy textbooks. All the structures were modeled as no-compression linear spring, and the initial stiffness was assigned from the literature [10, 11, 13, 28–30]. The stiffness of each structure was varied within the specified range to obtain

the closest laxity prediction to the experimentally measured laxity in the intact knee, under the six loading regimes described previously. The same approach was previously used by Baldwin et al. [6].

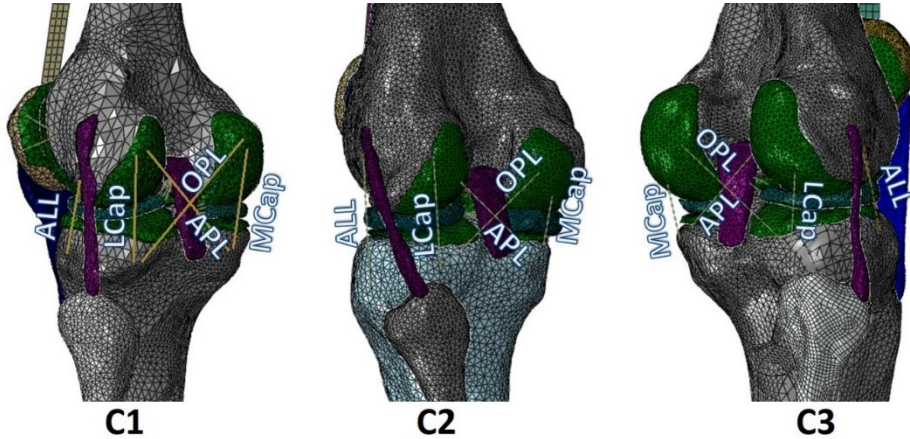


Figure 3: The validated subject-specific FE models of the three cadaveric knees (C1, C2 and C3) with five springs added to be representative for the dissected tissues as oblique popliteal ligament (OPL), arcuate popliteal ligament (APL), medial capsule (M_{Cap}), lateral capsule (L_{Cap}) and anterolateral ligament (ALL).

3. Results

In the following, the laxity outcomes of the specimens pre- and post-dissections were compared separately for anterior-posterior translational, internal-external rotational and valgus-varus rotational laxities. Despite the large inter-subject variability in some directions, the average laxity changes following dissection (\pm standard deviations) of the three specimens have been included in Table 1. Subsequently, the peripheral soft tissue stiffness values were incorporated in the FE models. Finally, the FE laxity predictions with and without these additional structures were compared with the experimental measurement.

Table 1: average laxity changes in the six loading conditions following the dissection (\pm standard deviations) for all three specimens.

		Loading Regimes					
		Internal Torque (5.16Nm)	External Torque (5.16Nm)	Varus Moment (12Nm)	Valgus Moment (12Nm)	Anterior Load (100N)	Posterior Load (100N)
		Internal Rotation (°)	External Rotation (°)	Varus Rotation (°)	Valgus Rotation (°)	Anterior Translation(mm)	Posterior Translation(mm)
Flexion Angle (°)	0	0.5 \pm 0.6	0.5 \pm 0.2	0.3 \pm 1.0	0.5 \pm 0.8	0.0 \pm 0.8	0.2 \pm 1.3
	30	1.5 \pm 0.8	0.2 \pm 0.8	0.2 \pm 1.0	0.9 \pm 1.2	0.1 \pm 0.5	0.1 \pm 1.8
	60	6.0 \pm 1.4	1.1 \pm 1.7	0.0 \pm 0.3	0.3 \pm 1.2	0.3 \pm 0.4	0.1 \pm 0.8
	90	6.3 \pm 3.5	0.9 \pm 2.1	0.1 \pm 0.6	0.3 \pm 1.7	0.2 \pm 0.6	0.4 \pm 0.8

3.1. Experimental Laxities

Anterior-posterior laxity: Figure 4 shows the anterior-posterior laxity in the three specimens, for the pre- and post-dissection cases.

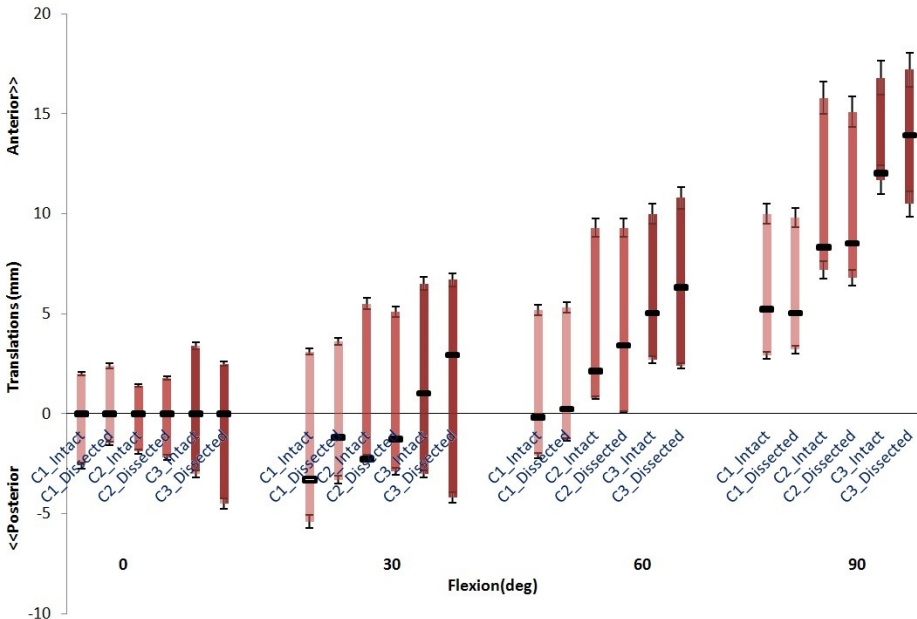


Figure 4: Anterior-posterior laxity of the three cadaveric knees at four flexion angles indicating unloaded (middle square), anteriorly loaded (upward bars) and posteriorly loaded (downward bars) cases.

All dissected knees showed a slightly larger average tibial anterior translation (1.0 to 2.1 mm at 30° and 0.4 to 1.3 mm at 60°). At 90°, the first two knees were negligibly affected by the dissection of the peripheral tissues, while the difference in the third knee was 1.9 mm. No considerable difference in anterior translation was found between the three knees.

Surprisingly, the posterior laxity of the first knee was reduced after dissection, although by less than 1.0 mm. In the second specimen, the posterior laxity increased by 1.7 and 1.0 mm at 30° and 60°, respectively. The third knee was more sensitive to peripheral soft tissues, as the posterior laxity at 0, 30, 60 and 90° increased by 1.5, 3.1, 1.6 and 3.1 mm, respectively.

Internal-external laxity: Internal-external rotations of the first and third specimens were negligibly influenced by dissection during flexion, whereas the second specimen maximally showed an external rotational perturbation of 2.9° at 90° (Figure 5).

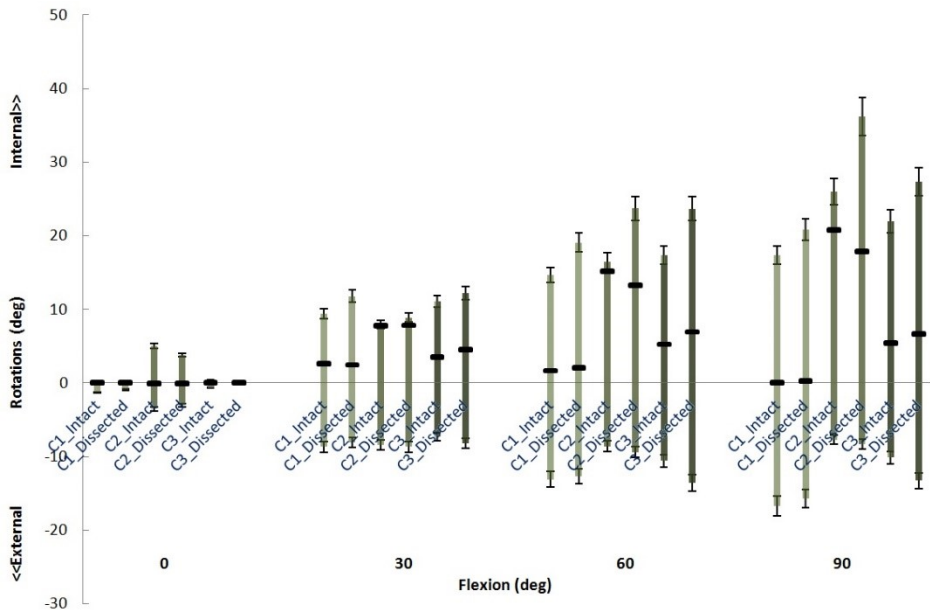


Figure 5: Internal-external rotations of three cadaveric knees at four flexion angles indicating unloaded joints (middle square), and with internal torque (upward bars) and external torque (downward bars).

Internal rotation increased by less than 1.2° after peripheral soft tissue removal for all specimens at full extension and 30° of flexion, except for the first knee (2.6° increase at 30°). At larger flexion angles, the laxity increased up to 12.9° .

Upon application of external, rotation of the first and second knees increased maximally by 1.7° after dissection, where in the third specimen it rotations increased up to 5.7° at 60° flexion and 4.4° at 90° flexion.

Valgus-varus laxity: In unloaded flexion, the first specimen showed only a slight valgus rotational increase at 90° by about 1.0° (Figure 6). The second and third knee inclined to more varus rotation at 30° and 60° of flexion, by less than 1.0° for the second knee and 2.9° (30° flexion) and 1.7° (60° flexion) for the third specimen. In 90° of flexion, only the second knee was considerably influenced by soft tissues removal (5.0° valgus).

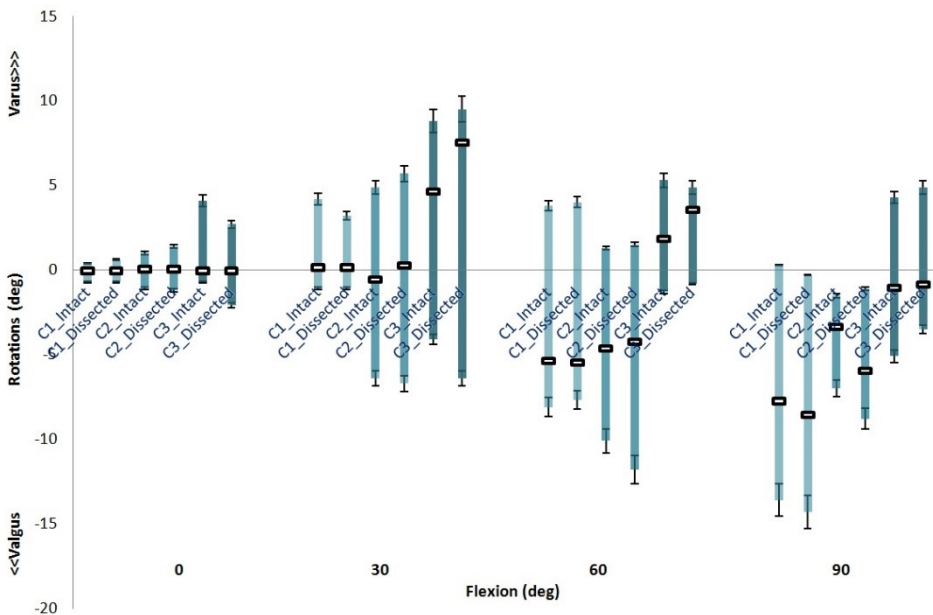


Figure 6: Varus-valgus rotations of three cadaveric knees at four flexion angles indicating unloaded joints (middle square), and with varus moment (upward bars) and valgus moment (downward bars).

Upon applying a varus moment, the maximum increase in varus rotational laxity occurred at 90° of flexion for the second specimen (3.0°), where for the first and third knees it was less than 1.0° in all flexion angles.

3.2. Finite Element Models

Table 2 shows the estimated stiffness for the modeled structures (APL, OPL, ALL, MCap and LCap), with which the closest intact knee laxity was obtained for all three knee specimens. The laxity outcomes for FE models with and without the additional structures were compared with the experimental laxity results in Figure 7 (anterior-posterior), Figure 8 (internal-external) and Figure 9 (valgus-varus).

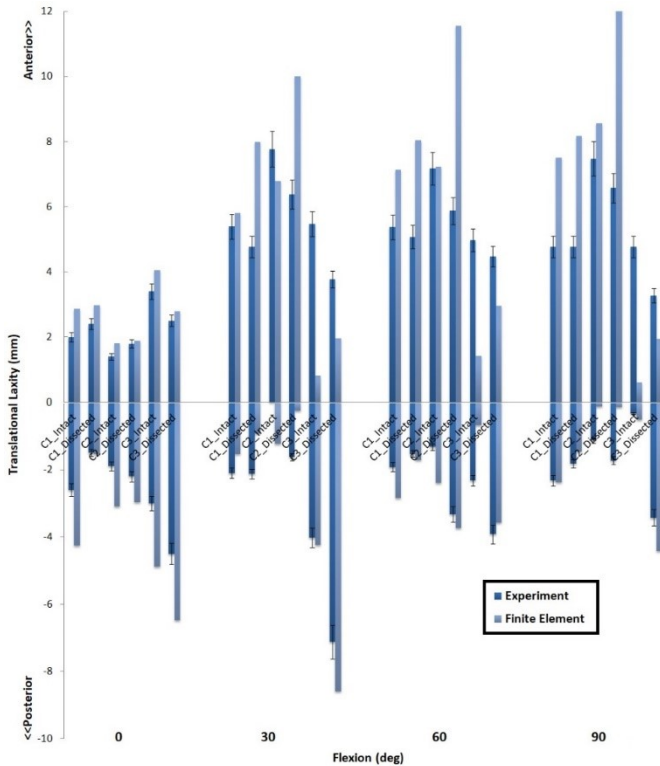


Figure 7: The anterior-posterior laxity predicted by FE models with (intact) and without (dissected) additional spring structures and measured in the experiment at different flexion angles.

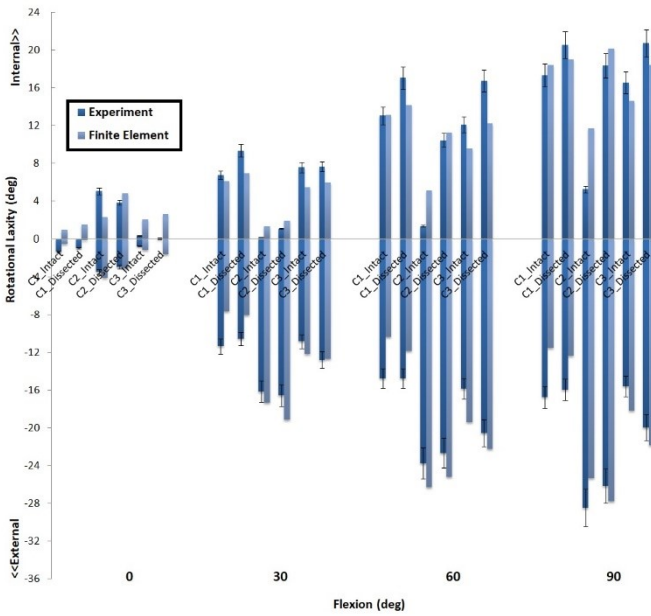


Figure 8: The internal-external rotational laxity predicted by FE models with (intact) and without (dissected) additional spring structures and measured in the experiment at different flexion angles.

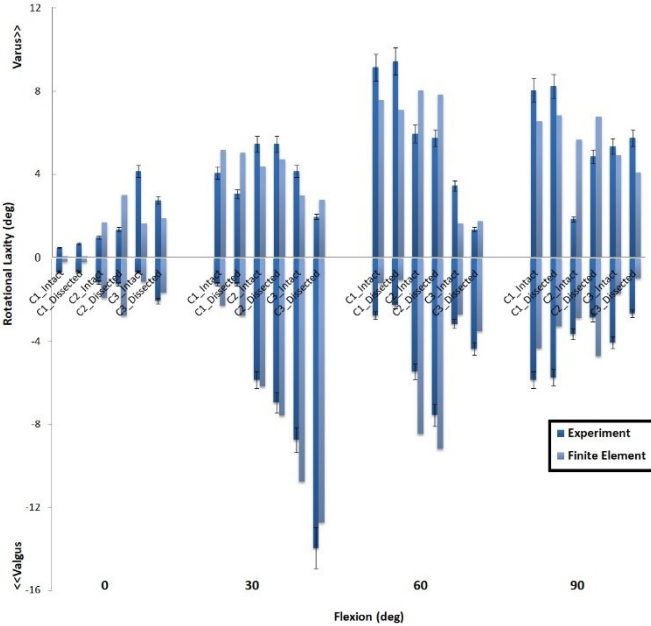


Figure 9: The valgus-varus rotational laxity predicted by FE models with (intact) and without (dissected) additional spring structures and measured in the experiment at different flexion angles.

Table2: the spring stiffness of the five modeled structures to be representative for the dissected structures, in three subject-specific FE models.

	The stiffness of the representative spring elements (N/mm)				
	APL	OPL	ALL	MCap	LCap
Initial Value \pm Range	28 \pm 14	28 \pm 14	42 \pm 26	15 \pm 10	15 \pm 10
C1	34	25	40	15	14
C2	40	30	45	19	17
C3	32	42	42	23	15

4. Discussion

In the current study the influence of the peripheral soft tissues and posterior capsule on knee joint laxity was investigated based on laxity tests in three human cadaveric specimens. Six different loading regimes were applied to each specimen pre- and post-dissection, at four different flexion angles. Based on the laxity outcomes additional structures were modelled in three validated specimen-specific FE models to achieve the pre-dissection knee laxities.

Removal of the peripheral soft tissues only had a limited effect on the anterior-posterior laxity, but it did effect the neutral (unloaded) position of the joint. At larger flexion angles, the peripheral tissue provided substantial internal rotational constraints, but it did not change the neutral rotational position in an unloaded state. In lax knees, the peripheral tissues showed a limited influence on neutral valgus-varus rotations and valgus rotational laxity.

The implication of omission of the peripheral and posterior capsular tissue in knee models can therefore vary depending on the simulated task and the loading conditions. Werner et al. showed that contact distribution and contact loads on medial and tibial compartments significantly changed with a valgus-varus variation as little as 3° in gait, based on the experiment on four cadaveric implanted knees [32]. Similar findings of Engin et al. on human native knee joint confirms the high sensitivity of knee contact biomechanics to valgus-varus rotational configurations [33].

Our results indicate a valgus-varus change beyond 3° at flexion angles of 60° and 90° with peripheral tissues and posterior capsule removal. The change in internal-external laxity by ignoring the peripheral tissues can alter not only tibiofemoral joint behavior, but also the biomechanics of patellafemoral joint. However, patellar kinematics and patellofemoral contact pressure were shown to be slightly more sensitive to internal rotation, where an internal rotational change of 5° can alter the patellofemoral joint biomechanical behavior [34]. The alteration in the posteriorly directed joint behavior by ignoring peripheral and capsular tissues can also lead to different cruciate ligament forces [5, 28]. According to Yao et al. an anterior-posterior perturbation of even 0.1 mm, which is less than what was measured in the current experiment, can lead to a considerable difference in tibiofemoral contact variables [36].

According to the study of Torzilli et al. the small difference between the intact and dissected knees at varus and external rotational and posterior translational mechanical loads could be attributed to the popliteofibular ligament [10]. They also reported a limited static mechanical resistance of the popliteal tendon in varus, more particularly at 30° , where the maximum varus difference occurred in the current study. In the study of Griffith et al., with loading conditions similar to the loads applied in the current study, a reduced internal and valgus rotational stiffness at low flexion was reported, in the knees with the OPL dissected [14].

In the subject-specific FE models of the three cadaveric knees used in this study, modeling only the main structures of the knee joint could not acceptably predict the pre-dissected knee laxity in the experiment. Adding APL, OPL, ALL, MCap and LCap as spring elements with adjusted stiffness in FE models, however, improved the replication of the pre-dissected knee behavior.

The main limitation of this study was the low number of specimens, which makes it impossible to draw general conclusions from the results, except demonstration of the inter-specimen variation in the effect of peripheral soft tissue on joint kinematics. A second limitation is the fact that the current in-vitro experiments were performed statically, while the in-vivo dynamics may be different specifically, as it has been proposed that the popliteal tendon mostly acts dynamically to stabilize the knee joint [37]. A larger tensile force could be more representative for the physiological patellar muscle force and might influence the stability of the joint. However, it previously was shown that proportional larger

quadriceps force would result in similar patellofemoral laxity patterns as the quadriceps loads applied in the current study [38]. In the FE models, the stiffness of the additional structures were manually adjusted, where following a more robust optimization routine could improve the stiffness estimation further. Nonetheless, even with the manual adjustment, the FE models revealed an improvement in the laxity prediction of pre-dissected knees.

5. Conclusions

Our findings indicated that in lax knees, ignoring the posterior capsule and peripheral soft tissues in computational models of the knee joint may lead to higher anterior translations and limited alterations in valgus rotations at 90° during unloaded flexion. Excluding these structures from the models may also result in an increase in posterior translational and valgus and internal rotational laxities when the knee is flexed. Consequently, if the simulation contains any flexion under posterior, internal and valgus loads or unloaded deep flexion, it is strongly recommended to incorporate the posterior capsule and peripheral tissues representations, as for instance incorporated in this study.

Acknowledgments

This study was a part of BioMechTools project (ERC-2012-ADG LS7), received funding from the European Research Council under the European Union's Seventh Framework Program (FP/2007-2013) / ERC Grant Agreement n. 323091.

References

- [1] M. Taylor and P. J. Prendergast, “Four decades of finite element analysis of orthopaedic devices: Where are we now and what are the opportunities?,” *J. Biomech.*, vol. 48, no. 5, pp. 767–778, 2015.
- [2] M. Kazemi, Y. Dabiri, and L. P. Li, “Recent advances in computational mechanics of the human knee joint,” *Comput. Math. Methods Med.*, vol. 2013, 2013.
- [3] K. E. Moglo and a. Shirazi-Adl, “On the coupling between anterior and posterior cruciate ligaments, and knee joint response under anterior femoral drawer in flexion: A finite element study,” *Clin. Biomech.*, vol. 18, no. 8, pp. 751–759, 2003.
- [4] H. Moeinzadehj and A. Erkan, “Response of a Two-Dimensional Dynamic Model of the Human Knee To the Externally,” vol. 5, pp. 281–291, 1983.
- [5] C. S. Shin, A. M. Chaudhari, and T. P. Andriacchi, “The effect of isolated valgus moments on ACL strain during single-leg landing: A simulation study,” *J. Biomech.*, vol. 42, no. 3, pp. 280–285, 2009.
- [6] M. a. Baldwin, C. W. Clary, C. K. Fitzpatrick, J. S. Deacy, L. P. Maletsky, and P. J. Rullkoetter, “Dynamic finite element knee simulation for evaluation of knee replacement mechanics,” *J. Biomech.*, vol. 45, no. 3, pp. 474–483, 2012.
- [7] O. C. Brantigan and A. F. Voshell, “The mechanics of the ligaments and menisci of the knee joint,” *J. bone Jt. Surg.*, vol. 23, pp. 44–66, 1941.
- [8] D. Geiger, E. Y. Chang, M. N. Pathria, and C. B. Chung, “Posterolateral and Posteromedial Corner Injuries of the Knee,” *Magn. Reson. Imaging Clin. N. Am.*, vol. 22, no. 4, pp. 581–599, 2014.
- [9] R. F. LaPrade, “The Anatomy of the Medial Part of the Knee,” *J. Bone Jt. Surg.*, vol. 89, no. 9, p. 2000, 2007.

- [10] P. a Torzilli, M. J. Maynard, and R. F. Warren, “The Role of the Popliteofibular Stability of the Human Knee Ligament in Study *,” *Am J Sport. Med.*, vol. 24, no. 1, pp. 19–27, 1995.
- [11] S. a Shahane, C. Ibbotson, R. Strachan, and D. R. Bickerstaff, “The popliteofibular ligament,” *J. Bone Jt. Surg.*, vol. 81, no. 4, pp. 636–642, 1999.
- [12] J. Michael, X. Deng, T. L. Wickiewicz, and R. F. Warren, “Winner of the 1994 Q ’ Donoghue Award The Popliteofibular Ligament Stability *,” pp. 311–316, 1994.
- [13] T. Sugita and a a Amis, “Anatomic and biomechanical study of the lateral collateral and popliteofibular ligaments.,” *Am. J. Sports Med.*, vol. 29, no. 4, pp. 466–472, 2001.
- [14] C. J. Griffith, C. A. Wijdicks, R. F. Laprade, B. M. Armitage, S. Johansen, and L. Engebretsen, “The American Journal of Sports Medicine Force Measurements on the Posterior Oblique Ligament and Superficial Medial Collateral Ligament Proximal and Distal,” *Am. J. Sports Med.*, vol. 37, no. 1, pp. 140–148, 2010.
- [15] H. H. Rachmat, D. Janssen, G. J. Verkerke, R. L. Diercks, and N. Verdonschot, “Material properties of the human posterior knee capsule,” *Biomed. Mater. Eng.*, vol. 25, no. 2, pp. 177–187, 2015.
- [16] A. Rood, G. Hannink, A. Lenting, K. Groenen, S. Koeter, N. Verdonschot, and A. van Kampen, “Patellofemoral Pressure Changes After Static and Dynamic Medial Patellofemoral Ligament Reconstructions,” *Am. J. Sports Med.*, vol. 43, no. 10, pp. 2538–2544, 2015.
- [17] H. H. Rachmat, D. Janssen, G. J. Verkerke, R. L. Diercks, and N. Verdonschot, “In-situ mechanical behavior and slackness of the anterior cruciate ligament at multiple knee flexion angles,” *Med. Eng. Phys.*, vol. 38, no. 3, pp. 209–215, 2016.
- [18] J. W. H. Luites, A. B. Wymenga, L. Blankevoort, J. M. G. Kooloos, and N. Verdonschot, “Computer-assisted anatomically placed

double-bundle ACL reconstruction: An in-vitro experiment with different tension angles for the AM and the PL graft,” *Med. Eng. Phys.*, vol. 34, no. 8, pp. 1031–1036, 2012.

[19] F. Farahmand, W. Senavongse, and A. A. Amis, “Quantitative study of the quadriceps muscles and trochlear groove geometry related to instability of the patellofemoral joint,” *J. Orthop. Res.*, vol. 16, no. 1, pp. 136–143, 1998.

[20] F. Farahmand, M. N. Tahmasbi, and A. Amis, “The contribution of the medial retinaculum and quadriceps muscles to patellar lateral stability - An in-vitro study,” *Knee*, vol. 11, no. 2, pp. 89–94, 2004.

[21] D. L. Miranda, M. J. Rainbow, E. L. Leventhal, J. J. Crisco, and B. C. Fleming, “Automatic determination of anatomical coordinate systems for three- dimensional bone models of the isolated human knee,” *J. Biomchanics*, vol. 43, no. 8, pp. 1623–1626, 2010.

[22] W. J. Zevenbergen, “Improved Anatomical Coordinate System of the Distal Femur Based on 3D Bone Geometry & Evaluation of the Inter- and Intra- Observer Variability of the Knee Ligament Attachment Sites,” University of Twente, 2012.

[23] W. J. Grood, E.S.; Suntay, “A joint coordinate system for the clinical description of three-dimensional motions applications to the knee,” *J. Biomech. Eng.*, vol. 105, no. 2, pp. 136–144, 1983.

[24] D. L. Gollehon, P. A. Torzilli, and R. F. Warren, “The role of the posterolateral and cruciate ligaments in the stability of the human knee. A biomechanical study.,” *J. Bone Joint Surg. Am.*, vol. 69, no. 2, pp. 233–42, 1987.

[25] W. P. Seering, R. L. Piziali, D. A. Nagel, and D. J. Schurman, “The function of the primary ligaments of the knee in varus-valgus and axial rotation,” *J. Biomech.*, vol. 13, no. 9, pp. 785–794, 1980.

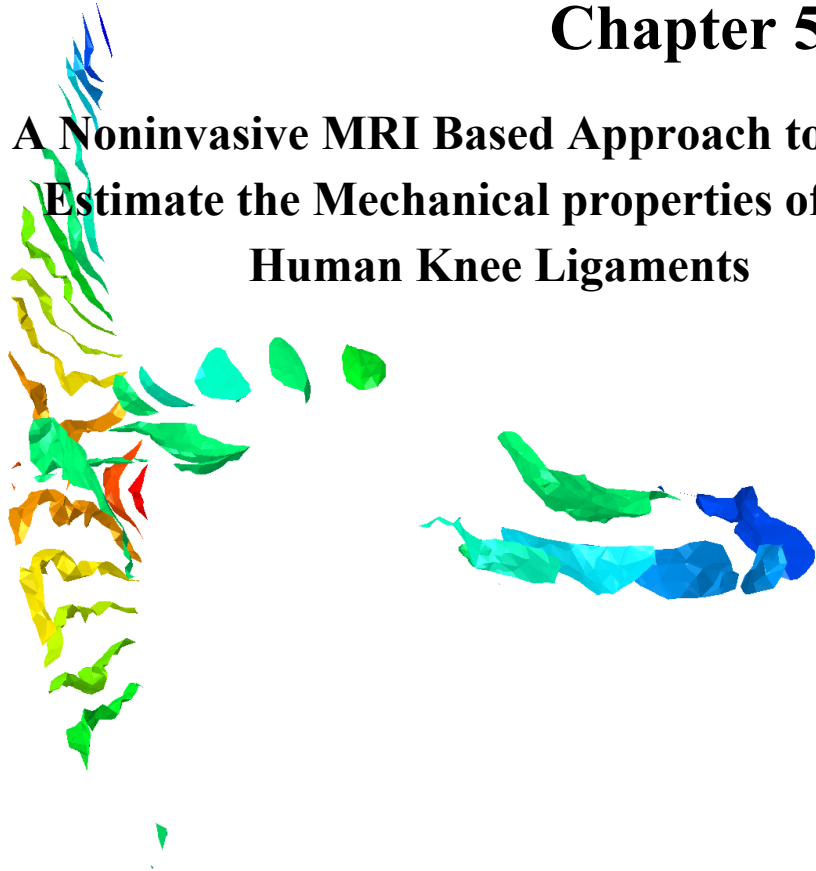
[26] Keith L. Markolf, J. S. Mensch, and Harlan C. Amstutz, “Stiffness and laxity of the knee - the contributions of the supporting structures,” *J. bone Jt. Surg.*, vol. 58, no. 5, 1976.

- [27] J. A. W. van Dommelen, M. Minary Jollandan, B. J. Ivarsson, S. A. Millington, M. Raut, J. R. Kerrigan, J. R. Crandall, and D. R. Diduch, “Nonlinear Viscoelastic Behavior of Human Knee Ligaments Subjected to Complex Loading Histories,” *Ann. Biomed. Eng.*, vol. 34, no. 6, pp. 1008–1018, 2006.
- [28] H. Naghibi Beidokhti, D. Janssen, S. Van De Groes, J. Hazrati, T. Van Den Boogaard, and N. Verdonschot, “The Influence of ligament Modelling Strategies on the Predictive Capability of Finite Element Models of the Human Knee Joint,” *J. Biomech.*, 2017.
- [29] Laprade, A. Tso, and F. Wentorf, “Force Measurements on the Fibular Collateral Ligament, Popliteofibular Ligament, and popliteus Tendon to Applied Loads,” *Am. J. Sports Med.*, vol. 32, no. 7, pp. 1695–1701, 2004.
- [30] R. F. Laprade, P. Morgan, F. Wentorf, S. Johansen, and L. Engebretsen, “The Anatomy of the Posterior Aspect of the Knee: An Anatomic Study,” *J. Bone Jt. Surg.*, vol. 89, no. 4, pp. 758–764, 2007.
- [31] H. Ishigooka, T. Sugihara, K. Shimizu, H. Aoki, and H. Kazuaki, “Anatomical study of the popliteofibular ligament and surrounding structures,” *J. Orthop. Sci.*, vol. 9, no. 1, pp. 51–58, 2004.
- [32] F. W. Werner, D. C. Ayers, L. P. Maletsky, and P. J. Rullkoetter, “The effect of valgus/varus malalignment on load distribution in total knee replacements,” *J. Biomech.*, vol. 38, no. 2, pp. 349–355, 2005.
- [33] A. E. Engin and M. S. Korde, “Biomechanics of normal and abnormal knee joint,” *J. Biomech.*, vol. 7, no. 4, 1974.
- [34] J. H. Heegaard, P. F. Leyvraz, and C. B. Hovey, “A computer model to simulate patellar biomechanics following total knee replacement: The effects of femoral component alignment,” *Clin. Biomech.*, vol. 16, no. 5, pp. 415–423, 2001.
- [35] H. Marouane, A. Shirazi-Adl, and J. Hashemi, “Quantification of the role of tibial posterior slope in knee joint mechanics and ACL force in simulated gait,” *J. Biomech.*, vol. 48, no. 10, pp. 1899–1905, 2015.

- [36] J. Yao, A. D. Salo, J. Lee, and A. L. Lerner, “Sensitivity of tibio-menisco-femoral joint contact behavior to variations in knee kinematics,” *J. Biomech.*, vol. 41, no. 2, pp. 390–398, 2008.
- [37] A. R. Guha, K. A. Gorgees, and D. I. Walker, “Popliteus tendon rupture: a case report and review of the literature,” *Br J Sport. Med*, vol. 37, pp. 358–360, 2003.
- [38] F. Farahmand, M. N. Tahmasbi, and A. A. Amis, “Lateral force-displacement behaviour of the human patella and its variation with knee flexion - A biomechanical study in-vitro,” *J. Biomech.*, vol. 31, no. 12, pp. 1147–1152, 1998.
- [39] R. Mootanah, C. W. Imhauser, F. Reisse, D. Carpanen, R. W. Walker, M. F. Koff, M. W. Lenhoff, R. Rozbruch, a T. Fragomen, Y. M. Kirane, S. R. Rozbruch, Z. Dewan, K. Cheah, J. K. Dowell, and H. J. Hillstrom, “Development and Verification of a Computational Model of the Knee Joint for the Evaluation of Surgical Treatments for Osteoarthritis,” *Computer methods in biomechanics and biomedical engineering*, vol. 17, no. 13. Taylor & Francis, pp. 1502–17, 2014.

Chapter 5

A Noninvasive MRI Based Approach to Estimate the Mechanical properties of Human Knee Ligaments



Naghibi Beidokhti, H., Mazzoli, V., Gijsbertse, k., Hannink, G., Sprengers, A., Janssen, D., Van den Boogaard, T., Verdonschot, N., 2018. Journal of the Mechanical Behavior of Biomedical Materials. Under review.

1. Introduction

For computational modeling of the knee joint, assigning realistic material properties is crucial. Among the knee tissues, the properties of the ligamentous structures are of special importance, as they have a distinct effect on the joint laxity [1], [2]. As shown previously, using the literature values for ligament stiffness can lead to inaccurate outcomes due to the wide range in reported properties [1]. By assigning personalized mechanical properties for knee ligaments in computational models, errors in model predictions caused by large inter-subject variability can be avoided [1].

In computational models with subject-specific ligament properties, usually invasive tests are required on cadaveric specimens, making the test unsuitable for in-vivo application [3]. Only few subject-specific studies have managed to introduce non-invasive experiments for the characterization of knee ligaments for FE modeling (i.e. [1], [4]).

We previously proposed a laxity-based workflow to estimate the mechanical properties of the main tibiofemoral ligaments, namely anterior and posterior cruciate ligaments (ACL and PCL) and medial and lateral collateral ligaments (MCL and LCL), in intact cadaveric knee joints, which would allow for in-vivo applications [1]. With a similar approach, Baldwin et al. (2009) also characterized the collateral ligaments properties in a cadaveric TKA implanted knee joint [4]. However, the time required for completion of the complicated workflow in these studies remains an obstacle for in-vivo (i.e. clinical) implementation.

In contrast with the invasive instruments used for the in-vivo characterization of ligament properties as reviewed by Fleming et al. (2004) [5], imaging techniques can be exploited to obtain information on ligament mechanical properties non-invasively. Previously, Magnetic Resonance Imaging (MRI) has been used to qualitatively assess knee ligaments. Only few studies tried to quantitatively use MR imaging techniques to find a correlation with the mechanical properties of the anterior cruciate ligament (ACL) [6]–[8]. Biercevicz et al. [8] showed that the volume and signal intensity from high-resolution T_2^* -weighted MRI scans are predictive of structural properties of ACL grafts in a porcine model. However, the signal intensity of a single gradient echo sequence, like the one used in their study, is more dependent to image acquisition parameters than to actual ligaments properties. In order to generalize this approach, in a follow-up study the

relaxation time T_2^* was used instead of signal intensity in 15 Yucatan pigs [6]. Their later study, however, failed to find a significant prediction of human biomechanical parameters using similar MR variables (T_2^*) based on 15 cadaveric samples [9]. The echo time used in the previous studies could lead to an overestimation of the T_2^* relaxation time; for instance [6] used only two echo times. Moreover, only the T_2^* parameter was measured in the previous studies, whereas T_2^* can directly be influenced by an MR artifact known as the *magic angle* effect, which can lead to defective maximum values in T_2^* [10], [11]. Including other parameters ($T_{1\rho}$ and T_2) may provide complementary information; particularly $T_{1\rho}$, which is believed to be affected less by the magic angle effect [12], [13]

In this study the aim was to assess if there is a correlation between quantitative MRI parameters (T_2^* , $T_{1\rho}$, and T_2) and structural properties, with the mechanical properties of tibiofemoral ligaments (ACL, PCL, MCL and LCL). The outcomes of this study may reveal the potential of utilizing MRI parameters, combined with structural properties, for determining subject-specific mechanical properties of ligaments.

2. Materials and Methods

Six fresh-frozen human cadavers with a mean age of 78 ± 11 years and with no obvious signs of injuries in the lower extremity were selected. The specimens were received from the Anatomy Department of Radboud University Medical Center with a permission statement for experimental use. From each cadaver one leg was prepared for the purposes of this study as schematically illustrated in Figure 1. Prior to MR scanning, the legs were cut approximately 15 cm above the knee joint space. The proximal end of rectus femoris muscle was separated and pulled by ~ 20 N in full extension using a rope through a block rigidly fixated to the femoral shaft. The force was applied to stabilize the patella in passive full extension and flexion [14].

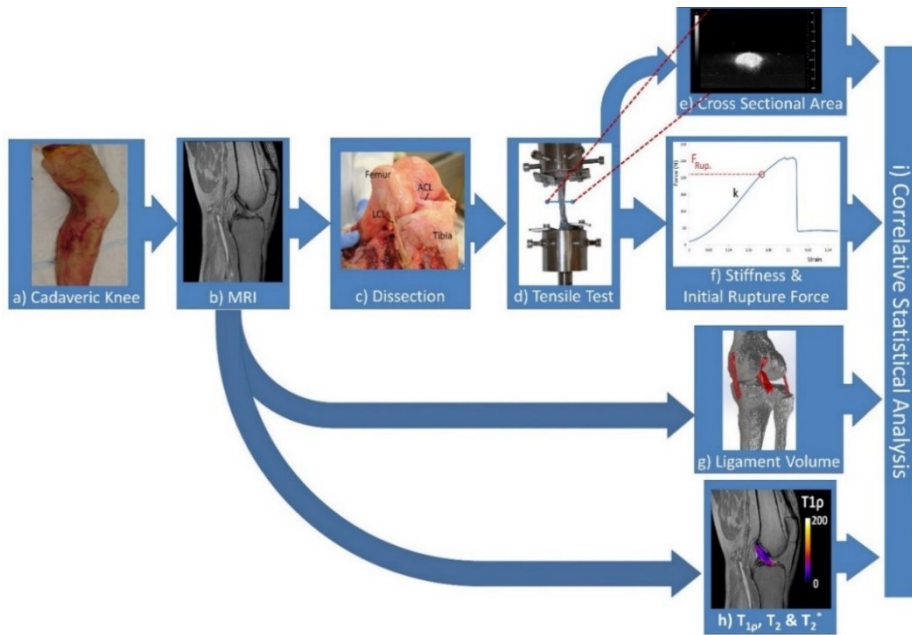


Fig1. Schematic illustration of the study: the cadaveric knee (a) was MRI scanned (b), based on which the ligaments were segmented to estimate their volume (g) and $T_{1\rho}$, T_2 & T_2^* were calculated (h). After knee dissection (c), the specimens were prepared for tensile test (d) where the cross-sectional area was measured by ultrasound (e) and initial rupture force and stiffness of each specimen were extract (f). The cross-sectional area, ligament volume and quantitative MR parameters were analyzed to find the best correlation with the mechanical properties (i).

2.1. MR Imaging

The legs were placed in a 3T Philips Ingenia MRI scanner (Philips Health-care, Best, The Netherlands) in full extension. As the MRI signal intensity of ligaments can be influenced by tension in the ligaments [15] and the magic angle effect [13], in addition to full extension, the knees were also scanned at 30° flexion, to prevent slackness of the PCL [16]. The images in full extension were used to study the ACL, MCL and LCL, and the images in flexed position were used for analysis of the PCL. At each position the following sequences were acquired:

- proton density-weighted (3D Turbo Spin Echo, voxel size = $0.31 \times 0.31 \times 0.52 \text{ mm}^3$, matrix size = $720 \times 720 \times 250$, TR = 1000 ms, TE = 41 ms, NSA = 2, acquisition time = 6 min 40 s);
- proton density-weighted with fat suppression (3D Turbo Spin Echo, SPAIR fat suppression, voxel size = $0.31 \times 0.31 \times 0.63 \text{ mm}^3$, matrix size = $720 \times 720 \times 206$, TR = 1300 ms, TE = 153 ms, NSA = 2, acquisition time = 12 min 35 s);

- $T_{1\rho}$ map (B_0 and B_1 compensated spin lock prepulse, 3D gradient echo readout, voxel size = $0.6 \times 0.6 \times 2 \text{ mm}^3$, matrix size = $320 \times 320 \times 131$, TR = 3.6 ms, TE = 2 ms, flip angle = 15° , spin lock time = 1, 5, 10, 20, 30, 40 ms, spin lock frequency = 500 Hz);
- T_2^* (3D gradient echo, voxel size = $0.6 \times 0.6 \times 1 \text{ mm}^3$, matrix size = $320 \times 320 \times 131$, TR = 104 ms, TE = 4.1, 8.1, 12.1, 16.1, 20.1, 24.1, 28.1, 32.1, 36.1, 40.1, 44.1, 48.1, 52.1, 56.1, 60.1, 64.1 ms, flip angle = 15°);
- T_2 (multislice multiecho spin echo, voxel size = $0.7 \times 0.7 \times 1 \text{ mm}^3$, matrix size = $320 \times 320 \times 131$, TR = 7000 ms, TE = 12.1, 18.2, 24.2, 30.3, 36.3, 42.4, 48.4, 54.5, 60.5, 66.6, 72.6, 78.7, 84.8 ms).

2.2. Image processing

The ligament geometries were segmented from either the proton density or proton density SPAIR sequences using Mimics v18.0 (Materialise, Leuven, Belgium). The ACL, MCL and LCL were segmented in full extension, and the PCL was segmented in the flexed knee. Based on the segmentation the volume of each ligament was measured in Mimics. Prior to data fitting of the MR data, the T_2 and T_2^* weighted scans were reformatted to the resolution of the $T_{1\rho}$ scan. $T_{1\rho}$, T_2 and T_2^* maps were calculated on a pixel-by-pixel fashion for the ACL, MCL and LCL in full extension, and the PCL in the flexed knee, using in-house developed Mathematica scripts (v11.0, WolframResearch, Champaign, IL). The values were averaged for the whole ligament using ImageJ 1.44 (NIH, Bethesda, MD, www.nih.gov).

2.3. Mechanical Tensile Tests

After completion of the MRI scans, the knees were dissected by an orthopedic surgeon to excise the ACL, PCL, MCL, and LCL, preserving the proximal and distal bone blocks (hence, 24 specimens in total). The Bone-ligament-bone specimens were then prepared following a standard protocol, for positioning of the specimens in a mechanical testing machine, while observing the anatomical orientation of the ligament in the joint [17]. The set-up allowed for further self-alignment during the tensile test in the remaining five degrees of freedom.

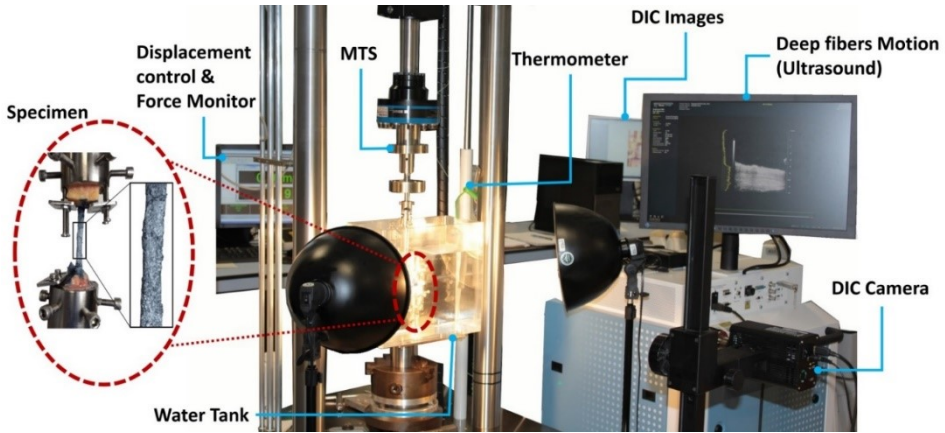


Figure 2: The experimental testing set-up for in-vitro ligament tensile test.

Digital image correlation (DIC) was applied in order to track the superficial strain of the ligament during the mechanical tensile test, while the in-depth strain of the ligament was captured using ultrasound. In order to create a high contrasted surface for DIC, each ligament was stained with a methylene blue (Methylthioninium chloride) solution to obtain a dark background, after which an oil-based paint was sprayed on the specimen surface to create a white speckle pattern [18], [19]. The set-up was positioned in a tank filled with warm water ($\sim 35^{\circ}\text{C}$), which kept the ligaments at a physiological temperature, and simultaneously acted as conducting substance for the ultrasound measurements (Figure 2).

Prior to the tensile test, the specimens were preloaded at 10 N to measure the ligament reference length. To minimize the hysteresis behavior of the ligaments without damaging the specimen, cyclic displacements of 5% (for ACL and PCL) and 4% (for MCL and LCL) were repeated 30 times [19]. Subsequent to ligament preconditioning, the ligament cross-sectional area (CSA) was measured using a high-frequency ultrasound along the length of the ligament, as defined by the two insertion sites. The cross-sectional area of the collateral ligaments (MCL and LCL) were measured at five equidistant locations, whereas, due to the short length of the cruciate ligaments, the cross-sectional area was measured at three locations along the length of the ACL and PCL.

Eventually, a displacement-controlled tensile test with a strain rate of 0.1 s^{-1} was performed until total rupture occurred in the ligament. The strain rate was selected

to be representative for an intermediate physiological loading condition [20]. Force-strain curves for each ligament were extracted as shown for a single specimen in Figure 3. The stiffness (k) was calculated for each ligament based on the model described by Blankevoort and Huiskes [21] for non-linear mechanical properties as follows:

$$f(\varepsilon) = 0 \quad \text{when } \varepsilon < 0$$

$$f(\varepsilon) = k \frac{1}{4} \varepsilon^2 / \varepsilon_l \quad \text{when } 0 \leq \varepsilon \leq 2\varepsilon_l \quad (1)$$

$$f(\varepsilon) = k(\varepsilon - \varepsilon_l) \quad \text{when } \varepsilon > 2\varepsilon_l$$

Where f is the tensile force in a line element, k is the ligament stiffness, ε is the strain in the ligament and ε_l is a strain constant.

Initial rupture force for each specimen was also extracted from the force-strain curve as for instance indicated in Figure 3 in a representative specimen. The region of the specimen where the rupture occurred was also defined from DIC and checked using ultrasound data. Among the multiple cross-sectional areas measured by ultrasound at each ligament, the lowest value was selected as the specimen cross-sectional area.

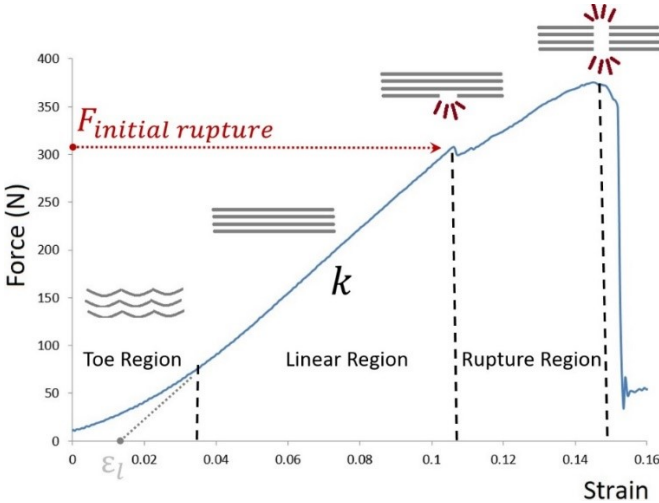


Figure 3: A representative Force-Strain curve for a single specimen (LCL) with different regions, stiffness and initial rupture force defined.

2.4. Statistical analysis

Descriptive statistics were used to summarize the data. Continuous variables were presented as mean values with their standard deviation/range.

Linear mixed models for repeated measures were used to examine the association of MRI parameters and measurements with structural properties (k , rupture force). MRI parameters ($T_{1\rho}$, T_2 , T_2^*) and measurements (cross-sectional area, volume), with and without ligament type incorporation, were included as fixed effects. Cadaver ID was included as a random effect. Conditional (fixed effects only) and marginal (fixed plus random effects) coefficients of determination (R^2) were calculated to provide information on the goodness of fit of the models/as a measure of model accuracy.

Statistical analyses were performed using R version 3.4.2 (R Foundation for Statistical Computing, Vienna, Austria) with package "nlme" and "MuMIn". P-values < 0.05 were considered statistically significant.

3. Results:

The DIC measurements and ultrasound data showed that most of the ligaments were ruptured at their insertion sites. The MR parameters ($T_{1\rho}$, T_2 and T_2^*) were calculated with a good fitting ($R^2 \geq 0.99$) as illustrated for a single representative specimen in Figure 4.

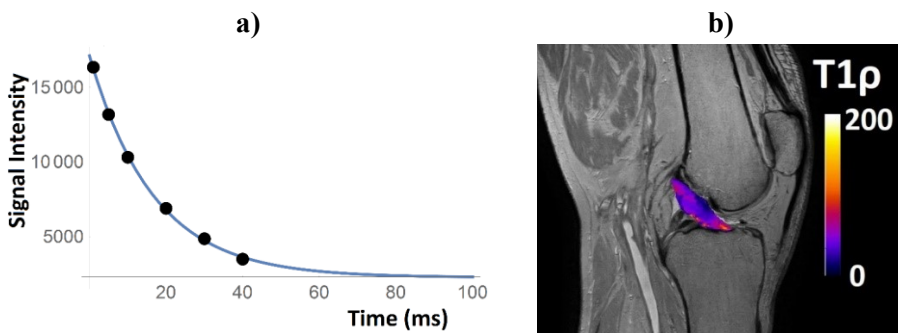


Figure 4: The curve fitting for calculating $T_{1\rho}$ in a sample region (a), and $T_{1\rho}$ mapped ACL in a single cadaveric knee (b).

Without putting the ligament type in perspective, both ligament stiffness (k ; $R^2 \approx 0.48$) and rupture force (F_{rup} ; $R^2 = 0.50$) showed similar correlations with T_{1p} , T_2 , and T_2^* combined with the ligament volume. The predictive functions for ligament stiffness and rupture force are presented in Table 1. The predicted ligament stiffness and rupture force using volume and T_{1p} , T_2 , and T_2^* were compared with the actual values in Figure 5.

In the second predictive model, based on the distribution of measured stiffness and rupture force for different ligaments (Figure 6), the correlation function was recalculated as shown in Table 2. With the ligament type incorporated in the predictive function, somewhat stronger correlations were found between the mechanical properties (stiffness and rupture force) and MR parameters (T_{1p} , T_2 and T_2^*) combined with the volume (Figure 7).

The results of the statistical analysis showed that if cross-sectional area was used instead of volume, the linear correlation between the mechanical properties and MR parameters was weakened, either with or without ligament type inclusion.

Table 1: The predictive equations for knee ligament stiffness and rupture force as functions of ligament volume and MR parameters (T_{1p} , T_2 and T_2^*).

T_i	$k = C_1 \times T_i + C_2 \times Vol + C_3$					$F_{Rup.} = C_5 \times T_i + C_6 \times Vol + C_7$			
	C_1	C_2	C_3	R^2		C_5	C_6	C_7	R^2
T_{1p}	12.3	1.3830	-199.0	0.48		0.8	0.2069	-160.7	0.53
T_2	38.0	1.4072	-702.8	0.49		3.8	0.2082	-221.5	0.53
T_2^*	14.3	1.3899	-118.5	0.47		2.1	0.2051	-171.4	0.53

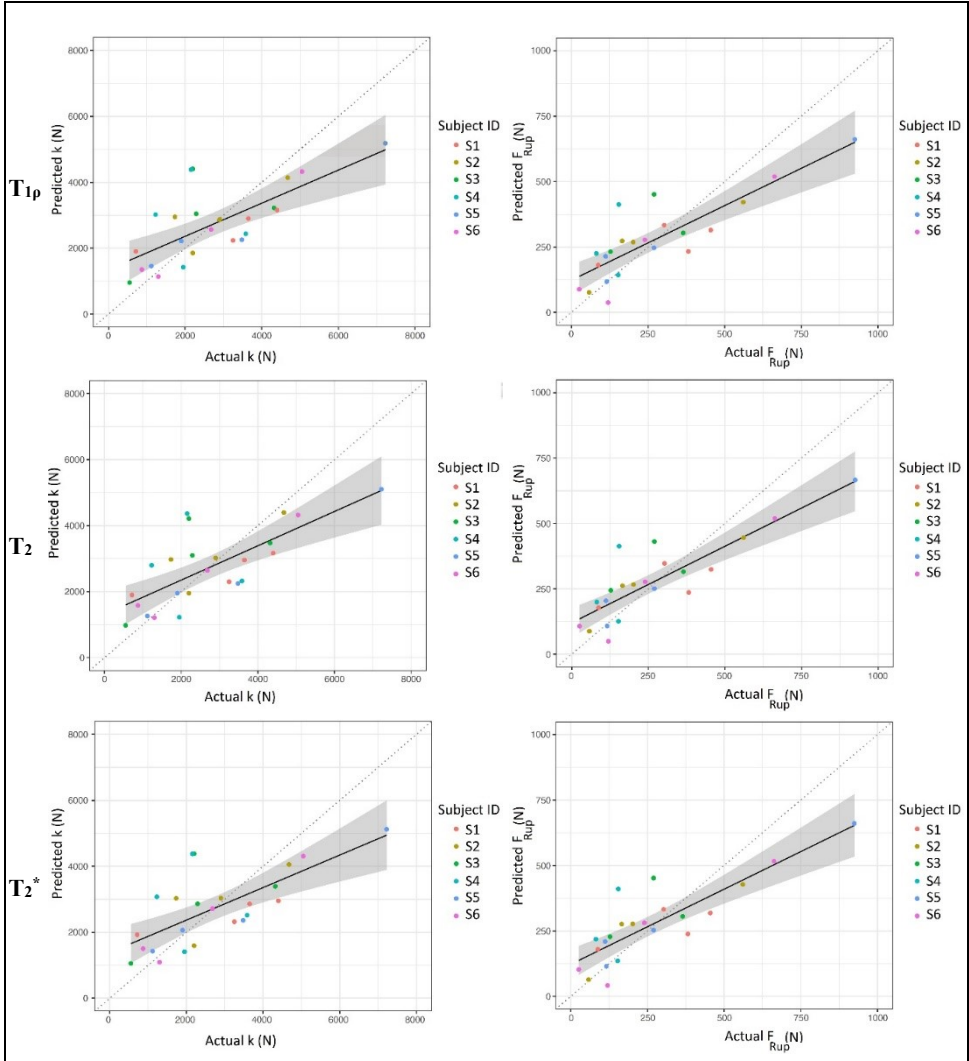


Figure 5: Actual versus predicted ligament stiffness (left column) and specimen rupture force (right column) determined using the predictive model based on the linear combination of ligament volume and T_{1p} , (first row) T_2 (second row) and T_2^* (third row).

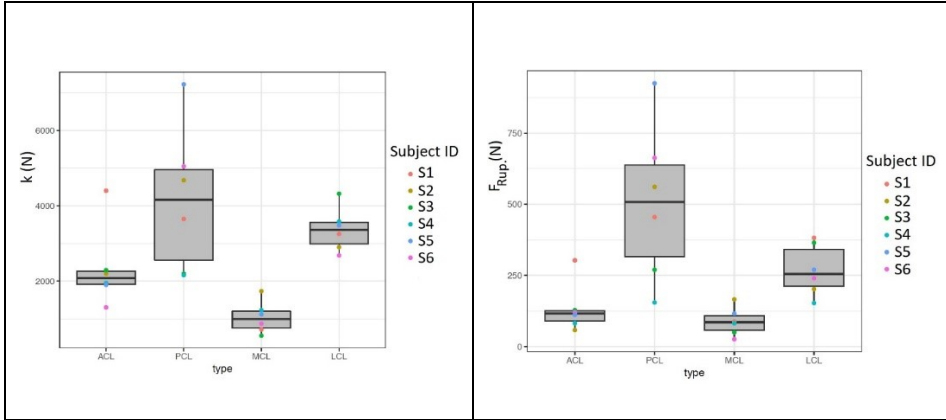


Figure 6: The distribution of stiffness and rupture force for different specimen type.

Table 2: The predictive equations for knee ligament stiffness and rupture force as functions of ligament volume, MR parameters (T_{1p} , T_2 and T_2^*) and specimen type.

T_i	Type	$k = C_1 \times T_i + C_2 \times Vol + C_3 + C_4(Type)$					$F_{Rup} = C_5 \times T_i + C_6 \times Vol + C_7 + C_8(Type)$				
		C_1	C_2	C_3	$C_4(Type)$	R^2	C_5	C_6	C_7	$C_8(Type)$	R^2
T_{1p}	ACL	22.5	1.0158	61.5	0 (Ref.)	0.60	-0.1	0.1183	-17.5	0 (Ref.)	0.57
	PCL				376.2					185.3	
	MCL				-829.4					-57.4	
	LCL				1099.4					60.3	
T_2	ACL	23.1	1.1175	290.0	0 (Ref.)	0.60	1.6	0.1194	-63.3	0 (Ref.)	0.57
	PCL				118.4					187.6	
	MCL				-1210.7					-42.5	
	LCL				527.9					74.9	
T_2^*	ACL	-10.4	1.0947	1093.8	0 (Ref.)	0.60	-2.8	0.1215	27.1	0 (Ref.)	0.57
	PCL				119.7					184.1	
	MCL				-1453.7					-73.3	
	LCL				295.6					41.3	

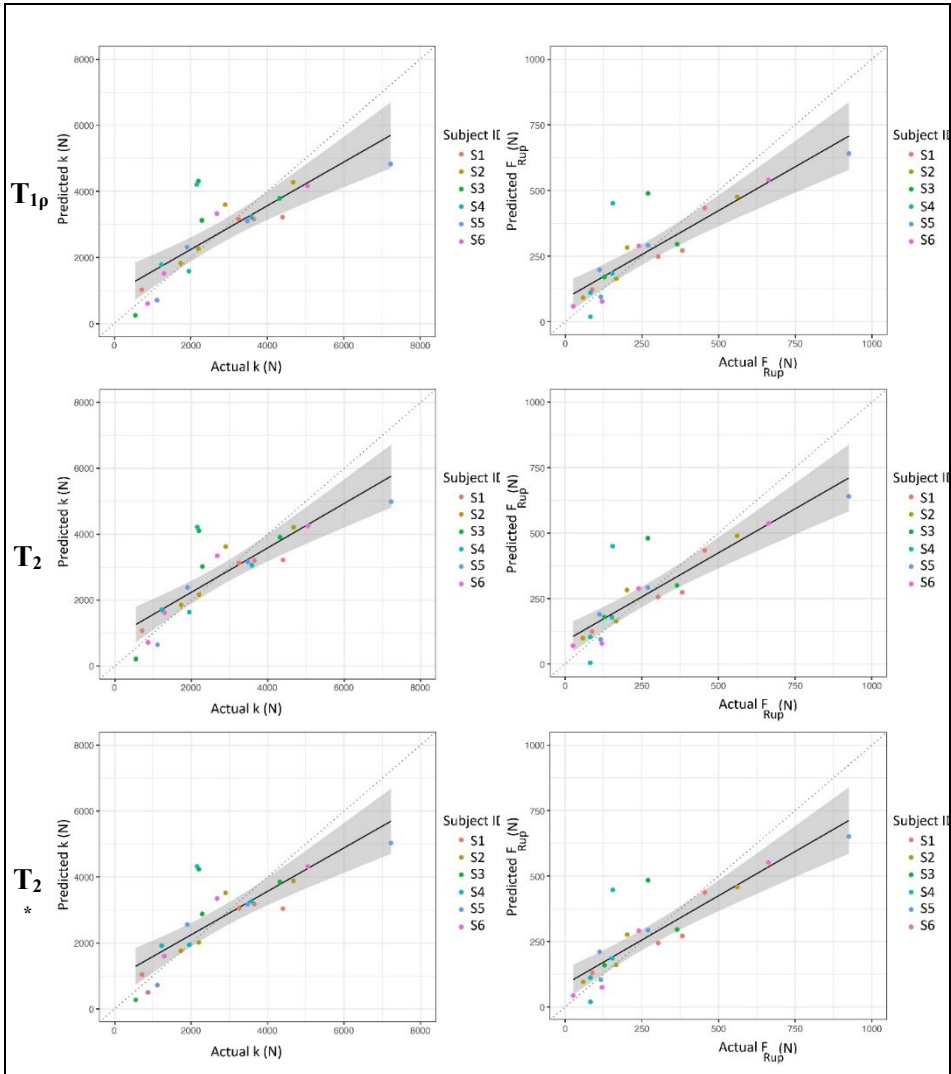


Figure 7: Actual versus predicted ligament stiffness (left column) and specimen rupture force (right column) determined using the predictive model based on the linear combination of ligament volume, specimen type and T_{1p} , (first row) T_2 (second row) and T_2^* (third row).

4. Discussion

In this study the stiffness and rupture force of the tibiofemoral ligaments were correlated to quantitative MRI parameters and geometrical specifications. The results revealed a significant correlation between the mechanical properties (stiffness and initial rupture force), and volume combined with the three MRI

parameters ($T_{1\rho}$, T_2 and T_2^*). While the mechanical properties were mostly correlated to the volume, inclusion of the MR parameters increased the correlation strength. This is in agreement with previous work by Fleming et al. (2011), who reported a significant correlation between the ACL stiffness and rupture force and ligament volume [22].

Inclusion of ligament type in the statistical analysis enhanced the correlation of mechanical properties with MR parameters and volume. The coefficient representative for ligament type was found to be different for ACL, PCL, MCL and LCL. This difference may be explained by the differences in the fractions of collagen types I and III in these ligaments. In a study investigating collagen type fractions in the ACL, PCL, MCL, and LCL, Wan et al. (2015) [23] found that ligaments with more collagen type I are stiffer than those with more collagen type III. The average proportion of collagen type I to type III, as an indication for ligament stiffness, resulted in a similar order of knee ligaments as derived from the statistical analysis in this study, based on the ligament-specific coefficients.

The model proposed by Blankevoort and Huiskes [21] for the description of ligament stiffness could acceptably represent the toe region and linear region of each specimen relative to the results of the tensile tests. In general, and as expected, the largest stiffness and rupture force was found for the PCL for each knee specimen.

The DIC and ultrasound measurements showed that almost all of the specimens were ruptured at their insertion sites, which may be due to the relatively old age of the tested specimens. Previously, it was shown that ligaments in aged donors are more likely to rupture at the insertion sites, while in younger donors the rupture may occur more frequently in the middle region [24].

The strains measured using ultrasound in the deep fibers of the collateral ligaments during the cyclic preconditioning loads revealed a good agreement with the surface strains measured using DIC (Figure 8), which gives confidence for employing DIC for these ligaments. Unfortunately, out-of-plane motions in the ultrasound measurements made such a comparison impossible for the more complex cruciate ligaments, and particularly the ACL.

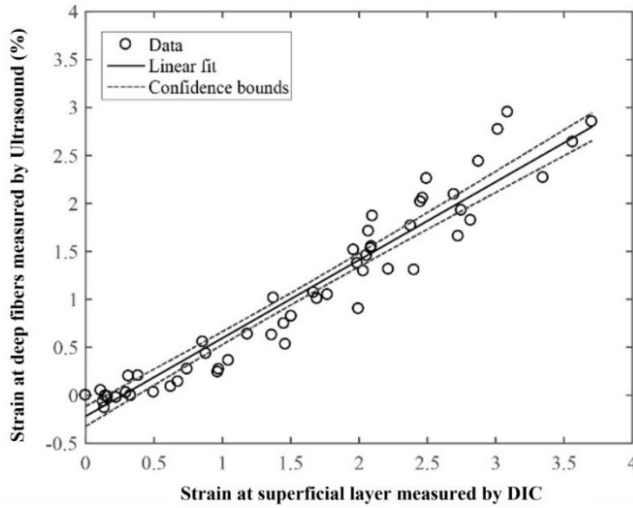


Figure 8: Linear correlation ($R^2=0.93$) between strain values derived from ultrasound data (deep fibers) and DIC (superficial strain) for all LCL specimens.

Assessment of the deviations between the predicted and measured stiffness shows that if T_{1p} or T_2 are utilized, the error in the ligament stiffness estimation rarely exceeds 500 N in the ACL, MCL and LCL (Figure 9). The deviation for the PCL of the fifth subject (S5) was considerably larger. Based on a series of sensitivity analyses in FE, [25] showed that the anterior translation and internal rotation of the knee joint is negligibly affected by variation of 500 N in ACL stiffness, during a walking cycle. Similarly, with the largest error in ACL stiffness prediction in this study (500 N), the average pressure at the tibial plateau changes maximally by 8%, and affects the center of pressure by less than 2 mm anteriorly, during a walking cycle. In the same study, the sensitivity of contact variables and the translational and rotational motions of the knee joint to PCL stiffness variations was shown to be negligible during a walking cycle. The changes in joint biomechanics due to the maximum error caused by our predictive model in MCL and LCL stiffness, also were concluded to be minor. However, it is important to consider the influence of the combined stiffness errors in all ligaments. We previously illustrated that a combined change in tibiofemoral ligament stiffness and initial strain can lead to inaccurate outcomes [1]. As a result, a sensitivity analysis, prior to implementation of the proposed predictive model, is recommended to assess the possible consequences of the combined errors in the estimation of all ligament stiffness values.

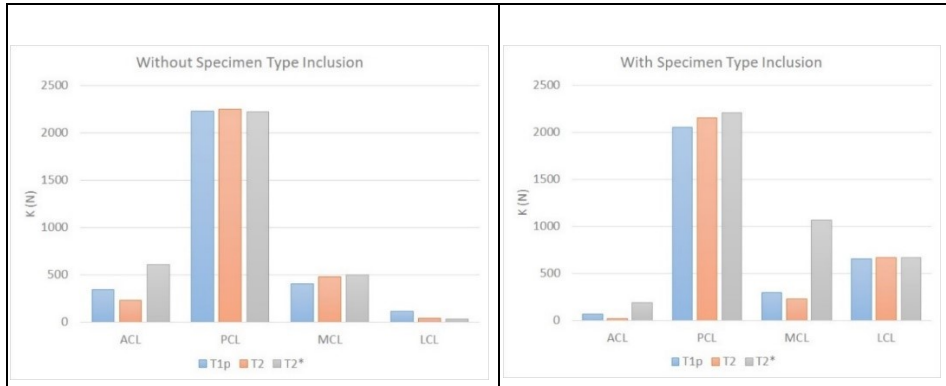


Figure 9: The largest differences between the actual and predicted stiffness from the predictive model with (right) and without (left) specimen type inclusion. The worse cases are from different subjects, as ACL (S1), PCL (S5), MCL (S2) and LCL (S3).

There were several limitations to this study. First, the study was performed on cadaveric specimens, which may lead to differences compared to the in-vivo situation. It particularly can have an influence on MR parameters. However, in order to characterize the mechanical properties of the ligaments, an in-vitro experiment with the isolated ligaments was unavoidable. Second, the specimens tested in the current study were selected from six cadavers. Increasing the number of specimens may improve the power of the statistical analysis. As to the best of Authors' knowledge this is the first study assessing the correlation of mechanical properties of all four tibiofemoral ligaments to MR parameters and structural properties, the 24 specimens still can provide valuable data for a statistical analysis. Another MR-related issue is the magic angle effect, which could lead to an artificial increase in signal intensity. Particularly T_2 and T_2^* are more sensitive to this MR artifact. In this study, T_{1p} was also added as one of the MRI parameters, as this parameter is believed to be less influenced by the magic angle effect. Also, the PCL was assessed in a different position than full extension, to ensure stretching of the bundles, and also to have more control over the orientation of the specimen in the MRI scanner. Another limitation was that the specimens tested in this study were from relatively old donors, due to the unavailability of younger specimens. The parameters assessed in this study, and particularly the mechanical properties of the ligaments can be different from younger tissues [24]. In average, the stiffness of the ligaments measured in this study were lower than

the values reported by Butler et al. who tested the tissues from younger donors [26]. The initial rupture force we measured for different ligaments were also considerably lower than what expected for younger tissues. It was previously shown that for instance the ACL rupture force in older donors as experimented in this study (61-97 years) can be 30% of the rupture force of ACL in younger donors (22-35 years) [17].

5. Conclusion

In conclusion, this study revealed the potentials in using quantitative MR parameters, $T_{1\rho}$, T_2 and T_2^* , combined with specimen volume to estimate the essential mechanical properties of all main tibiofemoral ligaments required for subject-specific FE modeling of human knee joint. $T_{1\rho}$ might, however, be more confidently used regardless of the inclusion or exclusion of the ligament type. Although the errors in the prediction of the mechanical properties for the individual ligaments may be acceptable, the effect of the combined errors of all four ligaments on the outcomes of FE models of the knee joint needs prior investigation in a sensitivity analysis.

Acknowledgments

This study was a part of BioMechTools project (ERC-2012-ADG LS7), received funding from the European Research Council under the European Union's Seventh Framework Program (FP/2007-2013) / ERC Grant Agreement n. 323091.

References

- [1] H. Naghibi Beidokhti, D. Janssen, S. Van De Groes, J. Hazrati, T. Van Den Boogaard, and N. Verdonchot, “The influence of ligament modelling strategies on the predictive capability of finite element models of the human knee joint,” *J. Biomech.*, vol. 65, pp. 1–11, 2017.
- [2] H. Naghibi, D. Janssen, S. Van De Groes, and N. Verdonchot, “The peripheral soft tissues should not be ignored in the finite element models of the human knee joint,” *Med. Biol. Eng. Comput.*, 2017.
- [3] J. C. Gardiner and J. a. Weiss, “Subject-specific finite element analysis of the human medial collateral ligament during valgus knee loading,” *J. Orthop. Res.*, vol. 21, no. 6, pp. 1098–1106, 2003.
- [4] M. a. Baldwin, C. Clary, L. P. Maletsky, and P. J. Rullkoetter, “Verification of predicted specimen-specific natural and implanted patellofemoral kinematics during simulated deep knee bend,” *J. Biomech.*, vol. 42, no. 14, pp. 2341–2348, 2009.
- [5] B. C. Fleming and B. D. Beynon, “In-vivo measurement of ligament/tendon strains and forces: A review,” *Ann. Biomed. Eng.*, vol. 32, no. 3, pp. 318–328, 2004.
- [6] A. M. Biercevicz, M. M. Murray, E. G. Walsh, D. L. Miranda, J. T. Machan, and B. C. Fleming, “T2* MR relaxometry and ligament volume are associated with the structural properties of the healing ACL,” *J. Orthop. Res.*, vol. 32, no. 4, pp. 492–499, 2014.
- [7] A. M. Biercevicz *et al.*, “MRI Volume and Signal Intensity of ACL Graft Predict Clinical, Functional, and Patient-Oriented Outcome Measures After ACL Reconstruction,” *Am. J. Sports Med.*, vol. 43, no. 3, pp. 693–699, 2015.
- [8] A. M. Biercevicz, D. L. Miranda, J. T. Machan, M. M. Murray, and B. C. Fleming, “In Situ, noninvasive, T2*-weighted MRI-derived parameters predict ex vivo structural properties of an anterior cruciate ligament reconstruction or bioenhanced primary repair in a porcine model,” *Am. J. Sports Med.*, vol. 41, no. 3, pp. 560–6, 2013.

- [9] A. M. Biercevicz, M. R. Akelman, L. E. Rubin, E. G. Walsh, D. Merck, and B. C. Fleming, "The uncertainty of predicting intact anterior cruciate ligament degeneration in terms of structural properties using T2* relaxometry in a human cadaveric model," *J. Biomech.*, vol. 48, no. 6, pp. 1188–1192, 2015.
- [10] N. M. Szeverenyi and G. M. Bydder, "Dipolar anisotropy fiber imaging in a goat knee meniscus," *Magn. Reson. Med.*, vol. 65, no. 2, pp. 463–470, 2011.
- [11] A. C. Wright, J. H. Yoder, E. J. Vresilovic, and D. M. Elliott, "Theory of MRI contrast in the annulus fibrosus of the intervertebral disc," *Magn. Reson. Mater. Physics, Biol. Med.*, vol. 29, no. 4, pp. 711–722, 2016.
- [12] N. Wang and Y. Xia, "Anisotropic analysis of multi-component T2 and T1 ρ relaxations in achilles tendon by NMR spectroscopy and microscopic MRI," *J. Magn. Reson. Imaging*, vol. 38, no. 3, pp. 625–633, 2013.
- [13] M. Bydder, A. Rahal, G. D. Fullerton, and G. M. Bydder, "The magic angle effect: A source of artifact, determinant of image contrast, and technique for imaging," *J. Magn. Reson. Imaging*, vol. 25, no. 2, pp. 290–300, 2007.
- [14] F. Farahmand, M. N. Tahmasbi, and A. A. Amis, "Lateral force-displacement behaviour of the human patella and its variation with knee flexion - A biomechanical study in-vitro," *J. Biomech.*, vol. 31, no. 12, pp. 1147–1152, 1998.
- [15] K. L. Smith *et al.*, "Effect of joint position and ligament tension on the MR signal intensity of the cruciate ligaments of the knee," *J. Magn. Reson. Imaging*, vol. 4, no. 6, pp. 819–822.
- [16] S. Nakagawa *et al.*, "The posterior cruciate ligament during flexion of the normal knee.," *J. Bone Joint Surg. Br.*, vol. 86, no. 3, pp. 450–456, 2004.
- [17] S. L. Woo, J. M. Hollis, D. J. Adams, R. M. Lyon, and S. Takai,

“Tensile properties of the human femur-anterior cruciate ligament-tibia complex. The effects of specimen age and orientation,” *Am. J. Sports Med.*, vol. 19, no. 3, pp. 217–225, 1991.

[18] T. Luyckx, M. Verstraete, K. De Roo, W. De Waele, J. Bellemans, and J. Victor, “Digital image correlation as a tool for three-dimensional strain analysis in human tendon tissue,” *J. Exp. Orthop.*, vol. 1, no. 1, pp. 1–7, 2014.

[19] G. Lionello, C. Sirieix, and M. Baleani, “An effective procedure to create a speckle pattern on biological soft tissue for digital image correlation measurements,” *J. Mech. Behav. Biomed. Mater.*, vol. 39, pp. 1–8, 2014.

[20] T. A. L. Wren, S. A. Yerby, G. S. Beaupré, and D. R. Carter, “Mechanical properties of the human achilles tendon,” *Clin. Biomech.*, vol. 16, no. 3, pp. 245–251, 2001.

[21] L. Blankevoort and R. Huiskes, “Ligament-bone interaction in a three-dimensional model of the knee,” *J. Biomech. Eng.*, vol. 113, no. 3, pp. 263–269, 1991.

[22] B. C. Fleming, S. Vajapeyam, S. A. Connolly, E. M. Magarian, and M. M. Murray, “The use of magnetic resonance imaging to predict ACL graft structural properties,” *J. Biomech.*, vol. 44, no. 16, pp. 2843–2846, 2011.

[23] C. Wan, Z. Hao, L. Tong, J. Lin, Z. Li, and S. Wen, “An update on the constitutive relation of ligament tissues with the effects of collagen types,” *J. Mech. Behav. Biomed. Mater.*, vol. 50, pp. 255–267, 2015.

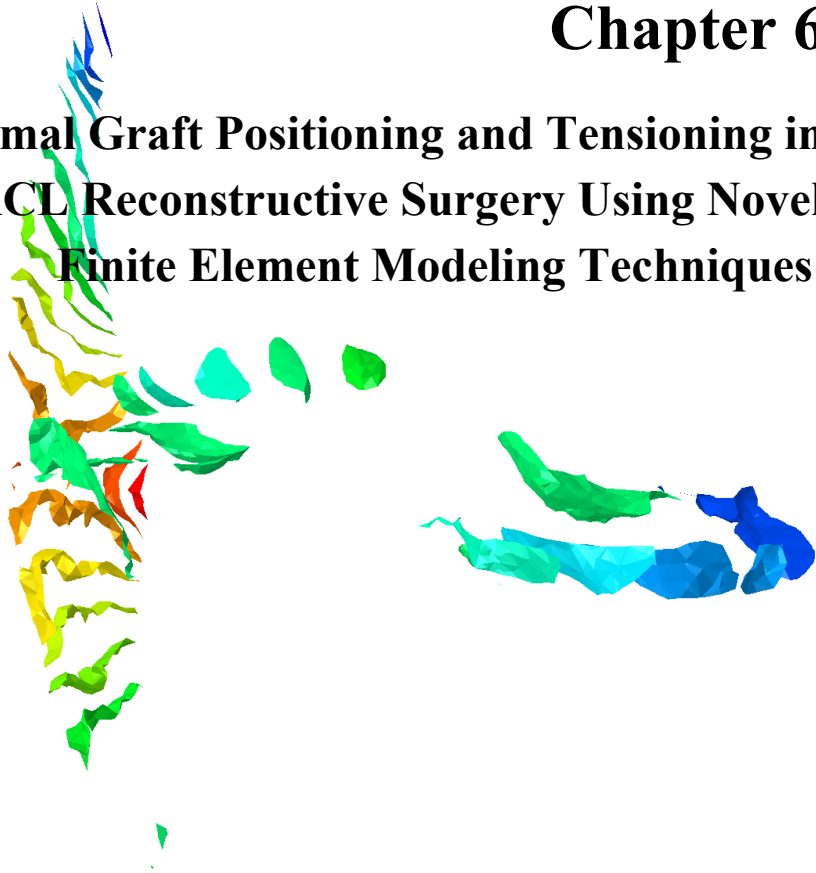
[24] F. R. Noyes and E. S. Grood, “The strength of the anterior cruciate ligament in humans and Rhesus monkeys,” *J Bone Jt. Surg Am*, vol. 58, no. 8, pp. 1074–82, 1976.

[25] C. R. Smith, R. L. Lenhart, J. Kaiser, M. F. Vignos, and D. G. Thelen, “Influence of Ligament Properties on Tibiofemoral Mechanics in Walking,” *J. Knee Surg.*, vol. 29, no. 2, pp. 99–106, 2015.

[26] D. L. Butler, M. D. Kay, and D. C. Stouffer, "Comparison of material properties in fascicle-bone units from human patellar tendon and knee ligaments.," *J. Biomech.*, vol. 19, no. 6, pp. 425–432, 1986.

Chapter 6

Optimal Graft Positioning and Tensioning in ACL Reconstructive Surgery Using Novel Finite Element Modeling Techniques



Naghibi Beidokhti, H., Janssen, D., Van Tienen, T., Van de Groes, S., Van den Boogaard, T., Verdonchot, N., 2018. The Knee Surgery, Sports Traumatology, Arthroscopy, Under review.

1. Introduction

Osteoarthritis (OA) development in the knee has been reported in both ACL-deficient and ACL-reconstructed knees [1]–[9]. In ACL reconstructed patients the post-operative knee biomechanics (i.e. laxity) may differ from the intact knee biomechanical behavior. This altered mechanical behavior can alter knee kinematics, which is believed to play an important role in the initiation or progression of knee OA [10]–[14]. It can also lead to a change in knee kinetics (forces), and as a result, tibiofemoral load transfer conditions (i.e. contact pressure at the cartilage surfaces), which may also result in OA [15]–[17]. Hence, in order to reduce the chance of OA progression in an ACL deficient patient the goal of the surgery should be to restore the kinematic and kinetic behavior of the intact knee as best as possible and optimize the surgical parameters to reach this goal.

A very important surgical parameter is the insertion site on the femur as well as on the tibia. Some surgeons prefer an isometric positioning, whereas some others aim for an anatomical placement of the graft [18]–[22]. Besides the variations in graft positioning, another parameter that may affect the post-operative mechanical behavior of the knee is the tension force applied to the graft at its fixation (fixation tension). Different graft fixation tension forces, ranging from 15 N to 150 N, have been proposed in the literature [23]–[27].

Finally, there are different preferences among orthopedic surgeons in terms of graft types and surgery technique (single bundle or double bundle) based on a variety of graft selection criteria [28]–[33]. The graft type of choice may just be a result of personal preference of the surgeon or other criteria (i.e. level of activity prior to surgery, sort of sport activity, etc.) or in some cases even based on the patient's special request [31]. The different graft types have different stiffnesses, strengths, sizes, and fiber orientations than the native ACL. As a result, a different mechanical response is expected for different graft choices. This means that different surgical variables (e.g. insertion site and fixation tension) may need to be applied for different graft choices in order to meet patient specific requirements and recreate the original intact knee behavior as best as possible. The surgeon that masters different techniques would be able to supply different choices for patient- or sport-specific requirements.

With the variations in insertion sites, fixation tension, graft type, and technique, the surgeon has many options to consider when reconstructing the ACL. Finite Element (FE) models can provide more insight on the implications of different choices on knee biomechanical outcomes [34]–[36]. We postulate that using an FE model of the knee joint as a pre-planning tool for ACL reconstructive surgery, may assist in optimizing the post-operative kinematics and kinetics.

It is known that the mechanical behavior of knees differs considerably amongst individuals. It has been shown previously that applying mechanical properties for the knee ligaments from the literature does not lead to a good representation of knee-specific mechanical behavior [37]. Hence, to enable simulation of a patient specific knee one needs patient specific geometry as well as patient specific fitting of the mechanical properties of the soft tissue structures. Patient specific geometry can be discerned from CT or MRI images [38], [39]. We propose that the mechanical properties of the soft tissues (i.e. ligaments) can be estimated from multi-directional laxity measurements. We furthermore postulate that if an ACL-deficient knee is reconstructed in a way such that the multi-directional knee laxity is very similar to that of the intact knee, this knee will also function adequately under weight-bearing conditions such as level walking.

The aim of this study was to demonstrate the potential of FE models to define the optimal choices in surgical parameters in terms of optimal graft positioning (insertion sites and fixation tension) in combination with graft type in order to restore the kinematic and kinetic behavior of the knee as best as possible. For this purpose we show 1) how ACL surgical parameters can be optimized to obtain (close to) intact knee joint laxity and 2) how these optimized choices progress into a more physiological behavior of the knee joint under level walking loading conditions.

2. Materials and Methods

The workflows proposed in this study is schematically illustrated in Figure 1 (block-B), based on the validated FE model developed in an earlier study (Figure 1: block-A) [37]. The methods as describe below are separated in three parts. Part I describes the anterior-posterior (AP) laxity tests in a cadaveric setting. The laxity tests (AP only) were selected so that they could relatively easy be applied under in-vivo patient conditions. Subsequently, Part II describes how a validated

FE model was utilized to select the optimal surgical parameters in order to generate a model of an ACL reconstruction that has a very similar biomechanical behavior as an intact knee model in terms of knee joint laxity (in AP laxity tests). In Part III we describe how the laxity-based optimization, as performed in Part II, affects knee joint kinematics and kinetics at loading conditions generated during level walking.

Part I: Cadaveric laxity tests

The specimens were received from the Anatomy Department of Radboud University Medical Center with a permission statement for experimental use. AP laxity tests (including Lachman and anterior drawer tests) were performed on the cadaveric intact knee in which an anterior load of 100N was applied to the tibia at approximately 5cm below the joint line at 0, 30, 60 and 90° of flexion. All translational and rotational motions of the joint were recorded during the tests using an electromagnetic tracking system (3Space Fastrak, Polhemus Incorporated, VT, USA).

To define the ACL footprint at femoral and tibial sites in the FE model, the ACL was removed from the insertion sites by an orthopedic surgeon and the femoral and tibial footprints were digitized using a calibrated pen-stylus. This information was used to provide geometrical boundaries for the calculations to determine the optimal insertion sites of the ACL reconstructions (see Part II).

Part II: Optimizing surgical parameters for ACL surgery

As shown in block-A in Figure 1, previously, based on imaging data, MRI and CT (Figure 1-a), and a series of internal-external (IE) and valgus-varus (VV) laxity tests on the human cadaveric specimen, a detailed computational (FE) model of a human intact knee joint was developed (Figure 1-b). Subsequently, the FE model was extensively validated against cadaveric measurements in a six-degree-of-freedom knee testing apparatus, focusing on joint kinematics and tibial cartilage contact pressures (Figure 1-c). This validated intact knee model developed in an earlier study [37] was then used to follow the workflow proposed in the current study as shown in block-B in Figure 1.

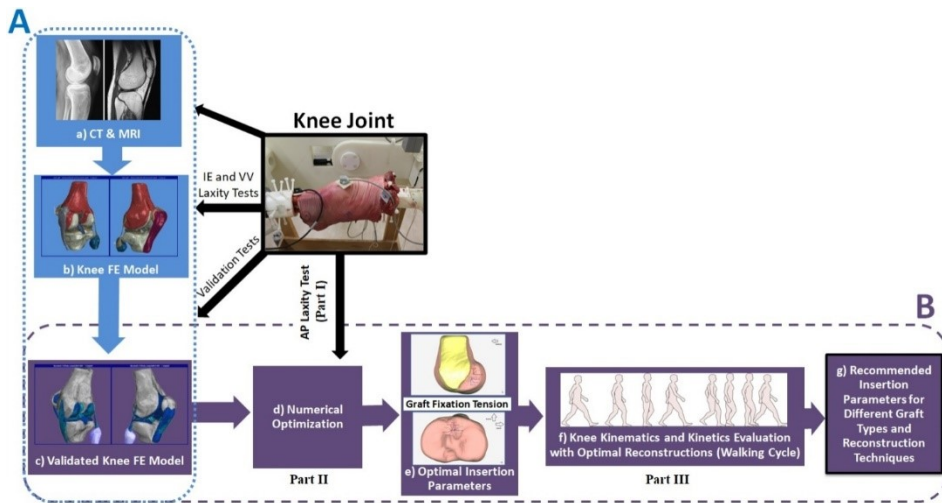


Figure 1: The ACL reconstruction pre-planning workflow proposed in this study, based on a validated FE model in an earlier study [37] (Block A), to recover intact knee biomechanics in an ACL-injured knee and minimize mechanically induced progression of OA (Block B). Based on imaging data (a), and IE and VV laxity tests (b), on a human cadaveric knee joint, a detailed FE model of the knee joint was developed which was validated against validation tests (c). In this study, based on the experimental AP laxity test, and implementing numerical optimizations on the FE model (d), the surgical graft insertion parameters (insertion sites and fixation tension) were optimized. The kinetics and kinematics of the knee joint during a walking cycle simulation was assessed with the optimized surgical parameters (f), in order to assess how these optimized choices progress into a more physiological behavior of the knee joint under level walking loading conditions. The recommended ACL-reconstruction insertion parameters can be created (g), in which the most optimal graft insertion parameters (insertion site and fixation tension) is presented for different graft types and different reconstruction technique (single bundle and double bundle).

The validated FE model was used to simulate various approaches for ACL reconstruction. Single bundle ACL reconstruction surgery was simulated with three different graft types: 1) bone-patellar tendon-bone (stiffness: 670 N/mm), 2) quadrupled hamstring tendon (stiffness: 776 N/mm) and 3) quadriceps tendon (stiffness: 465 N/mm). According to [29], hamstring tendon is the most used graft for double bundle reconstruction. Consequently, for the double bundle reconstruction simulation, doubled gracilis (stiffness: 370 N/mm) and semitendinosus (stiffness: 534 N/mm) grafts were utilized, respectively, as posterolateral (PL) and anteromedial (AM) bundles. The mechanical properties of all different graft types were based on the average stiffness values reported in the literature [33], [40]–[43]. To describe the nonlinear behavior of the grafts, for instance the negligible resistance in compression and toe- and linear regions in tension, the widely used model described by Blankevoort and Huiskes (1991) for ligament mechanical properties was used [44].

Computer simulation of the operative procedure: We chose to position the deficient knee joint in 30° of flexion to allow for graft fixation [45]. In single bundle reconstructions, the graft was inserted and tensioned with a 40N force before it was fixated at the centre of tibial and femoral footprints of the removed ACL [46]. In the double bundle case, the AM and PL bundles were tensioned by 50N and 30N, respectively [47]. After graft placement, the joint was fully extended again. The resulting models were representative for current standard surgical approaches. These models also served as the basis for subsequent optimization simulations to find the optimized surgical parameters.

Optimization of the insertion variables within the knee models: For each simulated operative case, a numerical optimization was performed. In brief, this optimization procedure aimed at mimicking the laxity of the intact joint as closely as possible, by varying and optimizing the femoral and tibial graft insertion sites, and the graft fixation tension. The laxity tests were simulating the experimental AP laxity tests on the intact knee joint, as explained previously (Part I). The insertion sites and fixation tension were optimized by sequentially running the model with adapted insertion sites and fixation tension parameters (Isight, Simulia, Providence, RI). The optimization model running continued until similar rotations (valgus-varus and internal-external) and anterior motion, to what measured experimentally (with the intact knee), were reached in the FE model of the grafted knee joint. This typically required 3000 FE simulations for each graft type.

During the optimization, the femoral and tibial insertion points were constrained within the footprints of native ACL as digitized during the experiment (Part I). The graft fixation tension was also constrained to be within the range of 0 to 150N.

After these optimizations three single bundle reconstructed knee models, using patellar tendon, hamstring and quadriceps grafts, and one double bundle reconstructed knee, with the optimized positioning parameters (insertion sites and fixation tension) were created.

In order to assess the significance of inserting the grafts with optimal parameters (insertion sites and fixation tension) as calculated in this study, the grafts in single bundle reconstruction, were also positioned in the opposite sites than the optimal

ones (with a fixation tension of 40 N) to be representative for a common non-optimal reconstruction. Moreover, in the double bundle reconstruction, the AM and PL bundles with common insertion sites (centers) and fixation tension was used as a non-optimal double bundle reconstruction.

Hence, in total the following ten models were generated:

- *ACL intact*: The intact knee joint model;
- *ACL ruptured*: A knee model with the ACL total rupture;
- *Optimal Patellar tendon*: A knee model with a single bundle reconstruction with optimized positioning (insertion sites and fixation tension) of the Patellar tendon graft;
- *Optimal Hamstring*: A knee model with a single bundle reconstruction with optimized positioning (insertion sites and fixation tension) of the Hamstring graft;
- *Optimal Quadriceps*: A knee model with a single bundle reconstruction with optimized positioning (insertion sites and fixation tension) of the Quadriceps graft;
- *Optimal double bundle*: A knee model with a double bundle reconstructed knee with optimized positioning (insertion sites and fixation tension) of AM and PL bundles;
- *Non-optimal Patellar tendon*: A knee model with a single bundle reconstruct with non-optimized positioning (opposite to the optimized sites) of the Patellar tendon graft (fixation tension: 40 N);
- *Non-optimal Hamstring*: A knee model with a single bundle reconstruction with non-optimized positioning (opposite to optimized sites) of the Hamstring graft (fixation tension: 40 N);
- *Non-optimal Quadriceps*: A knee model with a single bundle reconstruction with non-optimized positioning (opposite to optimized sites) of the Quadriceps graft (fixation tension: 40 N); and,
- *Non-optimal double bundle*: A knee model with a non-optimized double bundle reconstruction with AM (fixation tension: 50 N) and PL (fixation tension: 30 N) bundles inserted at the centre of AM and PL regions.

Part III: Demonstration of improved functional behavior of the ACL reconstructed knee using optimized surgical parameters

To evaluate the results of the optimization of the insertion sites and fixation tension, a full gait cycle was simulated with all ten models. The gait loads were based on the normalized in-vivo loads produced from eight subjects, as listed in the Orthoload database [48], and scaled to the weight of the cadaveric subject, and following the ASTM International standard guide (F3141-15) [49]. The tibia was fully constrained, and the loads and flexion were applied to femur, respectively in tibial and femoral frames (Figure 2).

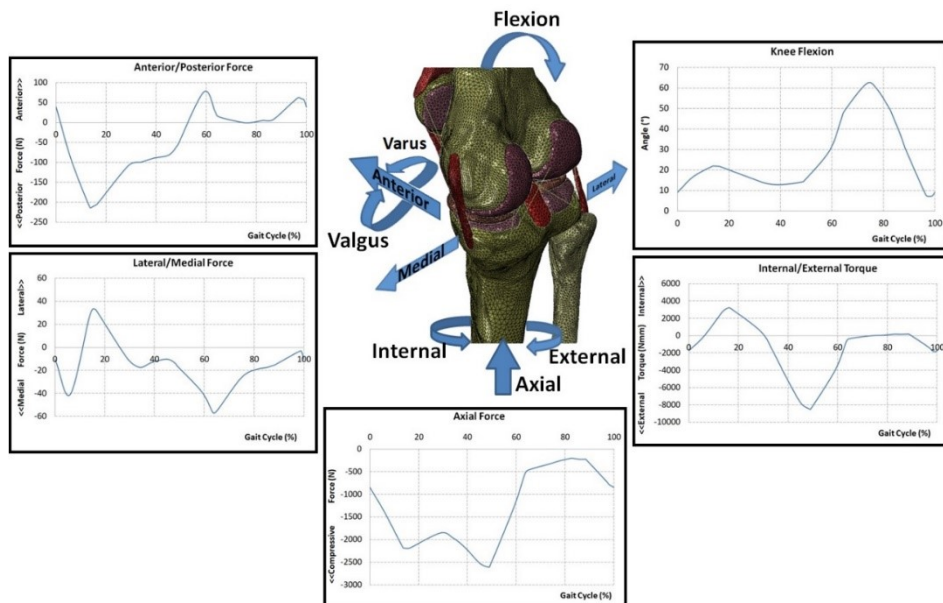


Figure 2: The loads and boundary conditions applied to the ten models generated in this study. Loads simulated a walking cycle, based on the normalized in-vivo loads in the Orthoload database [48].

As outcome parameters, the joint kinematics, contact pressure at tibial cartilage, force in the graft bundles and force in tibiofemoral ligaments were calculated and compared in the ten models. In order to compare the tibiofemoral articular condition improvements, achieved by different reconstructions in this study, the variations in peak contact pressure at tibial cartilage relative to the intact knee joint were compared. Consequently, for the medial and lateral tibial plateau, the averaged Root Mean Square (RMS) differences between the intact knee joint and

all the optimized and non-optimal reconstructed knees, as well as the deficient knee, during the stance and swing phases of a gait cycle, were compared.

3. Results

Graft insertion optimization: The optimization analyses revealed different optimal insertion sites, dependent on the graft type. For the quadriceps tendon, the intact knee laxity was best captured with the graft in the isometric regions, while for the patellar tendon and hamstring grafts the anatomical regions were calculated (Figure 3-a). Moreover, different fixation forces were calculated for the different grafts (Table 1). The quadriceps tendon required a higher fixation force (around 80N) than the patellar tendon and hamstring grafts (around 40N).

In the double bundle reconstruction case, the best fit with the intact knee laxity was achieved when the AM and PL bundles were positioned at, posterior distal and posterior proximal regions within the femoral footprint of the excised ACL, respectively (Figure 3-b). For an optimal fit with the intact knee laxity, both AM and PL bundles needed to be tensioned by about 50N (Table 1).

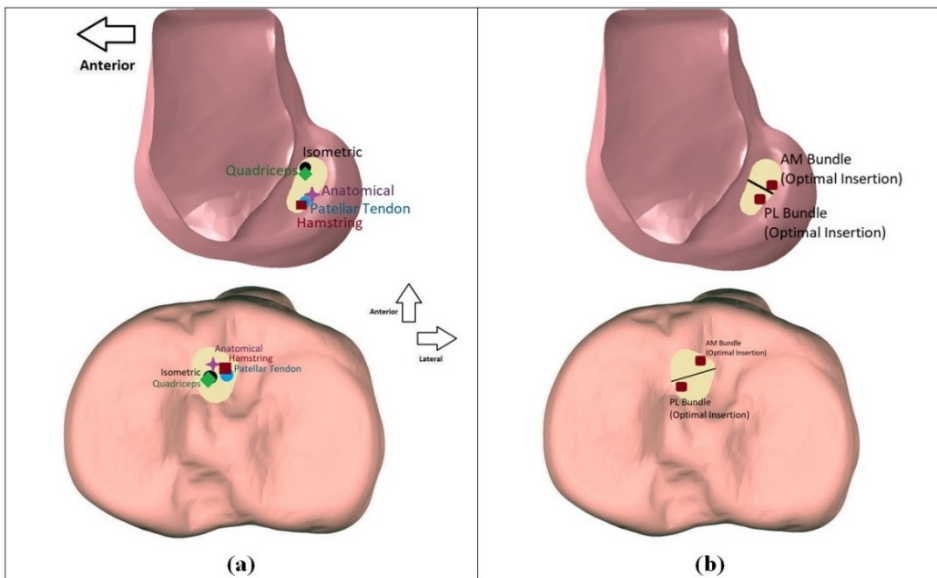


Figure 3: Optimal calculated graft insertion sites for single bundle (a) and double bundle (b) reconstructions, implementing the workflow of the current study.

Table 1: Optimal Graft tension at 30 degrees of flexion prior to the fixation (fixation tension) in order to recover the intact knee laxity during the AP laxity tests.

	Single Bundle Reconstruction			Double Bundle Reconstruction	
	Patellar Tendon	Hamstring (quadrupled)	Quadriceps tendon	AM Bundle (Semitendinosus)	PL Bundle (Gracilis)
Optimal Graft Fixation Tension	39 N	41 N	85 N	49 N	50 N

Gait Simulation: The ACL deficient knee showed a considerable increase in femoral posterior translation with a maximum of 14.3 mm at stance phase and 16.6 mm at swing phase (Figure 4). Moreover, ACL rupture led to an increase in femoral lateral translation at stance phase, maximally by 3.9 mm.

The reconstructed knees (single bundle and double bundle) with the optimized graft positioning and tension parameters, could recover the anterior-posterior (AP) and medial-lateral (ML) translation during a full walking cycle. In case of a non-optimal graft positioning (insertion sites and fixation tension) in single bundle reconstruction with hamstring and patellar tendons, the translational kinematics could not be recovered. The quadriceps tendon graft with non-optimal positioning parameters, could better follow the intact knee AP translation, whereas it over constrained the femoral lateral motion, particularly in swing phase.

Similarly to the translational kinematics, the intact knee rotational kinematics could be recovered using the optimized positioning variables in all three optimized single bundle reconstructions. The optimized double bundle reconstructed knee, revealed even a better improvement in the joint rotational kinematics recovery during the swing phase (Figure 5).

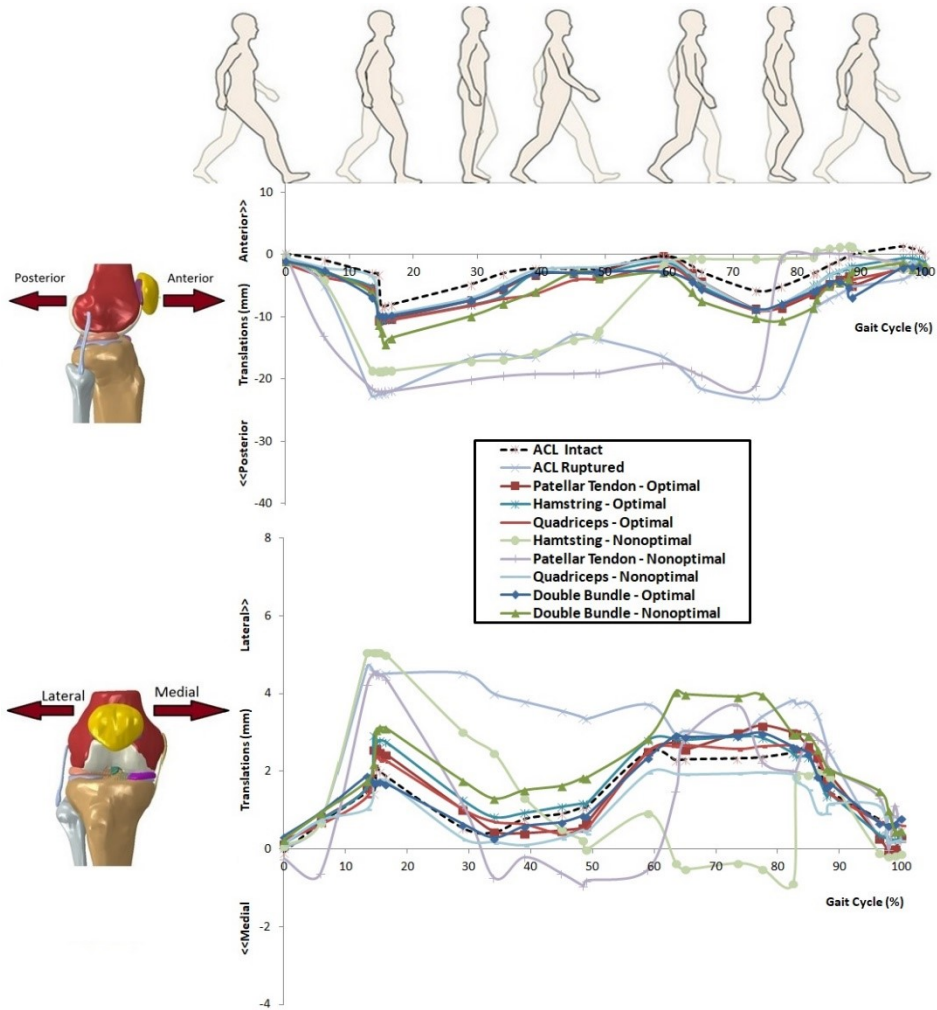


Figure 4: The knee Anterior-Posterior translation (top) and Medial-Lateral (bottom) translation during a full gait cycle for the ten models.

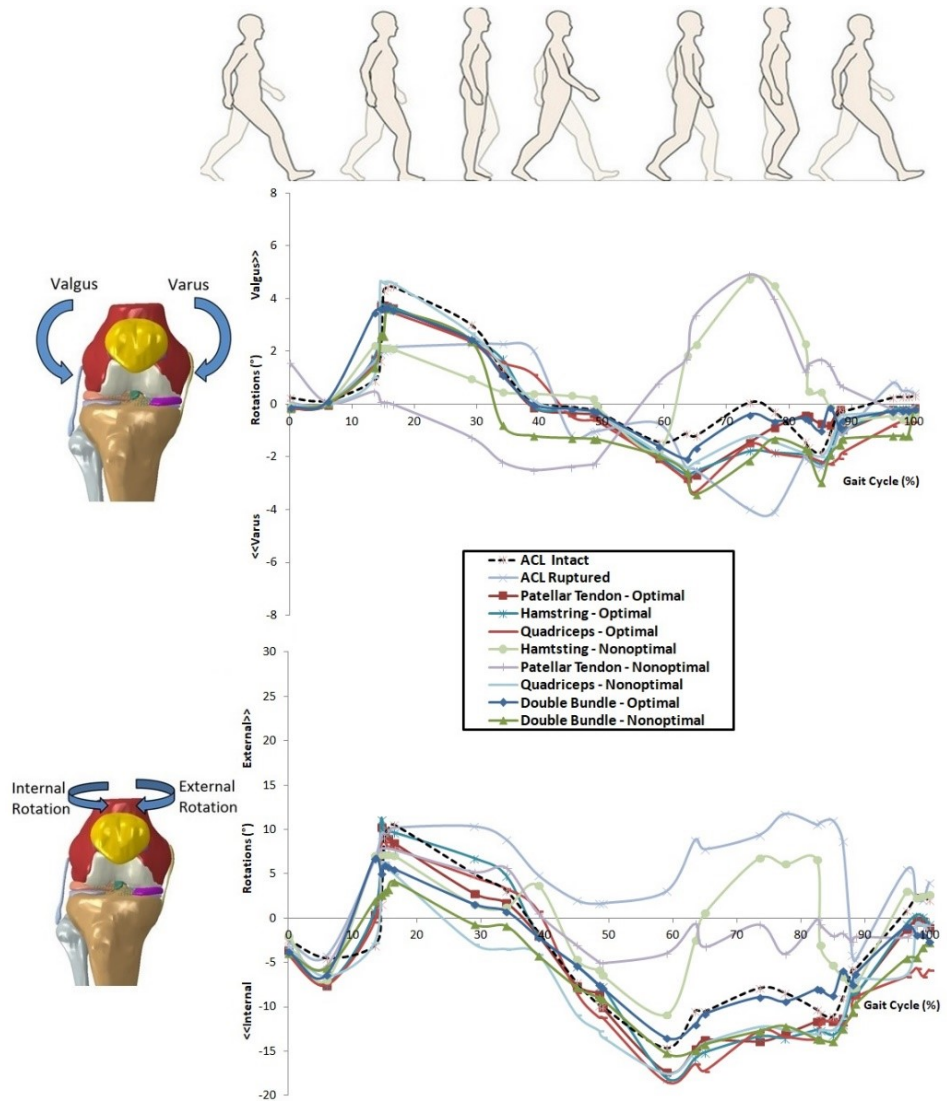


Figure 5: The knee Valgus-Varus rotation (top) and Internal-External rotation (bottom) during a full gait cycle for the ten models.

ACL rupture increased the peak contact pressure at the lateral tibial cartilage during the stance phase and particularly at mid-stance phase (20% of the gait cycle) where the increase in peak contact pressure was up to 2.3 MPa (37%), as shown in Figure 6. Not only in contact pressure magnitude, but also the contact pressure distribution pattern was influenced considerably by ACL rupture.

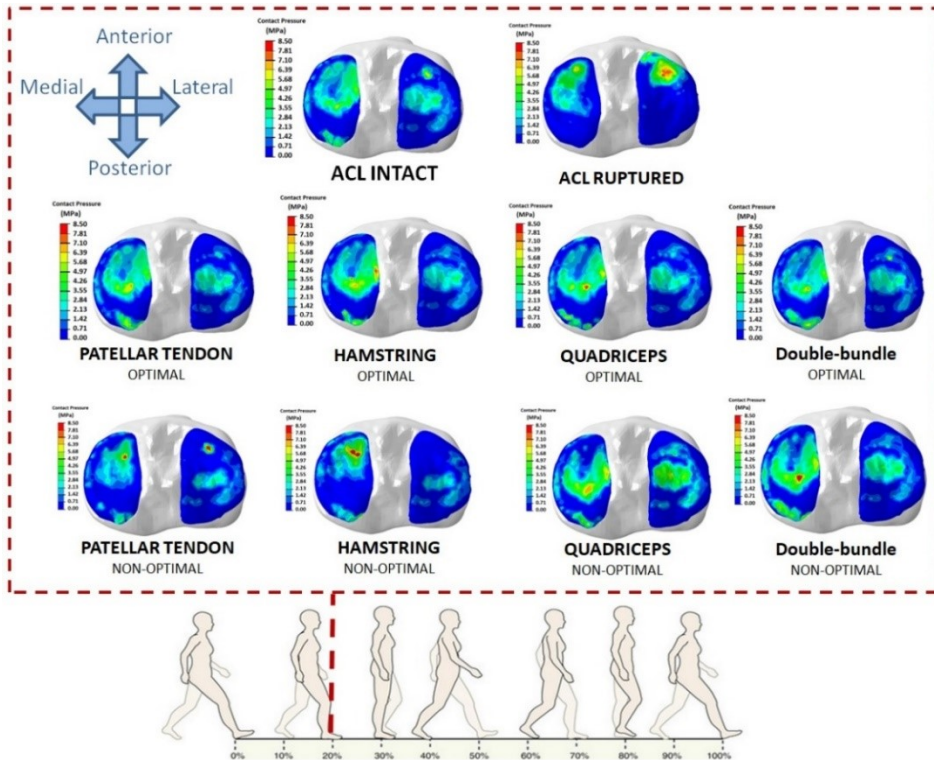


Figure 6: Contact pressure at tibial cartilage at 20% of a gait cycle for the intact knee, ACL-ruptured knee, three single-bundle and the double-bundle reconstructed knees with optimized grafting parameters, and three reconstructed knees with non-optimal common graft positioning.

The averaged Root Mean Square (RMS) differences between the peak contact pressure in the intact knee joint and all the optimized and non-optimal reconstructed knees, as well as the deficient knee, during the stance and swing phases of a gait cycle were presented in Table 2, separately for the medial and lateral tibial plateaus. As also the heat map illustrates, the lower values in Table 2 would mean that the reconstructed knee could better recover the intact knee peak contact pressure at tibial cartilage.

The results of the grafts biomechanics comparison indicated that the graft force in the optimized reconstructed cases was larger than the force in the native ACL. The force in the non-optimally positioned hamstring and patellar tendon grafts showed a drop to zero at some regions, more particularly in stance phase, revealing the graft slackness. In general, the quadriceps tendon graft, showed a larger force if non-optimal positioning applied.

Table2: The color-scaled averaged RMS difference between the intact knee and different reconstructed knees, for peak contact pressure at medial and lateral tibial cartilage, during the stance and swing phases of a gait cycle.

		Average RMS difference \pm standard deviation (MPa)			
		Stance Phase		Swing Phase	
Positioning		Medial Plateau	Lateral Plateau	Medial Plateau	Lateral Plateau
ACL-ruptured		1.18 \pm 1.40	1.14 \pm 1.80	2.19 \pm 3.34	1.52 \pm 2.41
Patellar Tendon	Non-optimal	0.92 \pm 0.89	1.76 \pm 4.08	1.10 \pm 1.28	1.21 \pm 2.09
	Optimal	0.39 \pm 0.31	0.28 \pm 0.23	0.26 \pm 0.28	0.40 \pm 0.33
Hamstring Tendon	Non-optimal	1.01 \pm 1.59	1.59 \pm 2.60	0.81 \pm 0.94	1.16 \pm 1.29
	Optimal	0.50 \pm 0.37	0.52 \pm 0.41	0.46 \pm 0.37	0.65 \pm 0.65
Quadriceps Tendon	Non-optimal	0.30 \pm 0.23	0.53 \pm 0.42	0.56 \pm 0.66	0.46 \pm 0.32
	Optimal	0.60 \pm 0.61	0.43 \pm 0.35	0.54 \pm 0.50	0.53 \pm 0.60
Double Bundle	Non-optimal	0.48 \pm 0.35	0.77 \pm 0.75	0.60 \pm 0.44	0.45 \pm 0.35
	Optimal	0.30 \pm 0.24	0.39 \pm 0.29	0.36 \pm 0.25	0.35 \pm 0.32

The tensile force in the PCL (at stance phase) and LCL (whole gait) increased dramatically in the model simulating an ACL rupture (Figure 7). All the grafted knees show similar PCL force and LCL force to intact knee joint. However, the non-optimal grafted knees with patellar tendon and hamstring tendon showed lower MCL force at stance phase and larger MCL force at swing phase.

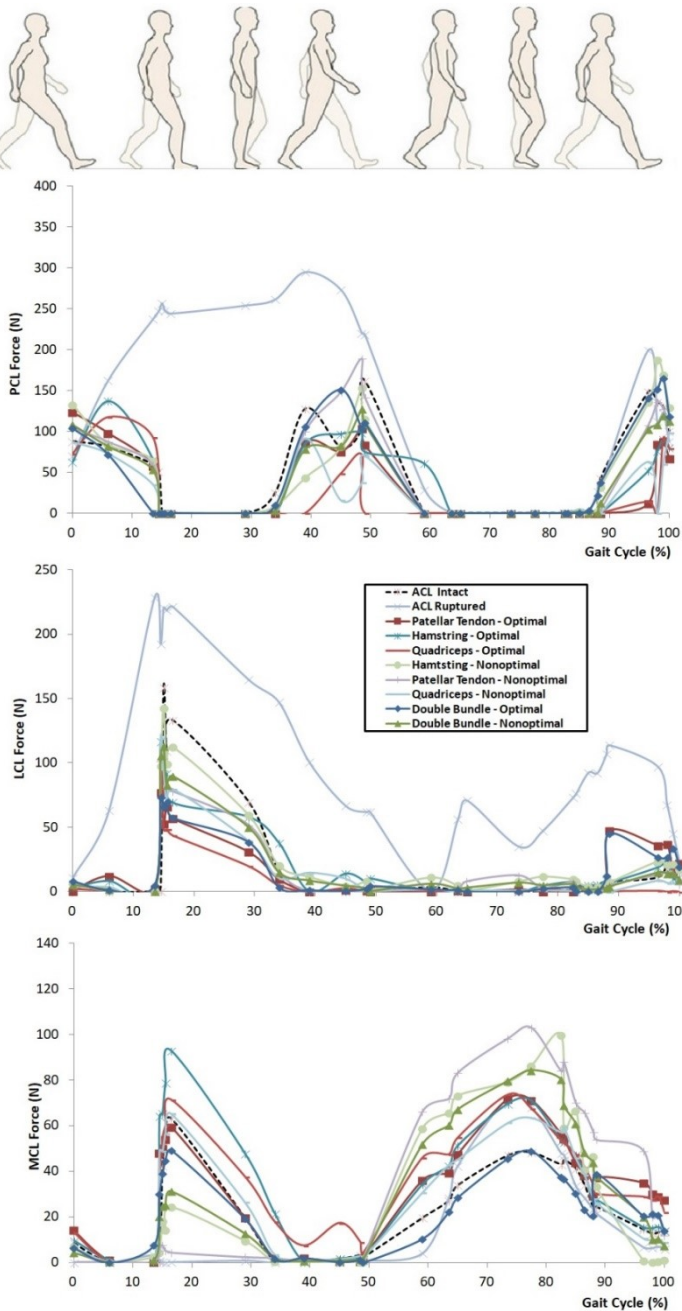


Figure 7: Force in PCL, LCL and MCL during a full gait cycle, for the intact knee, ACL-ruptured knee, single-bundle and double-bundle reconstructed knees with optimized positioning variables and the reconstructed knees with non-optimal common positioning parameters.

4. Discussion

In this study a workflow was proposed in order to recover the biomechanical behavior of the injured knee as physiological as possible. For this purpose, femoral and tibial graft insertion sites and graft fixation tension were optimized to obtain similar intact knee laxity, for three common single bundle reconstruction grafts (Hamstring, Quadriceps and Patellar tendons), as well as for a common double bundle reconstruction. Eventually, to verify the success of the surgery with the variables calculated with the proposed workflow, a full walking cycle was simulated with the intact, ACL-ruptured, optimal ACL reconstructed and non-optimal reconstructed knees to demonstrate that these optimized surgical parameters do indeed lead to more physiological knee biomechanics.

Implementing the proposed workflow to find the most optimal graft positioning parameters (insertion sites and fixation tension), in order to gain the intact knee laxity, for all three single bundle graft types and the double bundle grafts, did indeed improve the knee kinematics. The non-optimal, yet clinically applied, graft positioning protocol led to large deviations from intact knee kinematics and tibiofemoral articular behavior. We, furthermore, found clear biomechanical indications (instability and aberrant cartilage stresses) that ACL deficient knee may stimulate the onset or progression of OA (due to instability and aberrant cartilage stresses). This concurs with findings in the literature indicating a correlation between ACL injury and OA [11]–[14], [50].

The changes in the knee joint laxity due to the ACL deficiency observed in our simulations have been confirmed by the studies of Beynnon et al. (2002) and Liubarbara et al. (2007) who also reported an increase in tibial anterior and medial laxities and knee external rotational laxity [51], [52]. The kinematics prediction of the intact and ACL-deficient knee models during a full gait cycle is also in a good agreement with previous studies [50], [53]–[57]. Our calculated alterations in knee kinetics and force in tibiofemoral ligaments (PCL, LCL and MCL) due to the ACL rupture, were similar to the findings of Shelburne et al. (2004) [50].

Previously, studies reported an increased risk of OA development in untreated ACL rupture. For instance, Louboutin et al. reported a 60% increase risk of OA (after 10 years) for ACL-ruptured knees [4]. Our result indicates that, not only the untreated ACL-ruptured knee, but also non-optimally reconstructed knees,

can undergo larger contact pressure and also different contact pressure patterns than the intact knee joint. The larger contact pressure at tibial cartilage are shown to have a direct influence on OA development [11]. Moreover, the change in contact pressure pattern and as a result in peak contact pressure location can bring regions of tibial cartilage with a smaller thickness into contact, which is also believed to influence the OA development [58], [59].

For an optimal single bundle reconstruction, similar graft positioning parameters (insertion sites and graft fixation tension) were found for hamstring and patellar tendon grafts. Isometric positioning with a graft fixation tension of 40 N revealed the best kinematic (laxity) recovery for hamstring and patellar tendon grafts. With a quadriceps graft, anatomical positioning with 80 N graft fixation tension was required for the best outcomes. The reason for such differences might be sought in the larger stiffness of hamstring and patellar tendon, comparing with quadriceps tendon. Although both optimal single and double bundle reconstructions improved the knee joint biomechanics during gait cycle, optimal double bundle grafted knee indicated even better rotational improvement than the optimal single bundle reconstructions.

There were several limitations to this study. First, in-vitro cadaveric experiments were performed in this study, with no muscle activation involvement. Hence, the compensation mechanism of the quadriceps activation in ACL deficient patients was not considered. Therefore, in this respect the loading conditions divert from reality. However, as ACL-reconstruction is meant to recover a passive structure (ligament) function, passive experiments can sufficiently provide a realistic insight for assessing the biomechanical differences in different cases. Hence, we assume that if we are able to recover the soft-tissue stability envelope by optimizing ACL reconstruction, patients do not require to apply any muscle activation compensation strategies.

Another limitation was the fact that the detailed computational model was developed, validated and utilized based on a single cadaveric specimen. It is, however, emphasized that this is a methodological study as a novel approach to treat the ACL-ruptured knees in also a subject-specific manner. Consequently, for each patient, the proposed workflow can be followed. It is worth mentioning that the completion of this workflow for each patient requires almost one month.

Currently, investigations are underway to generate and optimize patient specific models in a much faster manner.

In this study, in order to simulate the ACL reconstruction procedure, the knee was positioned in 30° of flexion which was shown to have limited advantages over other flexions [45]. The workflow proposed in the current study is capable of implementing other flexion angles rather than 30° for graft insertion. In that case, a different graft fixation force combined with flexion might be expected as shown by Arnold et al. (2005) [60].

5. Conclusion

In conclusion, our results suggest that based on the surgeon's selected graft type (hamstring tendon, patellar tendon or quadriceps tendon) or surgery technique (single bundle vs. double bundle) numerical optimizations can be implemented prior to the surgery to find the most optimal graft positioning surgical parameters (graft insertion sites and fixation tension). For this purpose AP laxity tests (i.e. Lachman and Drawer tests) are required on the healthy knee (contralateral joint) as the control and on the deficient knee as the target joint for the optimization. With optimal graft positioning parameters, following the proposed workflow in this study, any of the single bundle graft types and surgical techniques (single vs. double-bundle) may be used to acceptably recover the intact knee joint biomechanical behavior.

Acknowledgments

This study was a part of BioMechTools project (ERC-2012-ADG LS7), received funding from the European Research Council under the European Union's Seventh Framework Program (FP/2007-2013) / ERC Grant Agreement n. 323091.

References

- [1] I. Holm, B. E. Øiestad, M. A. Risberg, and A. K. Aune, “No Difference in Knee Function or Prevalence of Osteoarthritis After Reconstruction of the Anterior Cruciate Ligament With 4-Strand Hamstring Autograft Versus Patellar Tendon – Bone Autograft,” pp. 448–454, 2010.
- [2] C. Hui *et al.*, “Fifteen-Year Outcome of Endoscopic Anterior Cruciate Ligament Reconstruction With Patellar Tendon Autograft for ““ Isolated ”” Anterior Cruciate Ligament Tear,” *Am. J. Sports Med.*, no. C, pp. 89–98, 1994.
- [3] A. R. Æ. M. S. Kuster, “Function , osteoarthritis and activity after ACL-rupture : 11 years follow-up results of conservative versus reconstructive treatment,” pp. 442–448, 2008.
- [4] H. Louboutin *et al.*, “Osteoarthritis in patients with anterior cruciate ligament rupture : A review of risk factors,” *Knee*, vol. 16, no. 4, pp. 239–244, 2009.
- [5] S. L. Keays, P. A. Newcombe, J. E. Bullock-saxton, M. I. Bullock, and A. C. Keays, “Factors Involved in the Development of Osteoarthritis After Anterior Cruciate Ligament Surgery,” pp. 455–463.
- [6] R. Mihelic, H. Jurdana, Z. Jotanovic, T. Madjarevic, and A. Tudor, “Long-term results of anterior cruciate ligament reconstruction : a comparison with non-operative treatment with a follow-up of 17 – 20 years,” pp. 1093–1097, 2011.
- [7] A. P. C. Study, “Prevalence of Tibiofemoral Osteoarthritis 15 Years After Nonoperative Treatment of Anterior Cruciate Ligament Injury,” pp. 1717–1725, 2008.
- [8] J. Struwer and T. M. Frangen, “Knee function and prevalence of osteoarthritis after isolated anterior cruciate ligament reconstruction using bone-patellar tendon-bone graft : long-term follow-up,” pp. 171–177, 2012.

- [9] R. A. Magnussen, A. A. Mansour, J. L. Carey, and K. P. Spindler, "Meniscus Status at ACL Reconstruction is Associated with the Presence of Radiographic Signs of Osteoarthritis at 5–10 Year Follow-up: A Systematic Review," *J. Knee Surg.*, vol. 22, no. 4, pp. 347–357, 2009.
- [10] H. F. Hart *et al.*, "Knee kinematics and joint moments during gait following anterior cruciate ligament reconstruction : a systematic review and meta-analysis," pp. 1–17, 2015.
- [11] F. Guilak, "Biomechanical factors in osteoarthritis," *Best Pract. Res. Clin. Rheumatol.*, vol. 25, no. 6, pp. 815–823, 2011.
- [12] K. D. Brandt, E. L. Radin, P. A. Dieppe, and L. van de Putte, "Yet more evidence that osteoarthritis is not a cartilage disease," *Ann. Rheum. Dis.*, vol. 65, pp. 1261–1265, 2006.
- [13] J. A. Buckwalter, "Osteoarthritis and articular cartilage use, disuse, and abuse: experimental studies.," *J. Rheumatol. Suppl.*, vol. 43, pp. 13–15, 1995.
- [14] T. M. Griffin and F. Guilak, "The role of mechanical loading in the onset and progression of osteoarthritis.," *Exerc. Sport Sci. Rev.*, vol. 33, no. 4, pp. 195–200, 2005.
- [15] A. Tp, S. Koo, and S. Sf, "Morphology and Osteoarthritis of the Knee," pp. 95–101, 2009.
- [16] T. P. Andriacchi, "Knee Kinematics, Cartilage Morphology, and Osteoarthritis after ACL Injury," *Med. Sci. Sport. Exerc.*, pp. 215–222, 2008.
- [17] T. P. Andriacchi, P. L. Briant, S. L. Beville, and S. Koo, "Rotational Changes at the Knee after ACL Injury Cause Cartilage Thinning," no. 442, pp. 39–44, 2006.
- [18] A. Hosseini, P. Lodhia, S. K. Van De Velde, P. D. Asnis, B. Zarins, and T. J. Gill, "Tunnel position and graft orientation in failed anterior cruciate ligament reconstruction : a clinical and imaging analysis," pp. 845–852, 2012.

- [19] E. S. Abebe *et al.*, “The effects of femoral graft placement on in-vivo knee kinematics after anterior cruciate ligament reconstruction,” *J. Biomech.*, vol. 44, no. 5, pp. 924–929, 2011.
- [20] V. Musahl *et al.*, “the Anatomical Footprint and Isometric Positions Effect on Kinematics of the Anterior Cruciate Ligament – Reconstructed Knee,” pp. 712–718, 2005.
- [21] F. Rayan *et al.*, “Review of evolution of tunnel position in anterior cruciate ligament reconstruction,” vol. 6, no. 2, pp. 252–262, 2015.
- [22] D. Biggs, P. Walker, and L. Jp, “Isometric Placement of a Synthetic ACL Graft,” no. 2288, p. 2288, 2012.
- [23] S. D. Abramowitch, C. D. Papageorgiou, J. D. Withrow, T. W. Gilbert, and S. L. Woo, “The effect of initial graft tension on the biomechanical properties of a healing ACL replacement graft : a study in goats,” vol. 21, 2003.
- [24] S. Yoshiya and T. Jack, “Graft tension in anterior cruciate reconstruction ligament,” *Am. J. Sports Med.*, vol. 15, no. 5, pp. 464–470, 1986.
- [25] S. G. Kim, H. Kurosawa, K. Sakuraba, H. Ikeda, and S. Takazawa, “The effect of initial graft tension on postoperative clinical outcome in anterior cruciate ligament reconstruction with semitendinosus tendon,” *Arch. Orthop. Trauma Surg.*, vol. 126, no. 4, pp. 260–264, 2006.
- [26] F. H. Fu, P. H. Araujo, and A. Lin, “Commentary & Perspective,” vol. 121, pp. 10–11, 2011.
- [27] J. Dargel, M. Gotter, K. Mader, D. Pennig, J. Koebke, and R. Schmidt-Wiethoff, “Biomechanics of the anterior cruciate ligament and implications for surgical reconstruction,” *Strateg. Trauma Limb Reconstr.*, vol. 2, no. 1, pp. 1–12, 2007.
- [28] P. Suomalainen, T. Järvelä, A. Paakkala, P. Kannus, and M. Järvinen, “Double-bundle versus single-bundle anterior cruciate ligament

reconstruction: A prospective randomized study with 5-year results,” *Am. J. Sports Med.*, vol. 40, no. 7, pp. 1511–1518, 2012.

[29] C. F. van Eck *et al.*, “‘Anatomic’ Anterior Cruciate Ligament Reconstruction: A Systematic Review of Surgical Techniques and Reporting of Surgical Data,” *Arthrosc. J. Arthrosc. Relat. Surg.*, vol. 26, no. 9, pp. S2–S12, 2010.

[30] P. B. Lewis, A. D. Parameswaran, J. H. Rue, and B. R. B. Jr, “Systematic Review of Single-Bundle Anterior Cruciate Ligament Reconstruction Outcomes A Baseline Assessment for Consideration of Double-Bundle Techniques,” vol. 36, no. 10, 2008.

[31] K. K. Middleton, T. Hamilton, J. J. Irrgang, J. Karlsson, C. D. Harner, and F. H. Fu, “Anatomic anterior cruciate ligament (ACL) reconstruction : a global perspective . Part 1,” pp. 1467–1482, 2014.

[32] G. Cerulli, G. Placella, E. Sebastiani, M. M. Tei, A. Speziali, and F. Manfreda, “ACL Reconstruction: Choosing the Graft.,” *Joints*, vol. 1, no. 1, pp. 18–24, 2013.

[33] D. E. Bonasia and A. Amendola, “Graft choice in ACL reconstruction,” *Knee Jt. Surg. Tech. Strateg.*, vol. 9782287993, no. 12, pp. 173–181, 2012.

[34] E. Pena, M. A. Martinez, B. Calvo, D. Palanca, and M. Doblare, “A finite element simulation of the effect of graft stiffness and graft tensioning in ACL reconstruction,” *Clin. Biomech.*, vol. 20, no. 6, pp. 636–644, 2005.

[35] H. Y. Kim, Y. J. Seo, H. J. Kim, T. Nguyenn, N. S. Shetty, and Y. S. Yoo, “Tension changes within the bundles of anatomic double-bundle anterior cruciate ligament reconstruction at different knee flexion angles: A study using a 3-dimensional finite element model,” *Arthrosc. - J. Arthrosc. Relat. Surg.*, vol. 27, no. 10, pp. 1400–1408, 2011.

[36] K. S. Halonen, M. E. Mononen, J. Töyräs, H. Kröger, A. Joukainen, and R. K. Korhonen, “Optimal graft stiffness and pre-strain

restore normal joint motion and cartilage responses in ACL reconstructed knee,” *J. Biomech.*, vol. 49, no. 13, pp. 2566–2576, 2016.

[37] H. Naghibi Beidokhti, D. Janssen, S. Van De Groes, J. Hazrati, T. Van Den Boogaard, and N. Verdonschot, “The influence of ligament modelling strategies on the predictive capability of finite element models of the human knee joint,” *J. Biomech.*, vol. 65, pp. 1–11, 2017.

[38] H. Pillet *et al.*, “Femur , tibia and fi bula bone templates to estimate subject-speci fi c knee ligament attachment site locations,” *J. Biomech.*, vol. 49, no. 14, pp. 3523–3528, 2016.

[39] M. A. Baldwin, J. E. Langenderfer, P. J. Rullkoetter, and P. J. Laz, “Development of subject-specific and statistical shape models of the knee using an efficient segmentation and mesh-morphing approach,” *Comput. Methods Programs Biomed.*, vol. 97, pp. 232–240, 2010.

[40] M. S. H. Frank R. Noyes, David L. Bulter, Edward S. Grood, Ronald F. Zernicke, “Biomechanical Analysis of Human Repairs Ligament Grafts used in,” *J. bone Jt. Surg.*, pp. 344–352, 1984.

[41] R. West and C. Harner, “Graft selection in anterior cruciate ligament reconstruction.,” *J. Am. Acad. Orthop. Surg.*, vol. 13, no. 3, pp. 197–207, 2005.

[42] R. H. Shani, E. Umpierrez, M. Nasert, E. A. Hiza, and J. Xerogeanes, “Biomechanical Comparison of Quadriceps and Patellar Tendon Grafts in Anterior Cruciate Ligament Reconstruction,” *Arthrosc. J. Arthrosc. Relat. Surg.*, vol. 32, no. 1, pp. 1–5, 2015.

[43] D. L. Hamner, C. H. Brown, M. E. Steiner, a T. Hecker, and W. C. Hayes, “Hamstring tendon grafts for reconstruction of the anterior cruciate ligament: biomechanical evaluation of the use of multiple strands and tensioning techniques.,” *J. Bone Joint Surg. Am.*, vol. 81, no. 4, pp. 549–557, 1999.

[44] L. Blankevoort, J. H. Kuiper, R. Huiskes, and H. J. Grootenboer, “Articular contact in a three-dimensional model of the knee,” *J. Biomech.*, vol. 24, no. 11, pp. 1019–1031, 1991.

- [45] T. Mae, K. Shino, and K. Nakata, "Optimization of graft fixation at the time of anterior cruciate ligament reconstruction. Part II: effect of knee flexion angle.," *Am. J. Sports Med.*, vol. 36, no. 6, pp. 1094–1100, 2008.
- [46] T. Mae, K. Shino, K. Nakata, Y. Toritsuka, H. Otsubo, and H. Fujie, "Optimization of Graft Fixation at the Time of Anterior Cruciate Ligament Reconstruction Part I : Effect of Initial Tension," *Am. J. Sports Med.*, vol. 36, no. 6, pp. 1087–1093, 2008.
- [47] Y. Hoshino *et al.*, "The effect of graft tensioning in anatomic 2-bundle ACL reconstruction on knee joint kinematics," *Knee Surgery, Sport. Traumatol. Arthrosc.*, vol. 15, no. 5, pp. 508–514, 2007.
- [48] A. Rohlmann *et al.*, "Standardized Loads Acting in Knee Implants," vol. 9, no. 1, 2014.
- [49] *ASTM F3141-15, Standard Guide for Total Knee Replacement Loading Profiles*. West Conshohocken, PA: ASTM International, 2016.
- [50] T. P. Andriacchi, A. Mundermann, R. L. Smith, E. J. Alexander, C. O. Dyrby, and S. Koo, "A Framework for the in-vivo Pathomechanics of Osteoarthritis at the Knee," *Ann. Biomed. Eng.*, vol. 32, no. 3, pp. 447–457, 2004.
- [51] D. Liu-barba and M. L. Hull, "Compressive Load in Intact and ACL-Deficient Knees : A Cadaveric Study," *J. Biomech. Eng.*, vol. 129, no. December, pp. 818–824, 2007.
- [52] B. D. Beynon, B. C. Fleming, R. Labovitch, and B. Parsons, "Chronic anterior cruciate ligament deficiency is associated with increased anterior translation of the tibia during the transition from non-weightbearing to weightbearing," *J. Orthop. Res.*, vol. 20, pp. 332–337, 2002.
- [53] H. Wang, J. E. Fleischli, N. N. Zheng, N. Carolina, and N. Carolina, "Transtibial Versus Anteromedial Portal Technique in Single-Bundle Anterior Cruciate Ligament Reconstruction Outcomes of Knee

Joint Kinematics During Walking,” pp. 1847–1856, 2013.

[54] M. Kozanek *et al.*, “Tibiofemoral kinematics and condylar motion during the stance phase of gait,” *J. Biomech.*, vol. 42, no. 12, pp. 1877–1884, 2009.

[55] H. Wang, T. Chen, P. Torzilli, R. Warren, and S. Maher, “Dynamic contact stress patterns on the tibial plateaus during simulated gait: A novel application of normalized cross correlation,” *J. Biomech.*, vol. 47, no. 2, pp. 568–574, 2014.

[56] K. B. Shelburne, M. R. Torry, and M. G. Pandy, “Muscle, Ligament, and Joint-Contact Forces at the Knee during Walking,” *Med. Sci. Sport. Exerc.*, no. 3, 2005.

[57] L. Zhang, T. J. Limbird, and J. M. Minorik, “Six degrees-of-freedom kinematics of ACL deficient knees during locomotion * compensatory mechanism,” *Gait Posture*, vol. 17, pp. 34–42, 2003.

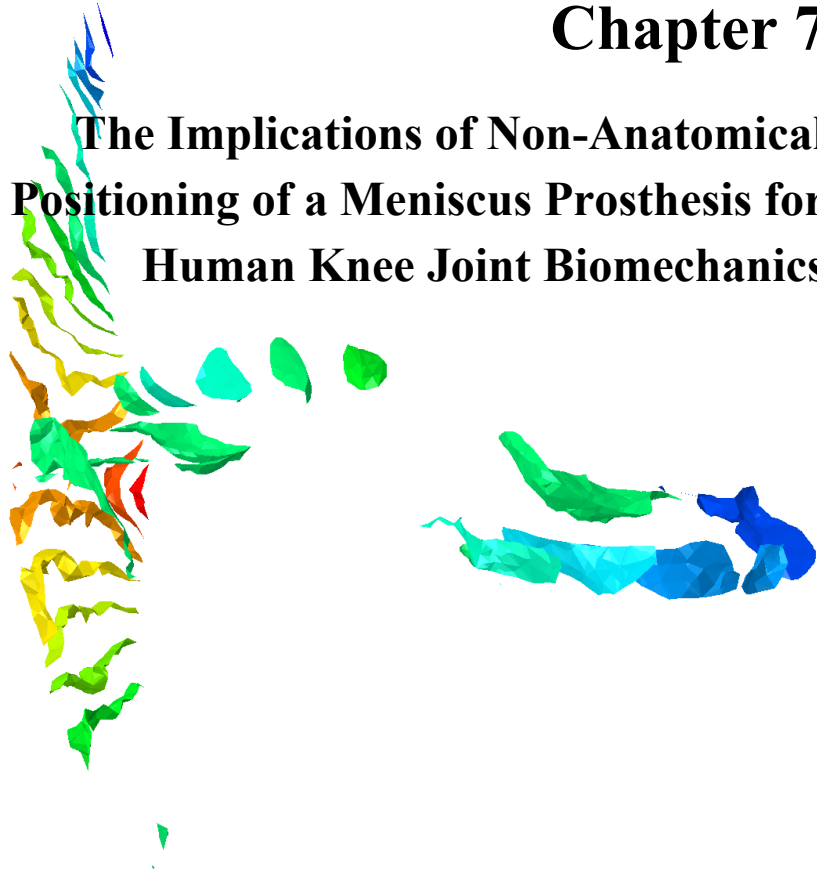
[58] S. K. Van De Velde *et al.*, “NIH Public Access,” *Arthritis Rheumatol.*, vol. 60, no. 12, pp. 3693–3702, 2010.

[59] Papannagari, N. P. Pathare, L. E. DeFrate, and T. J. Gill, “Anterior Cruciate Ligament Deficiency Alters the In-vivo Motion of the Tibiofemoral Cartilage Contact Points in Both the Anteroposterior and Mediolateral Directions,” *J. bone Jt. Surg.*, pp. 1826–1834, 2006.

[60] M. P. Arnold, N. Verdonshot, and A. Van Kampen, “The Normal Anterior Cruciate Ligament as a Model for Tensioning Strategies in Anterior Cruciate Ligament Grafts,” *Am. J. Sports Med.*, vol. 33, no. 2, pp. 277–283, 2005.

Chapter 7

The Implications of Non-Anatomical Positioning of a Meniscus Prosthesis for Human Knee Joint Biomechanics



Naghbi Beidokhti, H., Janssen, D., Van Minnen, B., Van den Boogaard, T., Van Tienen, T., Verdonchot, N., 2018. Scientific Reports. Under review.

1. Introduction

Medial meniscus injuries are among the most common knee-related injuries. When the medial meniscus cannot function properly due to severe damage or degeneration it might be partially resected (partial meniscectomy). The more meniscus tissue is resected the higher the chance on OA [1]. This increase of OA may lead to pain and functional impairment. When most of the meniscus is absent, replacement with a meniscal allograft may be an option. After transplantation the pain is reduced and patients typically have an improved quality of life [2]. However, problems related to the availability and sizing of allografts has driven the search for an alternative treatment [3]–[5]. An on-the-shelf meniscus prosthesis may overcome the shortcomings of meniscal allografts.

For a meniscus prosthesis, the geometry, material properties, fixation type, and prosthesis positioning are crucial factors, which need to be assessed thoroughly before clinical implementation. The influence of geometrical specifications of the medial meniscus prosthesis [6]–[8] and the material properties of the prosthesis [9]–[11] on the knee biomechanics have previously been studied, as have different meniscus prosthesis fixation types [12], [13].

In our lab, a novel anatomically shaped, polycarbonate urethane total meniscus prosthesis was recently developed using statistical shape modelling based on 35 subjects [14]. The composite structure of the meniscus prosthesis allows for flexible articulations, while simultaneously constraining excessive prosthesis deformation. Several studies have been performed to improve the geometry, material properties, and fixation technique of the meniscus prosthesis [14]–[16].

In analogy with meniscus allograft transplantation, positioning of a meniscus prosthesis may influence the biomechanical behaviour in the knee [17]. In clinical practise the success of the prosthesis, therefore, will depend on surgical factors such as the intra-operative positioning of the prosthesis. Wajsfisz et al. introduced a new arthroscopic technique for meniscal transplantation [18]. With their technique they could achieve a placement accuracy of about $\pm 2\text{mm}$ in anterior-posterior and $\pm 4\text{mm}$ in medial-lateral directions. However, the influence of the implantation offset on joint biomechanics was not reported in their study. Sekaran et al. assessed the impact of posterior attachment dislocation of autografts on the contact pressure on the medial tibia plateau in a cadaveric study [19]. Their results

revealed an alteration in contact pressures in a simplified loading condition, when the posterior horn of the native meniscus was fixated posteriorly. While the influence of the shifted placement of an allograft has previously been investigated [18], [19], a study on the significance of accurate meniscus prosthesis positioning on knee joint biomechanics is still missing.

The aim of this study was therefore to assess the implications of positional changes of the medial meniscus prosthesis. The outcome of this study may provide a better insight into the possible consequences of meniscus prosthesis positioning errors for the patient and the prosthesis functionality. This study may also open a discussion for possible risks of OA due to the mechanical factors induced by implantation errors.

2. Methods

All methods were carried out in accordance with the relevant guidelines and regulations. A pair of fresh frozen cadaveric knees, with no sign of injury and surgery was selected to follow the workflow of this study, as schematically illustrated in Figure 1. The specimens were received from the Anatomy Department of Radboud University Medical Centre with a permission statement for experimental use. After checking the symmetry of the knees (Appendix B), the left knee was used for in-vitro implantation experiment. The contralateral right knee was used for developing a detailed validated FE model [20]. The in-vitro experiment on the left knee was simulated with the validated FE model of the right knee, and the FE model predictions were further validated against experimental measurements. In addition to the anatomically positioned meniscus prosthesis, different non-anatomical prosthesis positioning was applied in the FE model. Eventually, a stance gait cycle was simulated with the intact knee model, anatomically positioned and non-anatomically positioned prostheses, to assess the influence of different implantations on the biomechanics of the joint and prosthesis.

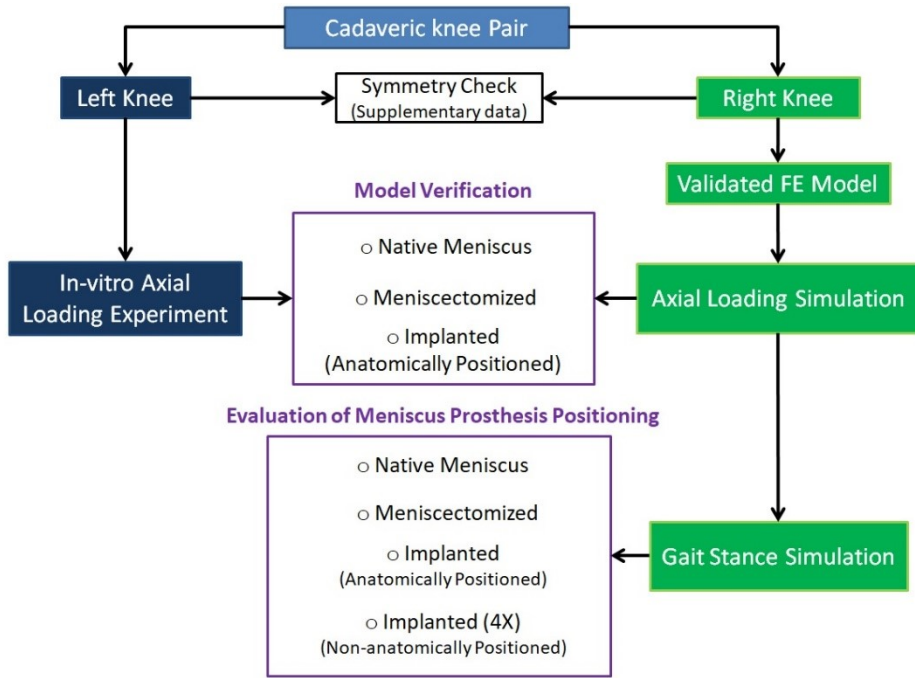


Figure 1: Schematic illustration of the workflow of the current study

2.1. In-vitro axial loading experiment:

The left knee was used for in-vitro implantation experiments (Figure 2-a). First, small tantalum markers (diameter: 1mm) were injected into the femur (three markers) and tibia (three markers). Next, the joint with the markers injected were CT-scanned in order to define the relative position of the markers with respect to the bony segment. Tantalum beads (diameter: 0.5 mm) were also injected into the native meniscus and the meniscus prosthesis in the anterior, posterior and middle region (Figure 2-b). During the experiment, the positions of the markers were captured using Roentgen Stereophotogrammetric Analysis (RSA; Figure 2-a) and in-house developed scripts (MATLAB R2013a, Natick, MA).

The joint was prepared to be positioned in a mechanical testing machine (MTS, MTS Systems Corporation, Eden Prairie, MN, USA) in an extended position. A calibrated pressure sensitive film (Type 4011, Tekscan Inc., Boston, MA, USA) was inserted from the anterior side underneath the medial meniscus by an experienced knee surgeon. An axial load of 1000 N was applied to the femur, and

the pressure map was recorded after 30s of applying the load. The medial meniscus was removed by the surgeon to replicate the total medial meniscectomy, and the same loading condition was applied to the joint. Eventually the meniscus prosthesis was inserted in the joint space using bone screw fixations at the centre of the anterior and posterior attachments of the excised native meniscus. The load was re-applied to the implanted knee while the contact pressure was recorded.

Based on the RSA techniques the medial-lateral (ML) and anterior-posterior (AP) motions of the injected titanium beads were calculated using in-house developed MATLAB scripts as indications for the native meniscus and meniscus prosthesis deformation at different regions. Eventually, the implanted joint was CT-scanned after the experiment for an accurate prosthesis positioning in the FE model, following the fixation screw holes in tibia.

2.2. Axial loading simulation (Finite Element Modelling of in-vitro experiment):

A detailed FE model of the right knee was developed in Abaqus v6.13 (Pawtucket, RI, USA) based on the laxity experiments. The FE model was subsequently validated based on validation tests against measured kinematics and contact pressure at tibiofemoral articular surfaces (Figure 2-d) [20], [21].

In the FE model, cartilage was modelled as nonlinear Neo-Hookean hyperelastic isotropic, in which the strain energy function ψ is described as a function of the first invariant of the left Cauchy-Green deformation tensor (I_1) and the elastic volume ratio (J):

$$\psi = C_{10}(I_1 - 3) + \frac{1}{2D}(J - 1)^2 \quad (1)$$

In this equation, C_{10} and D are the Neo-Hookean constant and the inverse of the bulk modulus, respectively, which were calculated based on experimental compressive tests on 11 cadaveric knees [22] ($C_{10}=0.86$ MPa and $D=0.048$ MPa⁻¹).

Menisci were modeled as transversely isotropic with circumferentially oriented fibers, implementing the Holzapfel-Gasser-Ogden (HGO) hyperelastic model [23]. The strain energy function ψ is described as a function of Neo-Hookean

terms, representing the non-collagenous matrix, and $\bar{I}_{4(\alpha\alpha)}$, pseudo-invariants of \bar{C} and A_α (directions of the fibers in the reference configuration):

$$\psi = C_{10}(\bar{I}_1 - 3) + \frac{1}{2D} \left(\frac{(J)^2 - 1}{2} - \ln(J) \right) + \frac{k_1}{2k_2} \{ \exp[k_2 \langle \bar{E}_\alpha \rangle^2] - 1 \} \quad (2)$$

With:

$$\bar{E}_\alpha = \kappa(\bar{I}_1 - 3) + (1 - 3\kappa)(\bar{I}_{4(\alpha\alpha)} - 1) \quad (3)$$

Constants k_1 and k_2 are material parameters and κ ($0 \leq \kappa \leq \frac{1}{3}$) describes the level of dispersion in the fiber directions. When $\kappa=0$, all fibers are perfectly aligned, and $\kappa = \frac{1}{3}$ describes an isotropic material [24]. The meniscus prosthesis materials (polycarbonate urethane, Bionates grade II 80A and 75D, DSM Biomedical, Geleen, Netherlands) were modeled as isotropic neo-Hookean materials for the prosthesis body ($C_{10}=1.93$ MPa and $D=0.001$ MPa⁻¹) and elastic material ($E=71$ MPa, $\nu=0.48$) for the stiff meniscus core, based on the material specifications.

The in-vitro experimental condition was replicated in the FE model of the right knee, following the initial joint orientation measured using RSA. In order to validate the prediction of the FE model, the contact pressure and contact area at the medial tibia plateau was compared with the experimentally measured values in three cases (native, meniscectomy, implanted). Moreover, the motions of the native meniscus and the meniscal prosthesis were compared in the FE model (Figure 2-c).

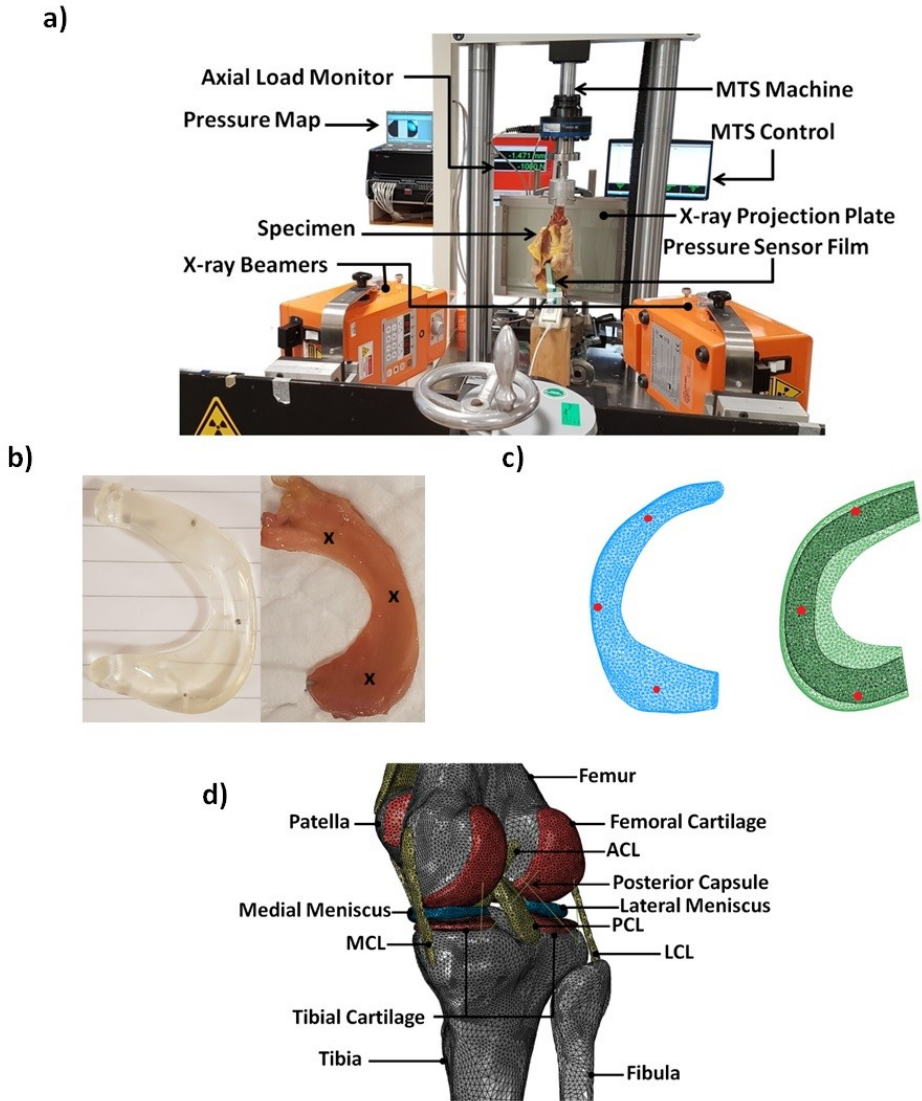


Figure 2: In-vitro experimental set-up (axial loading) to assess the biomechanical response of the cadaveric left knee (a), and the motion of the injected titanium beads could be quantified using RSA techniques in the native meniscus and meniscal prosthesis (b) which were compared with the representative nodes (c) in the detailed validated FE model (d) of the contralateral knee (right knee).

2.3. Gait stance simulation with different meniscus prosthesis positioning:

To investigate the effect of prosthesis malpositioning, prosthesis was then positioned 2mm anteriorly, 2mm posteriorly, 4mm laterally and 4mm medially, according to the reported positioning errors [18]. A full stance phase of straight walking cycle was simulated with the knee model with native meniscus (intact knee), the meniscectomized knee, the anatomically positioned prosthesis, and the four different shifted non-anatomical implantations (anterior, posterior, medial and lateral), with a dynamic explicit solver [25]. The loads were adjusted based on the normalized in-vivo loads produced from eight subjects, in the Orthoload database [26], and the weight of the cadaveric subject, following the ASTM International standard guide (F3141-15) [27]. The knee kinematics, the displacement of the native meniscus and meniscal prosthesis, the contact variables at tibial plateau, and the force at the attachment of the meniscal prosthesis were compared to assess the influence of prosthesis positioning on the knee joint biomechanics.

3. Results

3.1. Model verification (In-vitro experiment versus Finite element simulation:

In the axial loading case, the computational (FE) model could predict the changes in the contact pressure pattern comparable to the experimental measurement at the medial tibial plateau (Figure 3). As Figure 4 illustrates, a similar trend was seen between the experimental measurement and computational prediction for contact area at the medial tibial cartilage.

The motion of the native meniscus and meniscal prosthesis under axial loading, as measured during the experiment and calculated in the FE model, are shown in Table 1. The FE model could predict the motions of the markers in both medial and anterior directions, with a reasonable agreement with experimental measurements, for both the native meniscus and the prosthesis.

Table 1: The medial and anterior displacements of the injected tantalum markers in native meniscus and meniscus prosthesis and in the FE model, under axial loading.

		Medial displacement [mm]				Anterior displacement [mm]			
		Anterior marker	Middle marker	Posterior marker	Average	Anterior marker	Middle marker	Posterior marker	Average
Native Meniscus	Experiment	1.02	1.40	0.61	1.01	-0.89	-1.30	-0.86	-1.02
	FE Model	0.64	0.67	1.07	0.79	-0.43	-0.85	-1.89	-1.06
Meniscus Prosthesis	Experiment	0.60	0.63	0.27	0.50	0.63	0.38	0.31	0.44
	FE Model	0.49	1.66	0.39	0.85	2.80	1.85	0.48	1.71

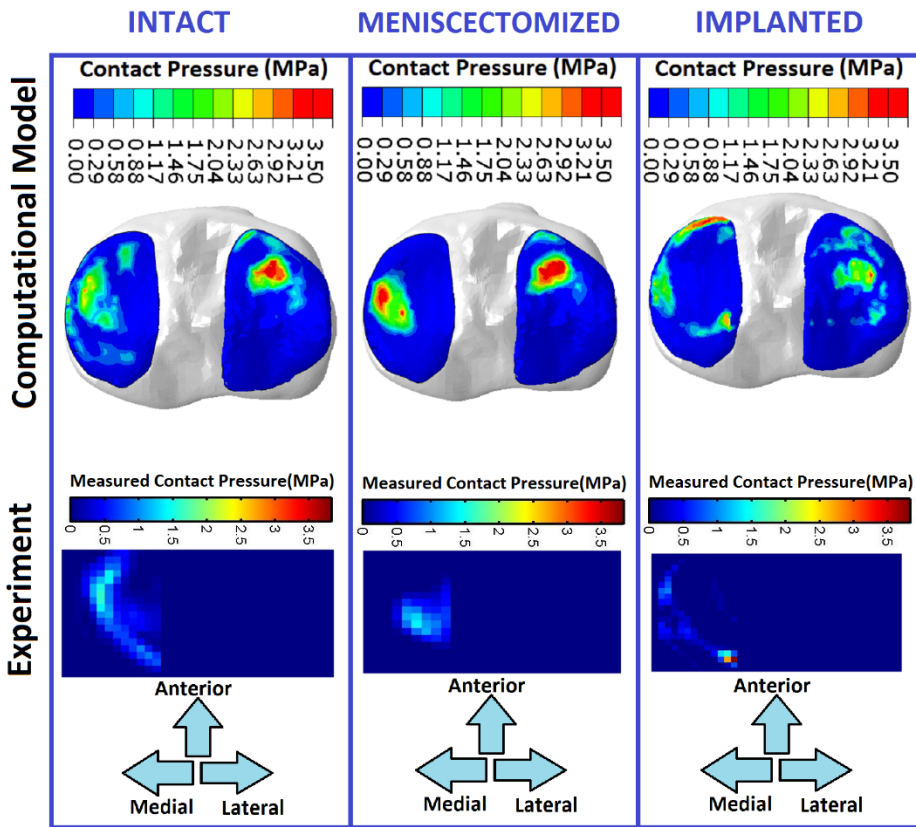


Figure 3: The contact pressure at tibial cartilage predicted by the FE model of the right knee (top) and measured during axial loading experiment (bottom) on the left knee, for the knees with native meniscus, total medial meniscectomy and meniscus prosthesis. In order to facilitate the comparison, the experimental pressure maps were horizontally flipped.

3.2. Evaluation of meniscus prosthesis positioning (Computational outcomes)

Knee kinematics: The FE model demonstrated that the meniscectomized knee joint had an increased medial-lateral translation (max. 4 mm) and anterior-posterior translation (max. 11 mm), both at the load acceptance phase (Figure 5). Valgus rotation was reduced by meniscectomy, as shown in Figure 6. Implantation at the anatomical position could partially recover the intact knee joint kinematics (Figure 5 and 6). A non-anatomical positioned prosthesis influenced the anterior-posterior motions by less than 3.5 mm, and the medial-lateral translations by less than 4 mm during the stance phase. A maximum alteration of 2° in valgus-varus and 6° in internal-external knee rotations was illustrated by non-anatomical positioning of the prosthesis.

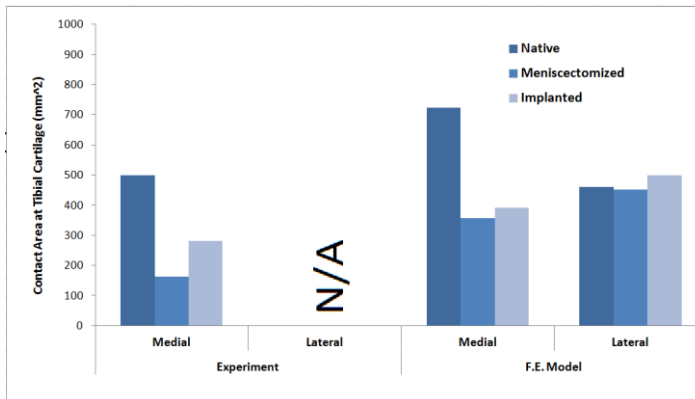


Figure 4: Articular contact area on tibial plateau (medial) during the axial loading experiment (left), and the calculated contact area in the FE model on both medial and lateral tibial plateaus in axial loading simulation.

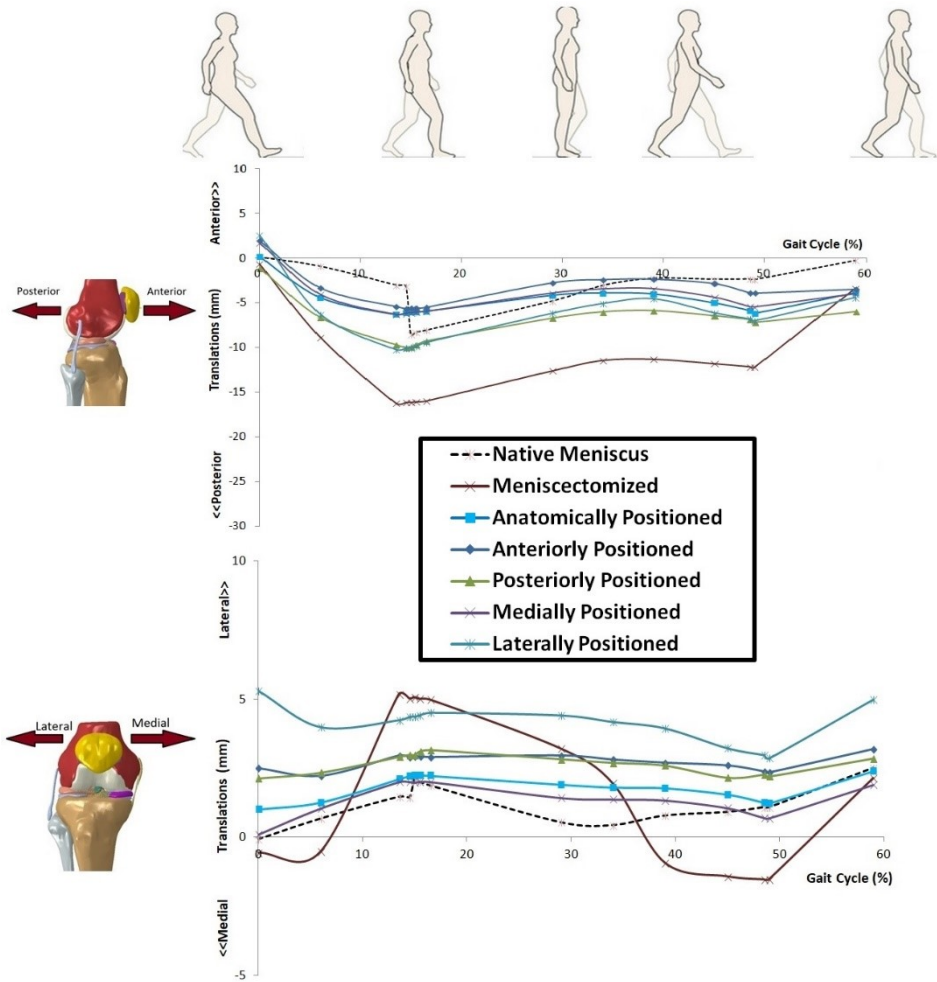


Figure 5: Translational (Anterior-posterior and medial-lateral) kinematics of the knee joint during a complete gait stance phase simulation, for the knees with native meniscus, total meniscectomy, anatomically positioned meniscus prosthesis, and four non-anatomically (anteriorly, posteriorly, medially and laterally) positioned meniscus prosthesis.

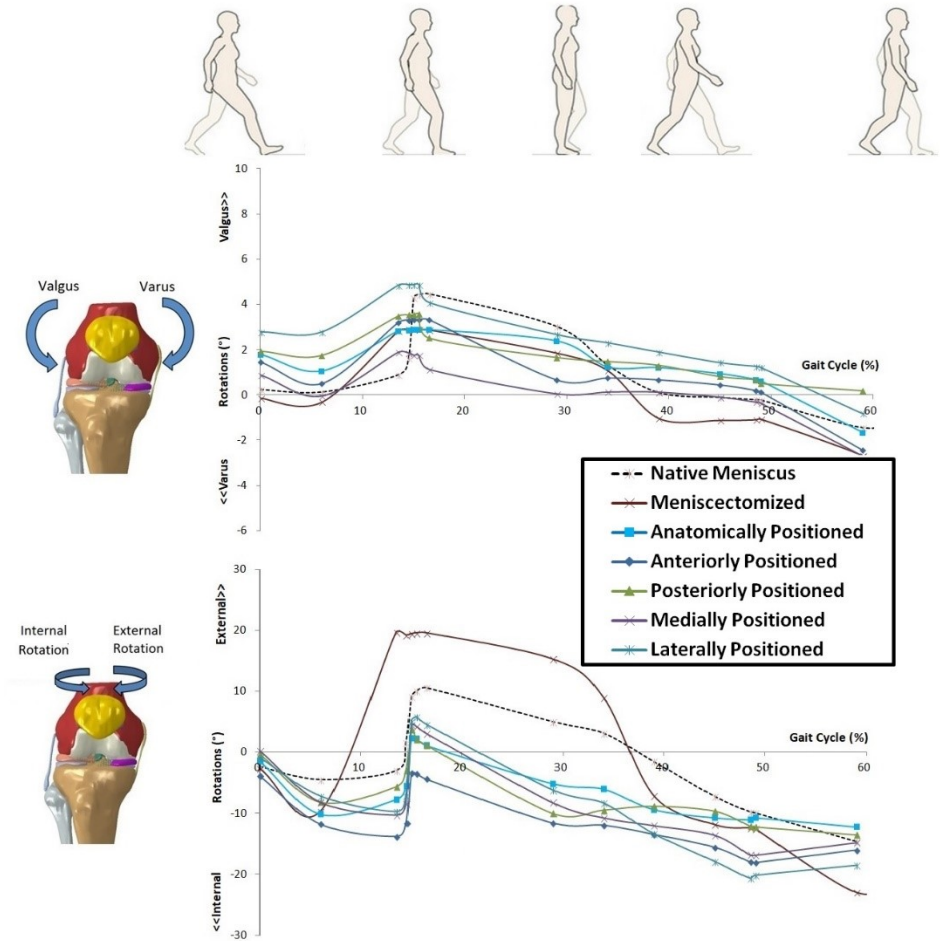


Figure 6: Rotational (valgus-varus and internal external) kinematics of the knee joint during a complete gait stance phase simulation, for the knees with native meniscus, total meniscectomy, anatomically positioned meniscus prosthesis, and four non-anatomically (anteriorly, posteriorly, medially and laterally) positioned meniscus prosthesis.

Meniscal prosthesis motion: Comparing the meniscal prosthesis displacement in coronal plane (ML), the non-anatomical lateral positioning caused the largest prosthesis motion during the whole stance phase (Figure 7). The posteriorly positioned prosthesis increased the displacement in the coronal plane, in the anterior region (30% to 60% of gait cycle) and posterior region (14% to 30% of gait cycle). The anteriorly positioned prosthesis resulted in a large motion in the coronal plane in the posterior region in the early stance (0% to 16% of gait cycle).

The medially positioned prosthesis showed the largest prosthesis motion in the sagittal plane (AP) at the end of the stance phase (30% to 50% of the gait cycle), maximally by ~4mm (Figure 7).

Contact variables: In comparison with the intact knee, total meniscectomy increased the peak contact pressure at medial and lateral plateau, respectively, by 1.4 MPa and 0.3 MPa, during the stance phase simulation. With the anatomically positioned meniscal prosthesis, the peak contact pressure decreased with an average difference of 0.04 MPa (medial plateau) and 0.03 MPa (lateral plateau) relative to the intact knee. While the peak contact pressure was revealed to be less sensitive to an anterior or posterior prosthesis position, a lateral or medial position led to a slightly larger peak contact pressure, respectively, at both the lateral and medial plateau (Figure 8).

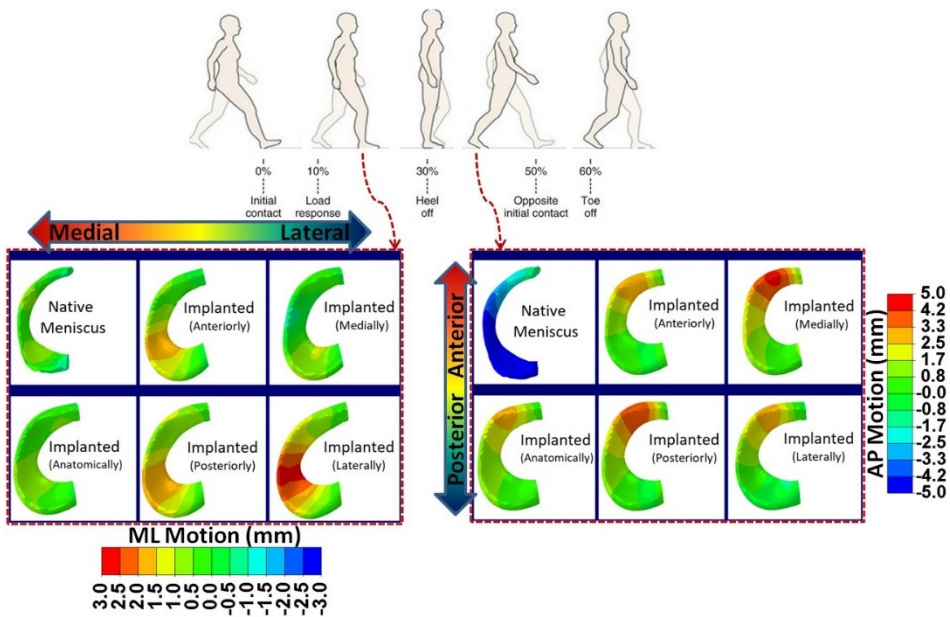


Figure 7: The displacements of native medial meniscus and medial meniscal prosthesis with the anatomical and four non-anatomical (anteriorly, posteriorly, medially and laterally) positioning in medial-lateral direction (ML) at 20% and in anterior-posterior direction (AP) at 35% of a gait cycle.

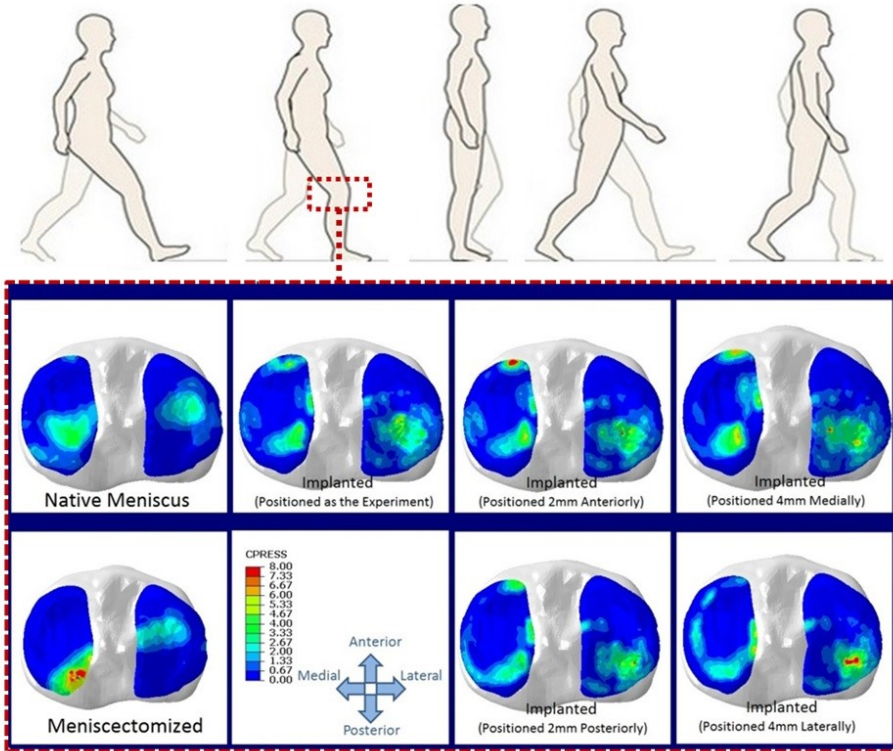


Figure 8: Contact pressure at tibial cartilages at loading response phase (20%) of a gait cycle for the knees with the native meniscus, total meniscectomy, anatomically positioned meniscus prosthesis, and four non-anatomical positioning of the meniscus prosthesis.

Meniscectomy predictably decreased the contact area at the affected plateau (medial plateau), while at the lateral plateau the influence was negligible (Figure 9). All the anatomical and non-anatomical implantation cases slightly increased the contact area at the medial plateau, although amongst the implantations the non-anatomical laterally positioned prosthesis showed the smallest contact area in this region.

Force at prosthesis horns: In the laterally and posteriorly positioned implantation cases, the force at the anterior attachment of the prosthesis increased considerably in heel strike phase and also after the heel-off phase (30% of gait cycle; Figure 10). Comparing with the anatomically positioned prosthesis, all the non-anatomically positioned prostheses displayed a larger force at the posterior attachment, of which the laterally positioned prosthesis underwent the largest force.

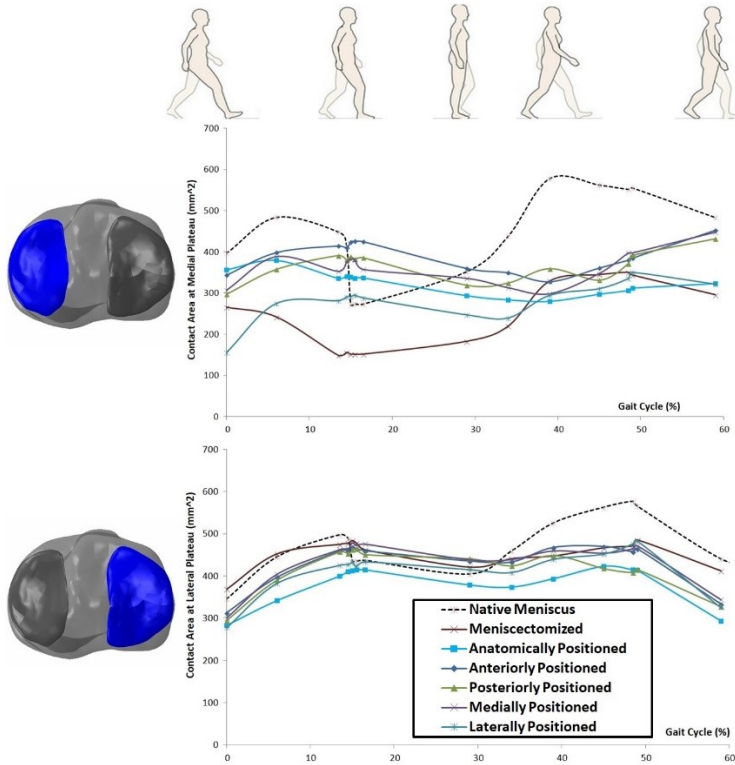


Figure 9: Articular contact area on tibial medial (top) and lateral (bottom) plateaus, during a complete gait stance simulation for the knees with native meniscus, total meniscectomy, anatomically positioned meniscus prosthesis, and four non-anatomical (anteriorly, posteriorly, medially and laterally) positioned meniscus prosthesis.

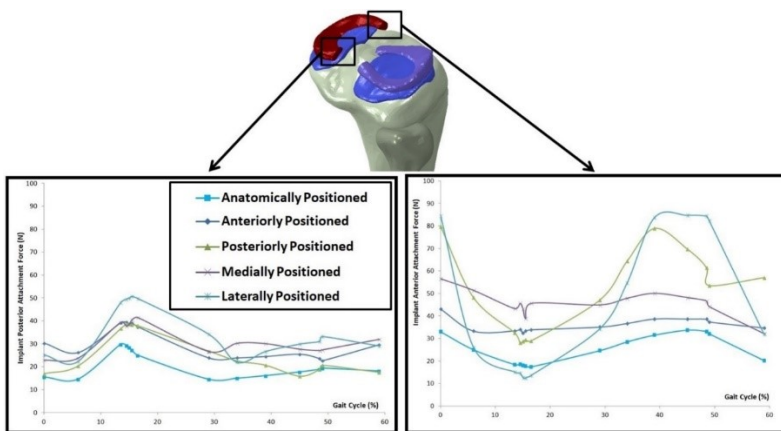


Figure 10: Total force at posterior (left) and anterior (right) fixations of meniscus prosthesis with anatomical and four non-anatomical positioning, during a gait stance simulation.

4. Discussion

In the current study the influence of a non-anatomical positioning of a meniscus prosthesis on the knee biomechanics was assessed during a complete gait stance phase. For this purpose, the right knee of a symmetrical cadaveric pair was used to develop a validated FE model, while the left knee was utilized for an in-vitro implantation experiment (axial loading) for further verification of the model outcomes validity (including the implanted knee model). Different non-anatomical prosthesis positions were applied in the FE model, and the biomechanical response during the stance phase of gait compared with an anatomically positioned prosthesis, as well as with the intact knee model.

The FE model was capable of predicting the motion of the native and meniscal prosthesis with an acceptable agreement with the in-vitro experimental results. The simulated contact pressure and area at the tibial medial plateau were comparable with the experimental measurements. However, the contact areas measured during the experiments were smaller than those in the FE models, which may be due to limitations in the pressure sensitive films of covering the joint contact surface. It is worth mentioning, that for in-vitro axial loading simulation the joint was constrained in valgus-varus direction to replicate the in-vitro loading condition for validation purposes. It should therefore be noted that the outcomes of the in-vitro loading simulation may not reflect the in-vivo knee re-alignment conditions. Re-alignment after implantation was considered, however, for gait simulations.

The kinematic predictions of the FE model during the stance phase of gait for the intact knee well agreed with the literature in both knee translations and rotations [28]–[31]. The results of our gait simulation showed an increase in tibial internal and varus rotations and posterior motion due to total medial meniscectomy. This is in agreement with the findings of Netravali et al (2010), in which similar changes were reported in 10 patients with medial meniscectomy comparing with their healthy contralateral knees [32].

The outcomes of the simulation of the stance phase of gait showed that an anatomically positioned meniscal prosthesis could improve the knee joint biomechanics, although it could not fully recover the intact knee joint function. Non-anatomical positioning of the meniscal prosthesis could lead to a limited

alteration in the joint kinematics. Werner et al. showed that contact distribution and contact loads on medial and tibial compartments significantly changed with a valgus-varus variation as little as 3° in gait, based on cadaveric experiments [33]. Similar findings of Engin et al. on human native knee joint confirm the high sensitivity of knee contact biomechanics to valgus-varus rotational configurations [34]. However, none of the non-anatomical prosthesis positionings led to a valgus-varus alteration beyond 2° , with respect to the anatomical positioning. The change in internal-external rotations during the gait simulation by non-anatomical prosthesis positioning, can alter not only tibiofemoral joint behavior, but also the biomechanics of patellafemoral joint. Patellar kinematics and patellofemoral contact pressure were shown to be slightly more sensitive to femoral internal rotation where an internal rotational change of 5° can alter the patellofemoral joint biomechanical behavior [35]. In anteriorly and laterally non-anatomical positioning cases, similar internal-external rotational change was reached. The alteration in the posteriorly directed joint behavior by non-anatomical posterior and lateral positioning, can also lead to different cruciate ligament forces [36], [37].

In our study we found that, in comparison with an anatomical prosthesis position, a non-anatomical position mostly resulted in a larger contact area at the medial tibial plateau. Sekaran et al. also reported an increase in contact area at the medial plateau when an allograft is positioned posteriorly or medially to the anatomical location [19].

When the meniscus prosthesis was fixated more laterally or posteriorly, the force at the fixations changed dramatically in both magnitude and trend. This may increase the risk of prosthesis loosening at fixations, and more particularly at the anterior fixation where the force fluctuation is larger [38]–[40]. The calculated forces at the fixations can be applied to another FE model with a non-rigid bone representation in order to assess the aseptic loosening risk due to the fatigue failure [39].

The large prosthesis motion in the coronal plane due to the lateral positioning of the prosthesis can be a result of the adoption of the prosthesis to femoral condyle. This may also be an indication for an increase in shear stress at medial tibial cartilage as a result of sliding of the prosthesis. This increase in shear stress at the tibial cartilage is a key factor in the progress of OA [41]. Despite the differences

in strain behaviour of meniscus prosthesis in different positioning, none of them reached beyond the failure strain of the materials implemented in the prosthesis.

There were several limitations in the current study. First, the computational FE model was developed and validated against an in-vitro experiment on cadaveric specimen, while an in-vivo model may give a more realistic insight into actual joint kinematics. However, due to the invasiveness of the measurements (contact pressure measurement, laxity measurement, RSA measurements, CT scanning), a cadaveric specimen-based computational modelling was unavoidable. Therefore, a cadaveric specimen-based detailed FE model was used which was intensively validated against in-vitro experiments in our earlier study [20]. Second, the bones were modelled as rigid bodies, which was shown to be an acceptable assumption when contact variables are of interest. A more realistic inhomogeneous modelling of bones could enrich the model with more details of the screw-bone interface. Third, the boundary conditions for the simulation of gait were assumed to be similar for all cases, whereas in the meniscectomized case the gait pattern might be different due to the lack of the meniscus, or due to pain. However, this model was force-controlled, meaning that loads were applied to the knee joint while allowing for free joint adjustment during gait. As a result, and in contrast with motion-controlled models, similar loading for different cases might acceptably be applied.

Despite the variations in the prosthesis mechanical properties and geometry, from the native meniscus, the anatomical placement of the meniscus prosthesis could better restore the intact knee biomechanics, comparing with all non-anatomical prosthesis positioning. An optimized subject-specific meniscus prosthesis positioning may improve the implantation outcomes furthermore. To achieve this, the developed FE model in the current study could be combined with optimization algorithms, in order to optimize the meniscus prosthesis position in the injured knee based on the intact knee joint (contralateral knee) biomechanical outcomes. Subsequently, the calculated optimal meniscus prosthesis placement can be applied, for instance, using 3D printed surgical guides.

5. Conclusion

This study showed that an anatomical positioning of the medial meniscus prosthesis could better recover the intact knee biomechanics, while a non-anatomical positioning of the meniscus prosthesis to a limited extent alters the knee kinematics, and increases the risk of implantation failure. Our results indicate that a medial or anterior positioning of the meniscus prosthesis may be more forgiving than a posteriorly or laterally positioned prosthesis.

Acknowledgments

This study was a part of BioMechTools project (ERC-2012-ADG LS7), received funding from the European Research Council under the European Union's Seventh Framework Program (FP/2007-2013) / ERC Grant Agreement n. 323091.

Reference

- [1] R. Verdonk, H. Madry, N. Shabshin, F. Dirisamer, and P. Angele, “The role of meniscal tissue in joint protection in early osteoarthritis,” *Knee Surg. Sport. Traumatol. Arthrosc.*, vol. 24, no. 6, pp. 1763–1774, 2016.
- [2] A. S. Lee, R. W. Kang, E. Kroin, N. N. Verma, and B. J. Cole, “Allograft Meniscus Transplantation,” *Sports Med. Arthrosc.*, vol. 20, no. 2, pp. 106–114, 2012.
- [3] B. Lee, J. Chung, J. Kim, W. Cho, K. Kim, and S. Bin, “Morphologic Changes in Fresh-Frozen Meniscus Allografts Over 1 Year A Prospective Magnetic Resonance Imaging Study on the Width and Thickness of Transplants,” *Am. J. Sports Med.*, vol. 40, no. 6, pp. 1384–1391, 2012.
- [4] Y. Wada, M. Amiel, F. Harwood, H. Oriya, and D. Amiel, “Architectural Remodeling in Deep Frozen Meniscal Allografts After Total Meniscectomy,” *J. Arthrosc. Relat. Surg.*, vol. 14, no. 3, pp. 250–257, 1998.
- [5] P. C. Rijk, “Meniscal Allograft Transplantation— Part I: Background, Results, Graft Selection and Preservation, and Surgical Considerations,” *J. Arthrosc. Relat. Surg.*, vol. 20, no. 7, pp. 728–743, 2007.
- [6] A. Huang, M. L. Hull, S. M. Howell, and T. H. Donahue, “Identification of Cross-Sectional Parameters of Lateral Meniscal Allografts That Predict Tibial Contact Pressure in Human Cadaveric Knees,” *J. Biomech. Eng.*, vol. 124, pp. 481–489, 2002.
- [7] T. L. H. Donahue, M. L. Hull, M. M. Rashid, and C. R. Jacobs, “The sensitivity of tibiofemoral contact pressure to the size and shape of the lateral and medial menisci,” *J. Orthop. Res.*, vol. 22, no. 4, pp. 807–814, 2004.
- [8] I. D. Mcdermott, F. Sharifi, A. M. J. Bull, C. M. Gupte, R. W.

Thomas, and A. A. Amis, “An anatomical study of meniscal allograft sizing,” pp. 130–135, 2004.

[9] J. R. Meakin, N. G. Shrive, C. B. Frank, and D. a. Hart, “Finite element analysis of the meniscus: the influence of geometry and material properties on its behaviour,” *Knee*, vol. 10, no. 1, pp. 33–41, 2003.

[10] K. Sommerlath, M. Gallino, and G. J., “Biomechanical characteristics of different artificial substitutes for rabbit medial meniscus and effect of prosthesis size on knee cartilage,” *Clin. Biomech.*, vol. 7, pp. 97–103, 1992.

[11] E. Linder-ganz, J. J. Elsner, A. Danino, and F. Guilak, “A Novel Quantitative Approach for Evaluating Contact Mechanics of Meniscal Replacements,” *J. Biomech. Eng.*, vol. 132, pp. 1–6, 2010.

[12] J. Vaquero and F. Forriol, “Meniscus tear surgery and meniscus replacement,” *Muscles. Ligaments Tendons J.*, vol. 6, no. 1, pp. 71–89, 2016.

[13] M. Alhalki, S. M. Howell, and M. L. Hull, “How Three Methods for Fixing a Medial Meniscal Autograft Affect Tibial Contact Mechanics,” *Am. J. Sports Med.*, vol. 27, no. 3, pp. 320–328, 1999.

[14] A. C. T. Vrancken *et al.*, “3D geometry analysis of the medial meniscus – a statistical shape modeling approach,” *J. Anat.*, vol. 225, no. 4, pp. 395–402, 2014.

[15] M. Khoshgoftar, A. C. T. Vrancken, T. G. van Tienen, P. Buma, D. Janssen, and N. Verdonschot, “The sensitivity of cartilage contact pressures in the knee joint to the size and shape of an anatomically shaped meniscal implant,” *J. Biomech.*, vol. 48, no. 8, pp. 1427–1435, 2015.

[16] A. C. T. Vrancken, W. Madej, G. Hannink, N. Verdonschot, T. G. Van Tienen, and P. Puma, “Short Term Evaluation of an Anatomically Shaped Polycarbonate Urethane Total Meniscus Replacement in a Goat Model,” *PLoS One*, vol. 10, no. 7, pp. 1–16, 2015.

[17] B. J. Cole, T. R. Carter, and S. A. Rodeo, “Allograft meniscal

transplantation: background, techniques, and results.," *Instr. Course Lect.*, vol. 52, pp. 383–396, 2003.

[18] A. Wajsfisz, A. Meyer, K. G. Makridis, and P. Hardy, "A new arthroscopic technique for lateral meniscal allograft transplantation: Cadaver feasibility study," *Orthop. Traumatol. Surg. Res.*, vol. 99, no. 3, pp. 299–304, 2013.

[19] S. V. Sekaran, M. L. Hull, and S. M. Howell, "Nonanatomic Location of the Posterior Horn of a Medial Meniscal Autograft Implanted in a Cadaveric Knee Adversely Affects the Pressure Distribution on the Tibial Plateau," vol. 30, no. 1, pp. 74–82, 2002.

[20] H. Naghibi Beidokhti, D. Janssen, S. van de Groes, J. Hazrati, T. Van den Boogaard, and N. Verdonschot, "The influence of ligament modelling strategies on the predictive capability of finite element models of the human knee joint," *J. Biomech.*, vol. 65, pp. 1–11, 2017.

[21] H. Naghibi Beidokhti, D. Janssen, S. Van De Groes, and N. Verdonschot, "The peripheral soft tissues should not be ignored in the finite element models of the human knee joint," *Med. Biol. Eng. Comput.*, 2017.

[22] D. E. Shepherd and B. B. Seedhom, "The 'instantaneous' compressive modulus of human articular cartilage in joints of the lower limb.," *Rheumatology (Oxford)*, vol. 38, no. 1, pp. 124–132, 1999.

[23] G. A. Holzapfel, T. C. Gasser, and R. W. Ogden, "A new constitutive framework for arterial wall mechanics and a comparative study of material models," *J. Elast.*, vol. 61, no. 1–3, pp. 1–48, 2000.

[24] A. Abaqus and Simulia, "ABAQUS 6.11 Documentation," *Dassault Syst. Simulia*, p. 1100, 2011.

[25] H. Naghibi Beidokhti *et al.*, "A comparison between dynamic implicit and explicit finite element simulations of the native knee joint," *Med. Eng. Phys.*, vol. 38, no. 2016, pp. 1123–1130, 2016.

[26] A. Rohlmann *et al.*, "Standardized Loads Acting in Knee

Implants,” vol. 9, no. 1, 2014.

[27] *ASTM F3141-15, Standard Guide for Total Knee Replacement Loading Profiles*. West Conshohocken, PA: ASTM International, 2016.

[28] H. Wang, J. E. Fleischli, N. N. Zheng, N. Carolina, and N. Carolina, “Transtibial Versus Anteromedial Portal Technique in Single-Bundle Anterior Cruciate Ligament Reconstruction Outcomes of Knee Joint Kinematics During Walking,” pp. 1847–1856, 2013.

[29] M. Kozanek *et al.*, “Tibiofemoral kinematics and condylar motion during the stance phase of gait,” *J. Biomech.*, vol. 42, no. 12, pp. 1877–1884, 2009.

[30] H. Wang, T. Chen, P. Torzilli, R. Warren, and S. Maher, “Dynamic contact stress patterns on the tibial plateaus during simulated gait: A novel application of normalized cross correlation,” *J. Biomech.*, vol. 47, no. 2, pp. 568–574, 2014.

[31] K. B. Shelburne, M. R. Torry, and M. G. Pandy, “Muscle, Ligament, and Joint-Contact Forces at the Knee during Walking,” *Med. Sci. Sport. Exerc.*, no. 3, 2005.

[32] N. A. Netravali, N. J. Giori, and T. P. Andriacchi, “Partial medial meniscectomy and rotational differences at the knee during walking,” *J. Biomech.*, vol. 43, no. 15, pp. 2948–2953, 2010.

[33] F. W. Werner, D. C. Ayers, L. P. Maletsky, and P. J. Rullkoetter, “The effect of valgus/varus malalignment on load distribution in total knee replacements,” *J. Biomech.*, vol. 38, no. 2, pp. 349–355, 2005.

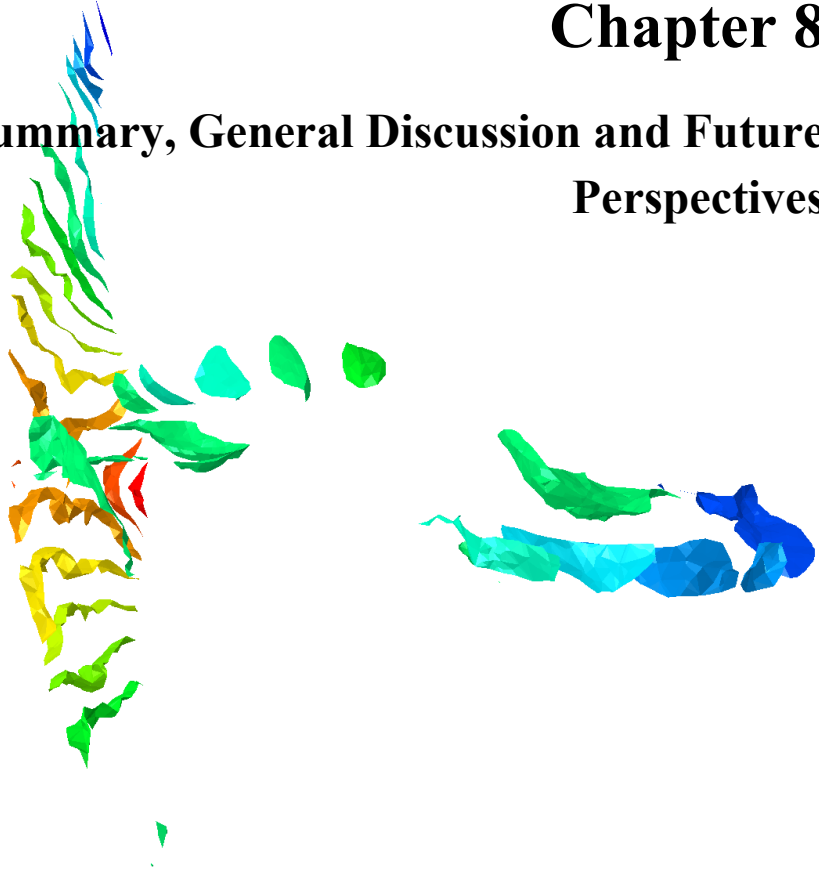
[34] A. E. Engin and M. S. Korde, “Biomechanics of normal and abnormal knee joint,” *J. Biomech.*, vol. 7, no. 4, 1974.

[35] J. H. Heegaard, P. F. Leyvraz, and C. B. Hovey, “A computer model to simulate patellar biomechanics following total knee replacement: The effects of femoral component alignment,” *Clin. Biomech.*, vol. 16, no. 5, pp. 415–423, 2001.

- [36] C. S. Shin, A. M. Chaudhari, and T. P. Andriacchi, “The effect of isolated valgus moments on ACL strain during single-leg landing: A simulation study,” *J. Biomech.*, vol. 42, no. 3, pp. 280–285, 2009.
- [37] H. Marouane, A. Shirazi-Adl, and J. Hashemi, “Quantification of the role of tibial posterior slope in knee joint mechanics and ACL force in simulated gait,” *J. Biomech.*, vol. 48, no. 10, pp. 1899–1905, 2015.
- [38] N. P. Zant, C. K. Y. Wong, and J. Tong, “International Journal of Fatigue Fatigue failure in the cement mantle of a simplified acetabular replacement model,” *Int. J. Fatigue*, vol. 29, no. 7, pp. 1245–1252, 2007.
- [39] R. Of and P. Mechanisms, “NIH Public Access,” *acta Biomater.*, vol. 9, no. 9, pp. 8046–8058, 2013.
- [40] Y. Abu-amer, I. Darwech, and J. C. Clohisy, “Aseptic loosening of total joint replacements: mechanisms underlying osteolysis and potential therapies,” *Arthritis Res. Ther.*, vol. 9, pp. 1–7, 2007.
- [41] P. Wang, P. Guan, C. Guo, F. Zhu, K. Konstantopoulos, and Z. Wang, “Fluid shear stress-induced osteoarthritis: roles of cyclooxygenase-2 and its metabolic products in inducing the expression of proinflammatory cytokines and matrix metalloproteinases,” *J. Fed. Am. Soc. Exp. Biol.*, vol. 27, pp. 4664–4677, 2013.

Chapter 8

Summary, General Discussion and Future Perspectives



1. Summary

The knee joint can be analyzed by using finite element model in a static or dynamic way, either using implicit or explicit methods. In general, the implicit method gives more accurate outcomes, due to the iterative solution in which the numerical errors must meet a tolerance value. However, convergence problems may require substantial simplifications to the FE models. In contrast, the direct forward explicit method allows for the inclusion of more complex features in the models. The explicit algorithm is conditionally stable, and can be quite time consuming. Although the computational time can be reduced by using mass-scaling, it may alter the outcomes if it is inappropriately implemented. In chapter 2 it was illustrated that ignoring dynamic effects in a simulation of a daily activity can result in unacceptable results. However, it was also shown that explicit analyses can be suitably used to simulate dynamic loading of the knee joint in high-speed activities, as this method offers a substantial reduction of computational time, while predicting similar cartilage contact pressures and meniscus strains as in a (time consuming) implicit simulation. Although mass-scaling can reduce computational time even more, it is not recommended for high-speed activities, in which inertial forces play a significant role.

In FE models of the knee joint, different material models have been used to capture the mechanical response of the tissues. Particularly, material models for knee ligaments have a large effect on the joint laxity, kinematics and, as a result, joint biomechanics (e.g. contact stresses). Traditionally, tibiofemoral ligaments have been modeled as one-dimensional spring elements, which reduces the computational costs. Only in a few FE models of either native or implanted knees (i.e. TKA, meniscus prosthesis, etc.), the geometry of the ligaments were physically represented, which enables modeling of ligament wrapping. In most models, the geometrical representation of the ligaments and the mechanical properties are based on data reported in literature, while only in a limited number of models the properties were adjusted specifically for the studied subject. In chapter 3, FE models were created based on in-vitro experiments with three cadaveric specimens. That study revealed that, for a more reliable FE simulation, both in models using springs or continuum elements to represent the ligaments, the material parameters need to be determined based on subject-specific properties. Although both the continuum and spring-based subject-specific FE

models improved the knee kinematics predictions, with ligaments modeled using continuum elements the contact pressure at the tibial cartilages was enhanced most.

In addition to the main tibiofemoral ligaments, there are other ligamentous structures that may influence the knee joint kinematics, particularly at the posterior side of the knee joint. In most FE models of the knee joint these structures are ignored, mostly because their influence has not been well-described and considered to be of minor effect for the overall biomechanical behavior of the knee. In chapter 4, a comparative study based on in-vitro experiments on three cadaveric knee joints demonstrated the importance of including the peripheral soft tissue envelope. According to the results, modeling the knee joint with only main tibiofemoral ligaments may not be a realistic representation for an intact knee joint, particularly, when the joint is under a (tibial) posterior load, internal torque, or valgus moment. Modeling the anterolateral ligament and posterior capsule improves the laxity prediction.

One of the biggest challenges in developing a patient-specific FE model is characterization of the patient's tissues. In this thesis, and as explained in chapter 3, based on laxity tests, and implementing parallel optimizations, the ligament properties could be calculated for three individuals. The laxity tests were selected such that they could also be implemented in-vivo. To the best of the author's knowledge, this was the first time an FE model of an intact knee was developed in subject-specific manner based on laxity tests. The main obstacle in implementing the same methodology for in-vivo applications, is the time required for model development (almost one month), mostly due to the laxity-based optimization. To address this obstacle, in chapter 5, it was assessed whether the mechanical properties of the knee joint ligaments can be estimated from quantitative MRI parameters, ($T_{1\rho}$, T_2 and T_2^*) and structural specifications (i.e. volume or cross-sectional area). For this purpose, the MR relaxation times ($T_{1\rho}$, T_2 and T_2^*) of all four main tibiofemoral ligaments (ACL, PCL, MCL and LCL) of six cadaveric knees were determined. Subsequently, the volume (based on segmentation of the MRI data) and cross-sectional area (based on ultrasound measurements) were measured. Eventually, in-vitro tensile tests were performed to measure the stiffness and rupture force. The results illustrated that if selected MR parameters are used in combination with ligament volume, the mechanical properties can be estimated acceptably, with an R^2 of 0.53 for the rupture force,

and 0.48 for ligament stiffness. If the ligament type (ACL, PCL, MCL and LCL) is also included in the predictive model, the correlation was further improved ($R^2=0.57$ for initial rupture force, and 0.60 for stiffness).

In order to demonstrate the capability of the developed FE models of the native knee joint, the models were used as surgical pre-planning tools for two common orthopedic procedures. Consequently, ACL reconstruction and meniscal implantation surgeries were studied in chapter 6 and chapter 7, respectively.

In patients with an ACL reconstruction the post-operative situation may differ from the intact situation, which can lead to changes in knee kinematics and kinetics, which is believed to play an important role in the initiation or progression of knee OA after an ACL injury. The aim of the study as described in chapter 6 was to demonstrate the potential of FE models to define the optimal surgical parameters in terms of graft positioning (insertion sites and fixation tension) in combination with graft type of choice, in order to restore the kinematic and kinetic behavior of the knee as good as possible.

A workflow was proposed based on cadaveric experiments to reconstruct the biomechanical behavior of the injured knee as physiologically as possible. Femoral and tibial graft insertion sites and the graft fixation tension were optimized to obtain a similar intact knee laxity, for three common single-bundle reconstruction grafts (hamstring, and quadriceps and patellar tendons), and for a common double-bundle reconstruction. Eventually, to verify the success of the surgery with the optimized parameters, a full walking cycle was simulated with the intact, the ACL-deficient, and the optimal and non-optimal reconstructed knees, to demonstrate that these optimized surgical parameters do indeed lead to more physiological knee biomechanics.

It was demonstrated that, based on the selected graft type (hamstring tendon, patellar tendon or quadriceps tendon) or surgical technique (single-bundle vs. double-bundle), numerical optimizations can be implemented prior to the surgery to find the most optimal graft positioning parameters (insertion sites and fixation tension) to replicate the intact knee behavior.

Despite efforts to optimize a meniscus prosthesis system (geometry, material and fixation type), the clinical success will depend on surgical factors, such as intra-

operative positioning of the meniscus prosthesis. In the study described in chapter 7, the aim was therefore to assess the implications of positional changes of the medial meniscus prosthesis for knee biomechanics.

A detailed validated FE model of intact and meniscal implanted knees was developed based on a series of in-vitro experiments. Different non-anatomical prosthesis positions were applied in the FE model, and the biomechanical response during the stance phase of gait was compared with an anatomically positioned prosthesis, and with the intact knee model.

The results showed that an anatomical positioning of the medial meniscus prosthesis could better replicate the intact knee biomechanics, while a non-anatomical positioning of the prosthesis to a limited extent altered the knee kinematics, and increased the failure risk of the meniscus prosthesis. The outcomes indicate that a medial or anterior positioning of the meniscus prosthesis may be more forgiving than a posteriorly or laterally positioned prosthesis. The outcome of this study may provide a better insight into the possible consequences of meniscus prosthesis positioning errors for the patient and the prosthesis functionality.

2. General Discussion and Future Perspectives

In this thesis the aim was to develop FE models of human knee joint, as a surgical pre-planning tool in order to improve the orthopedic surgical outcomes. For this purpose, first the essence of some modeling aspects were assessed. Subsequently, two approaches to develop knee models with personalized ligament properties were investigated. Eventually, the FE models were utilized as surgical pre-planning tools to improve the outcome of two common orthopedic surgeries; ACL reconstruction and meniscus implantation. As a part of the BioMechTools project, all the methodologies were designed in a way that they are expandable to an in-vivo application as a diagnostic, surgery pre-operative planning and decision tool for knee surgeons. This means that all the steps to build up an FE model should be able to be performed minimal- or non-invasively.

Figure 1 illustrates the developed workflow with the adjustments needed for modeling a knee of a patient. In order to measure the laxity in-vivo an MR-compatible device can be used inside the MRI-scanner, and static MR data pre-

and post-loading can be acquired (Figure 1-a, 1-b & 1-c). By implementing registration techniques, the tibiofemoral laxity can be calculated and transferred to the knee joint coordinate system, which can be used to tune the patient-specific soft tissue envelope (Figure 1-d). In addition, the motion of the joint can be estimated using dynamic MRI, as for instance implemented by Mazzoli et al. (2017) [1].

To build the FE model of a patient's knee, first, the geometries of the hard and soft tissues are extracted from MRI (Figure 1-c & 1-e). Compared with manual segmentation, automatic segmentation or statistical shape modeling can substantially reduce the time needed for extracting the geometries [2]–[4]. After geometry extraction, realistic material properties need to be assigned to each segment (hard and soft tissues).

In this FE-based framework, modeling the bones as rigid bodies can be an acceptable assumption when simplified contact variables (e.g. contact pressure) are investigated, or when more sophisticated variables (e.g. cartilage stress) are assessed in comparative studies [5], [6]. As a result, with rigid bodies representing the bones, the FE model predictions for cartilage contact pressures are suitable for comparative studies, as presented in chapter 6 (ACL-deficiency) and chapter 7 (meniscectomy). If the biomechanical response of the bones (e.g. due to cartilage degeneration) is of interest, a more realistic material definition is essential. Bone remodeling around cementless and cemented prosthetic knees (e.g. TKA), micro-motion analysis at the interface, or stress shielding of the prosthesis are some examples where a more sophisticated representation of bone is needed. In these cases, the bone material properties can be estimated from CT [7]. However, this increases the computational costs substantially. As a result, the majority of the studies with a realistic mechanical description of bone typically explore only a limited set of loading conditions, focusing on peak forces (e.g. stance phase of gait), which is the main drawback of these FE models [8].

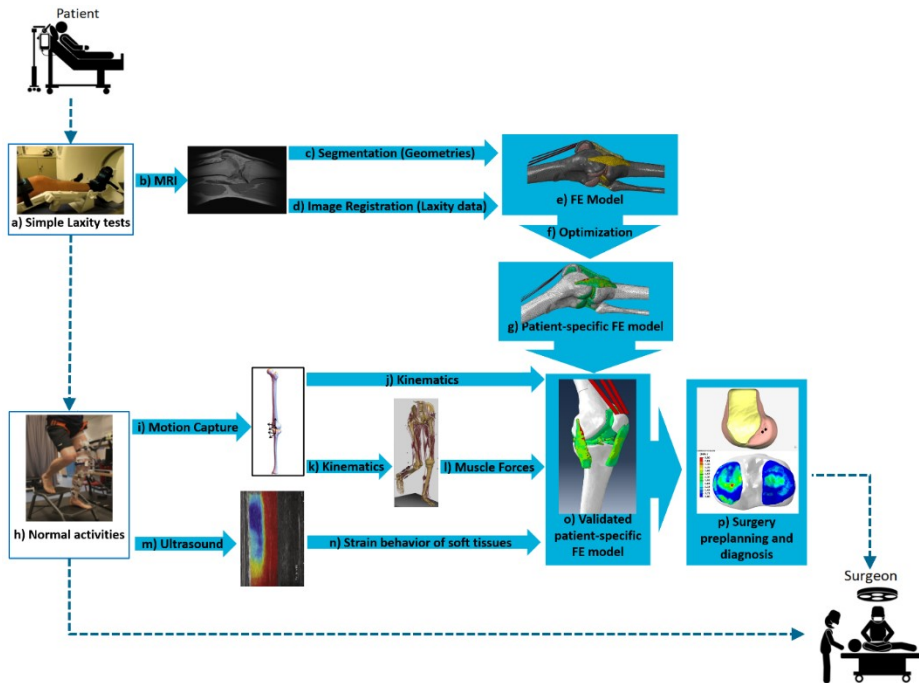


Figure 1: The studied workflow for developing FE models as surgery pre-planning and diagnostic tools, with the adjustments for implementation in clinic (BioMechTools projects). Based on simple laxity tests (a), inside the MR-scanner (b), the geometries can be extracted (c), and the laxity data can be calculated using image registration techniques (d). The properties of the soft tissues (e) are calculated following optimization routines (f), to develop a patient-specific FE model of the knee (g). The patient is asked to perform some activities (h), during which the kinematics is measured using motion capture techniques (i), e.g. with A-mode ultrasound. The kinematics (j) is used to validate the FE predictions. It is also utilized in a musculoskeletal model (k) to estimate muscle forces (l) as the input loads for the patient-specific FE model. Using ultrasound (m), strain in soft tissues (n) (e.g. in collateral ligaments) is measured to further validate the patient-specific FE model (o). The validated FE model is implemented in clinics as an surgeon assistive tool for surgery pre-planning (p).

In order to determine the loading conditions on the FE models one could combine them with musculoskeletal (MS) models (Figure 1-1). These models can also be generated from MRI scans and are able to calculate forces in the joints (as shown for example by Marra et al. [22]). The output (muscle and joint forces) can be applied to FE models in order to simulate more realistic boundary conditions. This multi-model (or multi-scale) approach is rather time-consuming, but it can be expected that in the future model generation and analysis will be greatly accelerated.

Articular cartilage biomechanics is of importance in the FE models of the knee joint, as it can give an insight into the risk of OA-development in the knee joint

[9]. In the current thesis, due to the rather simple mechanical description of the cartilage, the results on the actual cartilage stress levels should be interpreted with care. Although we used a rather simple model, the contact pressures appeared to be very similar to what has been reported previously [10], [11]. In a more sophisticated FE model, Wilson et al. (2003) demonstrated that the local stress and strain response of the cartilage also depends on the local architecture of the collagen network [12], [13], which can be incorporated with a multi-scale modeling approach. The resultant force or contact pressure at the cartilage articular surfaces from the current model can be applied to a more detailed representation of cartilage such as modeled by Wilson et al. (2003). Hence, using a combined approach of a ‘macroscopic’ model, that captures the overall, subject-specific knee kinematics and kinetics, with a ‘microscopic’ model capturing the mechanically induced collagen degeneration would be a powerful way to quantify the OA-risk in an individualized manner.

The dynamic explicit algorithm can be used with suitable simulation parameters, such as the viscosity parameter and the mass-scaling factor, and meshing properties following from sensitivity analyses. The comparative study in chapter 2 can be an example of how a proper solution strategy in FE analysis of the knee joint should be selected. The solution parameters found in this chapter cannot simply be adopted in other knee FE models built in a different manner (i.e. different material models or number or type of elements, etc.). However, any FE model of the knee joint can follow a similar methodology to that presented in chapter 2 for an efficient gain in terms of computational time and outcome accuracy. For instance, only the heel strike phase was simulated in chapter 2, in which the largest variation in the major axial load occurs. Depending on the biomechanical outcomes of interest (e.g. center of contact pressure) the swing phase of the gait cycle, which involves the joint with larger flexions and rotations, may also be required to simulate.

Relative to the soft tissue biomechanics around the knee joint, the exact representation required in the FE model depends on the research question. Particularly the descriptive model for ligaments should be selected with care, as it can considerably influence the knee laxity and biomechanics (chapter 3). The personalized coefficients in the mathematical description can be obtained through model optimization based on a series of laxity test (e.g. IE and VV rotational

laxity). One of the most time-consuming steps in the whole workflow was the optimization of the ligament coefficients based on the laxity data (Figure 1-f). To shorten the time required for the optimization, a more efficient sampling (on ligament coefficients) can be achieved using a generic probabilistic study based on a series of sensitivity analyses on the input variables [14], [15]. A similar approach can be implemented for calculating patient-specific surgical parameters based on laxity data, for instance in ACL-ruptured patients. For this purpose, the distribution of the surgical variables and of the variables required to characterize the patients' knee joint (i.e. geometry and mechanical properties) is sampled. As a result of the probabilistic analysis, the distribution in performance metrics (i.e. laxity data and/or cartilage contact pressure) and the sensitivity factors are determined.

Simple FE models can be used to study any isolated structure of the knee joint under simplified loading conditions. However, for an enhanced clinical application, modeling of only the salient structures of the knee, as modelled in most of the knee FE models, may not be acceptable, as patient's laxity and/or kinematics data are dealt with as inputs and outputs for the FE model. The altered laxity by ignoring the peripheral tissues, as shown in chapter 4, can result in inaccurate kinematics predictions in the force-controlled FE models. In some FE models complex loading patterns, such as gait, have been implemented using displacement-controlled simulations [6], [16]–[18]. Thus, in a sense, the effect of these soft tissues has already been taken into account in the kinematics. However, even in the models with prescribed kinematics, excluding the peripheral tissues can lead to inaccurate joint reaction forces and moments, and hence to inaccurate results at even salient structures (e.g. tibiofemoral ligament forces). More importantly, when any clinical condition (i.e. ligament deficiency, meniscectomy, etc.) needs to be simulated with an FE model, only the force-driven model can capture the changes in kinematics and laxity.

In order to implement the workflow more practically in-vivo, the quantitative MRI parameters of the patient (T_2 , T_2^* or $T_{1\rho}$) and also the ligament volume can be calculated, and based on the method presented in chapter 5 the ligament mechanical properties could be estimated. Moreover, the force within the ligaments in different patients might be different, which also may influence the quantitative MR parameters. The results of chapter 5 illustrated the potential of utilizing MR parameters combined with ligament volume to estimate the stiffness

and partial rupture force. The data may not be directly applicable for in-vivo use due to the limitations and deviations of the sample conditions from in-vivo, as explained in chapter 5. A library containing the MR quantitative parameters (T_2 , T_2^* or $T_{1\rho}$) and specimen volume (from segmentation) for patients' ligaments, and the mechanical properties, as for instance calculated by laxity-based optimization, can be created. Based on such a library, by including subjects from different ages, genders, etc., the correlative model can be extracted. Furthermore, it can be expected that new MRI sequences or ultrasound techniques or other multi-modal imaging techniques may reveal correlations with the mechanical properties of the soft tissues in the future.

Eventually, validation tests need to be performed to compare the joint kinematics predictions of the FE model with the actual in vivo kinematics. In this thesis, the resultant force at the tibiofemoral joint was applied in the simulations (i.e. gait) based on the Orthoload database [19]. Applying patient-specific muscle forces calculated by a musculoskeletal model to the FE model can give a more realistic replication of the in-vivo condition (Figure 1-l). It should be noted, however, that most of the musculoskeletal models lack some crucial knee soft tissues (e.g. menisci), or model those tissues unrealistically (e.g. rigid body). The influence of such unrealistic representations needs to be studied beforehand. One manner to represent soft tissue mechanics in rigid body models may be the implementation of a surrogate model. This surrogate model can be based on a more detailed FE model as for instance proposed by Lin et al. (2010), and also implemented by Marra et al. (2017) [20], [21].

A musculoskeletal model (e.g. [22]) usually calculates the muscle forces based on the imposed kinematics (Figure 1-k). Hence, these models are sensitive to the accuracy of the applied kinematics. Different approaches were implemented to measure the in-vivo kinematics (Figure 1-i). Comparing with traditional skin markers tracking, an ultrasound tracking system (Figure 1-h), as a novel technique, revealed to be a promising method to measure the knee kinematics in six degree of freedom [23]. These measured kinematics, can also be compared with the FE model predictions for validation purposes (Figure 1-j).

As demonstrated in this thesis, even with fitting of the kinematics of the knee joint by tuning the ligament properties, a correct prediction of non-kinematics variables (e.g. contact pressure) is not guaranteed. Therefore, any data on the

behavior of soft tissues can be used for further validation of the FE model (Figure 1-n). For this purpose, strains in the collateral ligaments (Figure 1-m), for instance measured by ultrasound (e.g. [24], [25]), or meniscus deformation and contact pressure distributions estimated from overlapping MR images pre- and post-loading (e.g. [26]–[28]) are methods to further improve patient-specific finite element models.

Currently, FE models are widely used for luxation simulations and cartilage stress estimations in the hip joint. For the knee joint, accurate predictions are more challenging. FE models of the knee suffer from many simplifications, and are often only suitable for a very limited application area. In this thesis we developed an FE model of the knee joint with personalized properties for a wider range of clinical applications. With collaborative platforms, such as BioMechTools or Open-knee, the modeling community makes rapid progress, and by networking efforts an accelerated progress can be obtained, allowing the introduction of patient-specific modeling techniques in clinical practice. Whether these modeling techniques have clinical benefits requires long term clinical studies. In any case, the most effective way to enhance modeling capabilities seems to be the better coordination of the imaging, modeling and clinical communities, working together to obtain true patient-specific predictions of the effects of surgical decisions, which will aid in selecting the best treatment in an individualized manner.

References

- [1] V. Mazzoli *et al.*, “Accelerated 4D self-gated MRI of tibiofemoral kinematics,” *NMR Biomed.*, vol. 30, no. 11, pp. 1–11, 2017.
- [2] C. Ahn, T. D. Bui, Y. W. Lee, J. Shin, and H. Park, “Fully automated, level set-based segmentation for knee MRIs using an adaptive force function and template: Data from the osteoarthritis initiative,” *Biomed. Eng. Online*, vol. 15, no. 1, pp. 1–14, 2016.
- [3] J. Pang, P. Li, M. Qiu, W. Chen, and L. Qiao, “Automatic Articular Cartilage Segmentation Based on Pattern Recognition from Knee MRI Images,” *J. Digit. Imaging*, vol. 28, no. 6, pp. 695–703, 2015.
- [4] M. A. Baldwin, J. E. Langenderfer, P. J. Rullkoetter, and P. J. Laz, “Development of subject-specific and statistical shape models of the knee using an efficient segmentation and mesh-morphing approach,” *Comput. Methods Programs Biomed.*, vol. 97, no. 3, pp. 232–240, 2010.
- [5] T. L. H. Donahue, M. L. Hull, M. M. Rashid, and C. R. Jacobs, “A finite element model of the human knee joint for the study of tibio-femoral contact,” *J. Biomech. Eng.*, vol. 124, no. 3, pp. 273–280, 2002.
- [6] M. S. Venäläinen *et al.*, “Effect of bone inhomogeneity on tibiofemoral contact mechanics during physiological loading,” *J. Biomech.*, vol. 49, no. 7, pp. 1111–1120, 2016.
- [7] S. M. Snyder and E. Schneider, “Estimation of mechanical properties of cortical bone by computed tomography,” *J. Orthop. Res.*, vol. 9, no. 3, pp. 422–431, 1991.
- [8] M. Taylor and P. J. Prendergast, “Four decades of finite element analysis of orthopaedic devices: Where are we now and what are the opportunities?,” *J. Biomech.*, vol. 48, no. 5, pp. 767–778, 2015.
- [9] F. Guilak, “Biomechanical factors in osteoarthritis,” *Best Pract. Res. Clin. Rheumatol.*, vol. 25, no. 6, pp. 815–823, 2011.
- [10] M. E. Mononen *et al.*, “Effect of superficial collagen patterns and

fibrillation of femoral articular cartilage on knee joint mechanics—A 3D finite element analysis,” *J. Biomech.*, vol. 45, no. 3, pp. 579–587, 2012.

[11] R. Mootanah, F. Reisse, D. Carpanen, R. Walker, and H. J. Hillstrom, “The effects of the material properties of bones and soft tissues on knee joint contact stress,” in *10th international symposium on Biomechanics and Biomedical Engineering*, 2012.

[12] C. Mothersill, C. B. Seymour, and A. O’Brien, “Induction of c-myc oncoprotein and of cellular proliferation by radiation in normal human urothelial cultures,” *Anticancer Res.*, vol. 24, no. 4, pp. 220–228, 2006.

[13] W. Wilson, C. C. Van Donkelaar, B. Van Rietbergen, K. Ito, and R. Huiskes, “Stresses in the local collagen network of articular cartilage: A poroviscoelastic fibril-reinforced finite element study,” *J. Biomech.*, vol. 37, no. 3, pp. 357–366, 2004.

[14] M. A. Baldwin, P. J. Laz, J. Q. Stowe, and P. J. Rullkoetter, “Efficient probabilistic representation of tibiofemoral soft tissue constraint,” *Comput. Methods Biomech. Biomed. Engin.*, vol. 12, no. 6, pp. 651–659, 2009.

[15] C. T. C. Arsene and B. Gabrys, “Probabilistic finite element predictions of the human lower limb model in total knee replacement,” *Med. Eng. Phys.*, vol. 35, no. 8, pp. 1116–1132, 2013.

[16] L. P. Räsänen, M. E. Mononen, E. Lammentausta, M. T. Nieminen, J. S. Jurvelin, and R. K. Korhonen, “Three dimensional patient-specific collagen architecture modulates cartilage responses in the knee joint during gait,” *Comput. Methods Biomech. Biomed. Engin.*, vol. 19, no. 11, pp. 1225–1240, 2016.

[17] M. E. Mononen, J. S. Jurvelin, and R. K. Korhonen, “Implementation of a gait cycle loading into healthy and meniscectomised knee joint models with fibril-reinforced articular cartilage,” *Computer Methods in Biomechanics and Biomedical Engineering*, vol. 18, no. 2. Taylor & Francis, pp. 141–152, 2015.

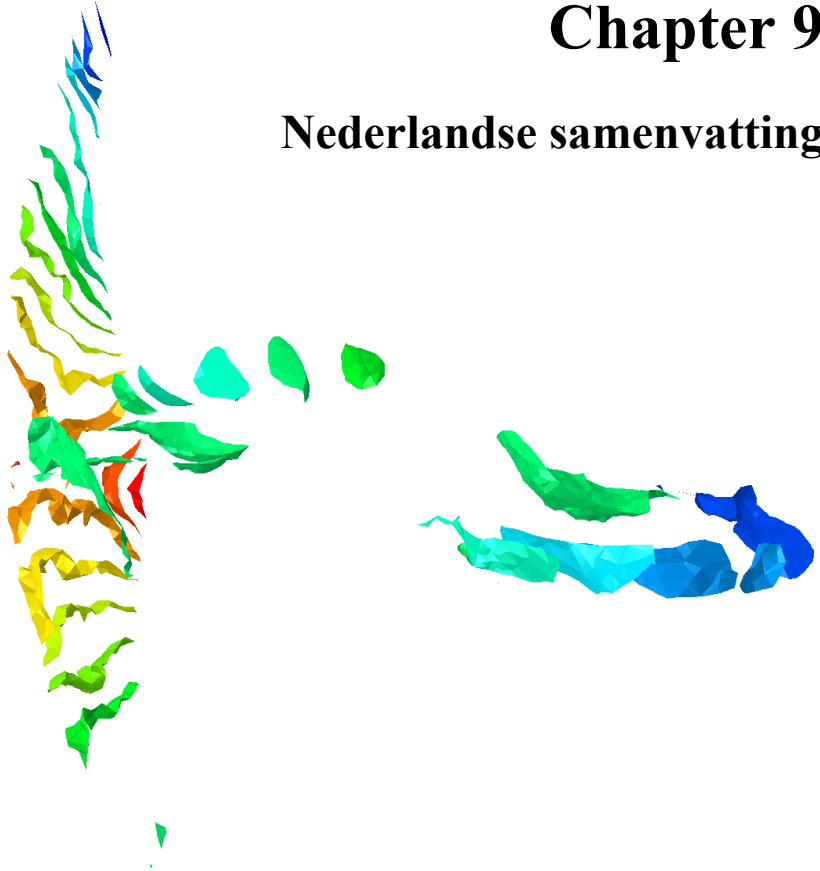
- [18] M. S. Venäläinen *et al.*, “Quantitative Evaluation of the Mechanical Risks Caused by Focal Cartilage Defects in the Knee,” *Sci. Rep.*, vol. 6, no. October, pp. 1–11, 2016.
- [19] A. Rohlmann *et al.*, “Standardized Loads Acting in Knee Implants,” vol. 9, no. 1, 2014.
- [20] M. A. Marra, M. S. Andersen, M. Damsgaard, B. F. J. M. Koopman, D. Janssen, and N. Verdonshot, “Evaluation of a Surrogate Contact Model in Force-Dependent Kinematic Simulations of Total Knee Replacement,” *J. Biomech. Eng.*, vol. 139, no. 8, p. 81001, Jun. 2017.
- [21] Y.-C. Lin, R. T. Haftka, N. V. Queipo, and B. J. Fregly, “Surrogate articular contact models for computationally efficient multibody dynamic simulations,” *Med. Eng. Phys.*, vol. 32, no. 6, pp. 584–594, 2010.
- [22] M. A. Marra, V. Vanheule, R. Fluit, B. Koopman, J. Rasmussen, and N. Verdonshot, “A Subject-Specific Musculoskeletal Modeling Framework to Predict In Vivo Mechanics of Total Knee Arthroplasty,” *J. Biomech. Eng.*, vol. 137, no. 2, pp. 1–12, 2015.
- [23] K. Niu *et al.*, “In situ comparison of A-mode ultrasound tracking system and skin-mounted markers for measuring kinematics of the lower extremity,” *J. Biomech.*, 2018.
- [24] M. De Maeseneer *et al.*, “Ultrasound of the knee with emphasis on the detailed anatomy of anterior, medial, and lateral structures,” *Skeletal Radiol.*, vol. 43, no. 8, pp. 1025–1039, 2014.
- [25] L. C. Slane, J. A. Slane, J. D’hooge, and L. Scheys, “The challenges of measuring in vivo knee collateral ligament strains using ultrasound,” *J. Biomech.*, vol. 61, pp. 258–262, 2017.
- [26] Y. Song, J. M. Greve, D. R. Carter, S. Koo, and N. J. Giori, “Articular cartilage MR imaging and thickness mapping of a loaded knee joint before and after meniscectomy,” *Osteoarthr. Cartil.*, vol. 14, no. 8, pp. 728–737, 2006.

[27] C. E. Henderson, J. S. Higginson, and P. J. Barrance, "Comparison of MRI-Based Estimates of Articular Cartilage Contact Area in the Tibiofemoral Joint," *J. Biomech. Eng.*, vol. 133, no. 1, pp. 1–12, 2011.

[28] T. D. MacLeod, K. Subburaj, S. Wu, D. Kumar, C. Wyatt, and R. B. Souza, "Magnetic resonance analysis of loaded meniscus deformation: a novel technique comparing participants with and without radiographic knee osteoarthritis," *Skeletal Radiol.*, vol. 44, no. 1, pp. 125–135, 2015.

Chapter 9

Nederlandse samenvatting



Het kniegewricht kan worden geanalyseerd met behulp van eindige elementen methode (EEM) modellen op een statische of dynamische manier, met impliciete of expliciete methoden. In het algemeen geeft de impliciete methode meer nauwkeurige resultaten, vanwege de iteratieve oplossing waarin de numerieke fouten aan een tolerantiewaarde moeten voldoen. Om convergentieproblemen te voorkomen zijn soms echter aanzienlijke vereenvoudigingen van de FE-modellen nodig. De direct forward expliciete methode maakt het daarentegen mogelijk om meer complexe kenmerken in de modellen op te nemen. Het expliciete algoritme is voorwaardelijk stabiel en kan behoorlijk tijdrovend zijn. Hoewel de computertijd kan worden verminderd door massa te schalen, kan dit de uitkomsten beïnvloeden als dit verkeerd wordt geïmplementeerd. In hoofdstuk 2 is aangetoond dat het negeren van dynamische effecten in een simulatie van een dagelijkse activiteit kan leiden tot onaanvaardbare resultaten. Er werd echter ook aangetoond dat expliciete analyses geschikt zijn om dynamische belastingen van het kniegewricht tijdens hoge snelheidsactiviteiten te simuleren, omdat deze methode een aanzienlijke vermindering van de computertijd oplevert, terwijl vergelijkbare kraakbeencontactdrukken en rekken in de meniscus worden voorspeld als in een (tijdrovende) impliciete simulatie. Hoewel massa schaling de computertijd nog meer kan verkorten, is het niet geschikt voor activiteiten met hoge snelheid, waarbij traagheidskrachten een belangrijke rol spelen.

In EEM-modellen van het kniegewricht zijn verschillende materiaalmodellen gebruikt om het mechanische gedrag van de weefsels te simuleren. Deze materiaalmodellen hebben een groot effect op de laxiteit, kinematica en als een resultaat, de biomechanische respons in het gewricht (bijvoorbeeld contactspanningen). Traditioneel worden tibiofemorale ligamenten gemodelleerd als eendimensionale veerelementen, wat de computerkosten verlaagt. Slechts in een paar EEM-modellen van intacte of geïmplanteerde knieën (d.w.z. TKA, meniscusprothese, enz.), is de geometrie van de ligamenten fysiek meegenomen, wat het mogelijk maakt om ‘wrapping’ van de ligamenten te simuleren. In de meeste modellen zijn de geometrie en de mechanische eigenschappen van de ligamenten gebaseerd op literatuur, terwijl slechts in een beperkt aantal modellen de eigenschappen subject-specifiek werden aangepast. In hoofdstuk 3 zijn EEM-modellen gemaakt op basis van in vitro experimenten met drie humane knieën. Deze studie toonde aan dat subject-specifieke materiaalparameters leiden tot betere resultaten, zowel in modellen die veren gebruiken als in modellen die

continu-elementen gebruiken om de ligamenten weer te geven. Beide typen modellen zorgen voor een betere simulatie van de kinematica van de knie. De tibiale contactdrukken kunnen echter het meest nauwkeurig gesimuleerd worden in modellen waarin ligamenten gemodelleerd worden met behulp van continu-elementen.

Naast de belangrijkste tibiofemorale ligamenten zijn er andere structuren die de kinematica van het kniegewricht kunnen beïnvloeden, vooral aan de achterkant van het kniegewricht. In de meeste EEM-modellen van het kniegewricht worden deze genegeerd, voornamelijk omdat hun invloed niet goed beschreven is en daarom beschouwd als structuren die weinig invloed hebben op het algehele biomechanische gedrag van de knie. In hoofdstuk 4 zijn in vitro experimenten uitgevoerd met drie knieën, waarin het belang van de perifere zachte weefsels aangetoond werd. De resultaten lieten zien dat het modelleren van het kniegewricht met alleen de belangrijkste tibiofemorale ligamenten geen realistische weergave geeft van het intacte kniegewricht, vooral wanneer het gewricht belast wordt met een posterieure belasting, een intern moment, of een valgusmoment. Het includeren van het anterolaterale ligament en de achterste gewrichtskapsel verbetert de voorspelling van de laxiteit.

Een van de grootste uitdagingen bij het ontwikkelen van een patiënt-specifiek EEM-model is de karakterisering van de weefsels. In dit proefschrift, en zoals uitgelegd in hoofdstuk 3, zijn op basis van laxiteitstesten en het implementeren van optimalisatie de ligament eigenschappen voor drie knieën worden berekend. De laxiteitstesten werden zodanig gekozen dat ze ook in vivo kunnen worden geïmplementeerd. Het belangrijkste obstakel bij het implementeren van dezelfde methodologie voor in-vivo-toepassingen, is de tijd die nodig is voor modelontwikkeling (bijna een maand), voornamelijk vanwege de op laxiteit gebaseerde optimalisatie. Om dit te verbeteren, werd in hoofdstuk 5 onderzocht of de mechanische eigenschappen van ligamenten kunnen worden bepaald op basis van kwantitatieve MRI-parameters ($T1\rho$, $T2$ en $T2^*$) en structurele specificaties (volume of dwarsdoorsnede). Voor dit doel werden de MR-relaxatietijden ($T1\rho$, $T2$ en $T2^*$) van de vier belangrijkste tibiofemorale ligamenten (ACL, PCL, MCL en LCL) van zes kadaverknieën bepaald. Vervolgens werden het volume (op basis van segmentatie van de MRI-gegevens) en de dwarsdoorsnede (op basis van ultrasound metingen) gemeten. Uiteindelijk werden in-vitro experimenten uitgevoerd om de stijfheid en de treksterkte te

meten. De resultaten laten zien dat als geselecteerde MR-parameters worden gebruikt in combinatie met ligament volume, de mechanische eigenschappen redelijk kunnen worden geschat, met een R^2 van 0,53 voor de treksterkte en 0,48 voor stijfheid. Als het ligament type (ACL, PCL, MCL en LCL) ook wordt meegenomen in het model, wordt de correlatie verder verbeterd ($R^2 = 0,57$ voor treksterkte en 0,60 voor stijfheid).

Om de klinische toepassing van de ontwikkelde EEM-modellen te demonstreren, werden de modellen gebruikt als chirurgische pre-planningstools voor twee veelvoorkomende orthopedische procedures. In hoofdstukken 6 en 7 is de methodologie gebruikt voor ACL-reconstructies en voor een meniscus-ervangend implantaat.

Bij patiënten met een ACL-reconstructie kan de postoperatieve situatie verschillen van de intacte situatie, wat kan leiden tot veranderingen in de kinematica, waarvan wordt aangenomen dat het een belangrijke rol speelt bij de initiatie of progressie van artrose na een ACL-ruptuur. Het doel van de studie in hoofdstuk 6 was om het potentieel van EEM-modellen om de optimale chirurgische parameters te definiëren te demonstreren, in termen van plaatsing van het transplantaat (insertieplaatsen en fixatiespanning), in combinatie met transplantaattype, om het kinematische gedrag van de knie zo goed mogelijk te herstellen.

Een workflow werd voorgesteld op basis van kadaverexperimenten om het biomechanische gedrag van de aangedane knie zo fysiologisch mogelijk te reconstrueren. Plaatsing van femorale en tibiale transplantaaten en de spanning van de transplantaatfixatie werden geoptimaliseerd om een vergelijkbare intacte knielaxiteit te verkrijgen. Hierbij werd gebruik gemaakt van drie gebruikelijke reconstructie-transplantaaten met een enkele bundeltechniek (hamstring en quadriceps en patellapezen) en voor een reconstructie met een dubbele bundeltechniek. Uiteindelijk, om het succes van de operatie met de geoptimaliseerde parameters te verifiëren, werd een volledige loopcyclus gesimuleerd met de intacte, de ACL-deficiënte, de geoptimaliseerde en niet-geoptimaliseerde knieën, om aan te tonen dat deze geoptimaliseerde chirurgische parameters inderdaad leiden tot een meer fysiologische kniebiomechanica.

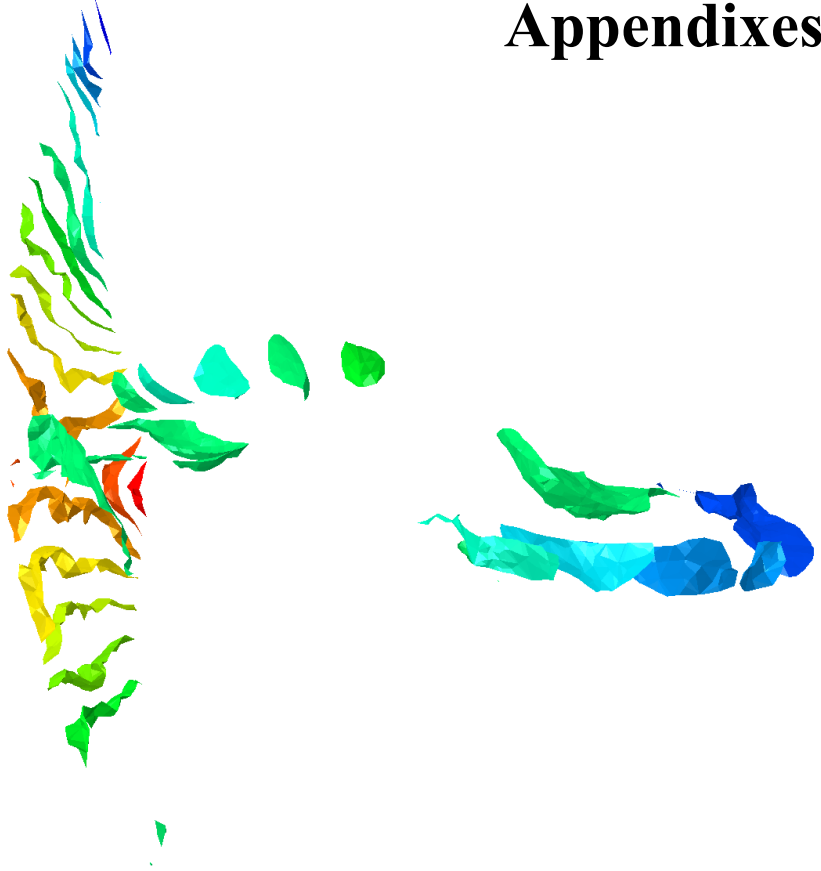
Er werd aangetoond dat, afhankelijk van het geselecteerde transplantaattype en de chirurgische techniek, numerieke optimalisaties kunnen worden geïmplementeerd om de optimale positie en fixatiespanning te vinden om het intacte kniegedrag te reconstrueren.

Ondanks pogingen om een meniscusprothesesysteem (geometrie, materiaal en fixatietype) te optimaliseren, zal het klinische succes afhangen van chirurgische factoren, zoals intra-operatieve positionering van de meniscusprothese. In de studie beschreven in hoofdstuk 7 was het doel daarom om de implicaties van positieveranderingen van de mediale meniscusprothese voor kniebiomechanica te beoordelen.

Een gedetailleerd gevalideerd EEM-model van de intacte en met meniscus geïmplanteerde knieën werd ontwikkeld op basis van een reeks in vitro experimenten. Verschillende niet-anatomische prothese-posities werden gesimuleerd in het EEM-model, waarna de biomechanische respons tijdens de standfase van het lopen werd vergeleken met een anatomisch geplaatste prothese en met het intacte kniemodel.

De resultaten toonden aan dat een anatomische positionering van de mediale meniscusprothese de intacte kniebiomechanica beter kon repliceren, terwijl een niet-anatomische positionering van de prothese de knie-kinematica veranderde en het faalrisico van de meniscusprothese verhoogde. De uitkomsten wijzen erop dat een mediale of anterieure positionering van de meniscusprothese meer vergevingsgezind kan zijn dan een posterieure of lateraal gepositioneerde prothese. De uitkomst van dit onderzoek geeft inzicht in de mogelijke gevolgen van positioneringsfouten van de meniscusprothese.

Appendix



Appendixes

Appendix A and Appendix B, respectively, provide the supplementary data for chapter 3 and chapter 7.

Appendix A

The knee testing apparatus described in chapter 3 and chapter 4 of in this thesis was schematically shown in Figure A1. Also, the number of elements each knee segment contains in FE model is presented for all three knee joints in Table A1.

The average RMS differences in experimental measured and computationally predicted rotational (Table A2 & A3) and translational (Table A4 – A6) kinematics during validation simulations were presented separately for different flexion angles.

The contact area at both medial and lateral plateaus calculated from experiment, spring models with literature and optimized properties and continuum models with literature and optimized properties for one sample (third knee) was presented in Figure A2.

The contact pressure at tibial cartilage predicted by four different developed FE models (for each specimen) in this study were compared with experimental measurements of the knees loaded axially (outlined with the model after registration), as illustrated in Figure A3, Figure A4, Figure A5 and Figure A6 at flexion angles of 0, 30, 60 and 110°, respectively. Figure 4 in chapter 3 presented the same outcomes for flexion of 90°.

Table A1: the number of elements in each FE model segment for three knee joints.

	Cartilages			Menisci		Ligaments (in Continuum models)			
	Tibial	Femoral	Patellar	Medial	Lateral	ACL	PCL	MCL	LCL
Knee 1	32231	117951	15936	8479	8881	5991	15076	9044	7247
Knee 2	58119	126063	36410	18028	13246	8641	19218	14609	8876
Knee 3	44967	120300	32394	10264	11775	6200	17003	6449	5400

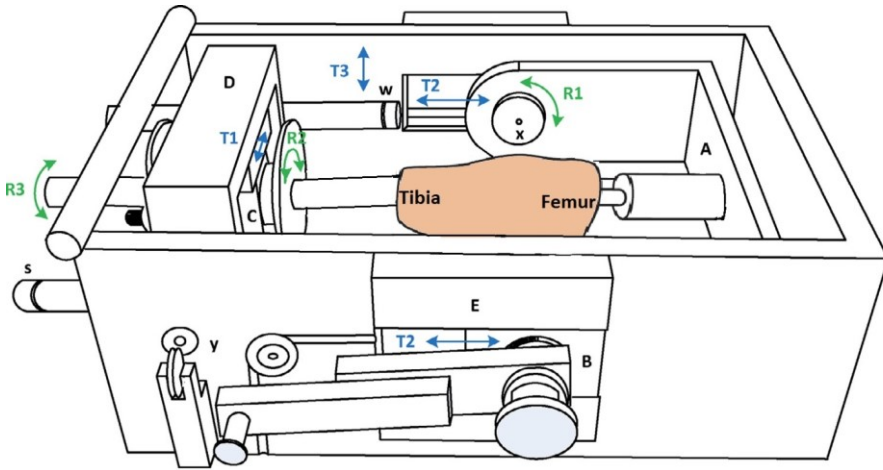


Figure A1: Knee joint testing rig. The femur was placed in a bracket (A), and the tibia was placed in the bracket D through sliding block C, allowing for medial-lateral translation (T1). Bracket A could be rotated around centre of rotation x, allowing knee flexion and extension (R1). Block B, which was also connected to bracket A, could slide within bracket E, to allow proximal-distal movement of the femur (T2) in addition to tibial shaft movement in block C. Block C could rotate to allow for varus–valgus rotation (R3) and internal–external rotation (R2). Bracket D could rotate around Y, to allow for an anterior and posterior movement (T3). (Figure was reused with minor changes from H. H. Rachmat, D. Janssen, G. J. Verkerke, R. L. Diercks, and N. Verdonschot, “In-situ mechanical behavior and slackness of the anterior cruciate ligament at multiple knee flexion angles,” *Med. Eng. Phys.*, vol. 38, no. 3, pp. 209–215, 2016; under permission number of 4134150889417.)

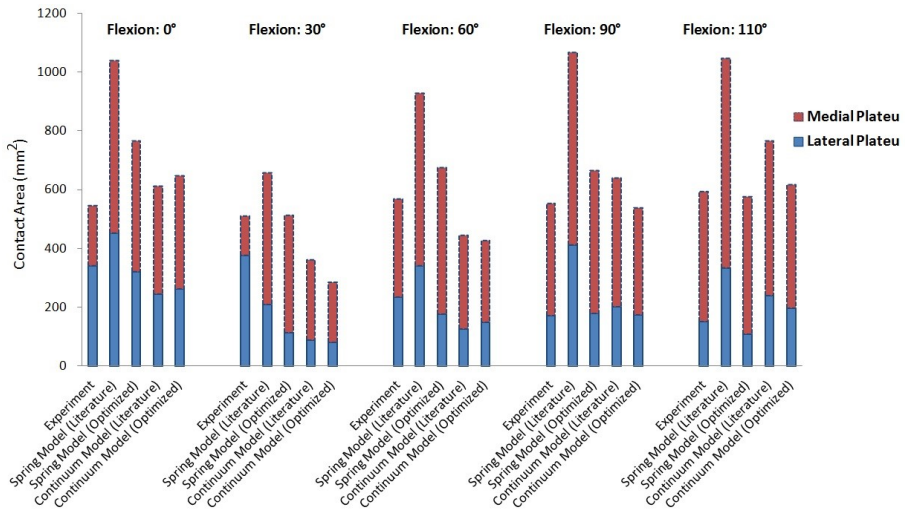


Figure A2: Contact area at both medial and lateral plateaus calculated from experiment, spring models with literature and optimized properties and continuum models with literature and optimized properties for one sample (third knee).

Table A3: Average RMS difference in valgus/varus rotations between experimental validation tests and two spring and continuum ligament FE models with literature-based and optimized ligament parameters for three specimens at different flexion angles; the best predictions at each validation loading case were marked in bold.

		Average RMS difference ± standard deviation											
		Unloaded deep flexion				Tibia axially loaded deep flexion				Tibia anteriorly loaded flexion			
Flexion: 110°		Flexion: 90°	Flexion: 60°	Flexion: 30°	Flexion: 0°	Literature-based spring model		Optimized spring model		Literature-based continuum model		Optimized continuum model	
		Flexion: 90°	Flexion: 60°	Flexion: 30°	Flexion: 0°								
10.7±8.7		4.8±5.1	4.6±3.6	3.9±1.2	1.5±2.7	Literature-based spring model		Optimized spring model		Literature-based continuum model		Optimized continuum model	
4.4±1.3		4.2±1.4	2.5±1.3	4.1±1.1	1.4±2.4								
8.5±16.1		6.3±12.3	5.5±10.3	4.0±6.6	1.5±3.0	Literature-based spring model		Optimized spring model		Literature-based continuum model		Optimized continuum model	
4.4±8.8		3.2±6.3	3.1±6.0	2.1±3.2	1.4±2.3								
11.1±6.3		4.0±2.2	4.5±3.3	3.4±2.7	2.8±5.6	Literature-based spring model		Optimized spring model		Literature-based continuum model		Optimized continuum model	
4.9±1.6		5.3±2.1	2.5±0.5	2.8±3.1	2.8±5.4								
5.6±10.6		4.2±8.1	3.3±6.4	4.0±7.0	2.9±5.6	Literature-based spring model		Optimized spring model		Literature-based continuum model		Optimized continuum model	
3.0±5.9		3.5±6.7	2.8±5.4	2.6±4.6	2.3±4.4								
N/A		5.6±3.4	4.0±1.9	6.3±4.1	1.8±2.2	Literature-based spring model		Optimized spring model		Literature-based continuum model		Optimized continuum model	
N/A		2.8±2.2	3.1±2.9	5.1±3.5	2.8±3.0								
N/A		6.2±9.3	2.6±3.9	3.6±3.1	3.2±3.4	Literature-based spring model		Optimized spring model		Literature-based continuum model		Optimized continuum model	
N/A		6.7±11.5	2.4±3.7	2.6±2.7	3.1±3.4								

Table A4: Average RMS difference in anterior/posterior translations between experimental validation tests and two spring and continuum ligament FE models with literature-based and optimized ligament parameters for three specimens at different flexion angles; the best predictions at each validation loading case were marked in bold.

		Average RMS difference ± standard deviation								
		Unloaded deep flexion				Tibia axially loaded deep flexion		Tibia anteriorly loaded flexion		
Anterior/Posterior translations (mm)		Flexion: 110°	Flexion: 90°	Flexion: 60°	Flexion: 30°	Flexion: 0°	Literature-based spring model	Optimized spring model	Literature-based continuum model	Optimized continuum model
		5.8±2.1	8.2±2.4	8.2±2.3	4.7±1.6	0.1±0.0				
		2.5±2.6	4.1±3.3	4.9±3.1	4.7±3.3	0.0±0.0				
		7.7±2.4	9.8±3.4	10.1±2.2	6.4±2.0	0.3±0.6	Literature-based spring model	Literature-based continuum model	Literature-based continuum model	Optimized continuum model
		3.2±1.5	5.7±2.3	5.9±1.9	2.6±1.5	0.6±0.8	Literature-based spring model	Literature-based continuum model	Literature-based continuum model	Optimized continuum model
		6.9±2.3	9.1±3.7	7.9±2.8	2.0±1.0	0.4±0.3	Literature-based spring model	Literature-based continuum model	Literature-based continuum model	Optimized continuum model
		3.4±2.6	4.9±3.5	5.2±4.1	2.3±2.8	0.9±0.5	Literature-based spring model	Literature-based continuum model	Literature-based continuum model	Optimized continuum model
		9.0±2.9	11.0±4.4	10.0±3.4	3.4±1.6	0.7±1.1	Literature-based spring model	Literature-based continuum model	Literature-based continuum model	Optimized continuum model
		4.2±1.5	6.6±2.3	5.7±1.8	0.4±0.7	1.2±1.5	Literature-based spring model	Literature-based continuum model	Literature-based continuum model	Optimized continuum model
		N/A	4.7±2.4	4.5±2.0	1.6±1.4	1.2±1.1	Literature-based spring model	Literature-based continuum model	Literature-based continuum model	Optimized continuum model
		N/A	2.0±2.8	2.5±2.8	1.9±2.8	2.3±0.7	Literature-based spring model	Literature-based continuum model	Literature-based continuum model	Optimized continuum model
		N/A	4.3±2.3	4.1±1.8	1.6±2.0	1.2±1.9	Literature-based spring model	Literature-based continuum model	Literature-based continuum model	Optimized continuum model
		N/A	4.1±2.7	4.0±2.3	2.1±2.2	0.7±0.8	Literature-based spring model	Literature-based continuum model	Literature-based continuum model	Optimized continuum model

Table A5: Average RMS difference in lateral/medial translations between experimental validation tests and two spring and continuum ligament FE models with literature-based and optimized ligament parameters for three specimens at different flexion angles; the best predictions at each validation loading case were marked in bold.

					Average RMS difference ± standard deviation											
					Unloaded deep flexion				Tibia axially loaded deep flexion				Tibia anteriorly loaded flexion			
Lateral/Medial translations (mm)					Flexion: 0°		Flexion: 30°		Flexion: 60°		Flexion: 90°		Flexion: 110°			
					Literature-based spring model	Optimized spring model	Literature-based continuum model	Optimized continuum model	Literature-based spring model	Optimized spring model	Literature-based continuum model	Optimized continuum model	Literature-based spring model	Optimized spring model	Literature-based continuum model	Optimized continuum model
Flexion: 0°					0.1±0.1	1.0±0.9	0.3±0.5	0.4±0.6	0.2±0.1	0.3±0.5	1.2±1.1	0.9±1.5	2.4±3.6	2.5±3.6	1.8±2.6	2.4±3.7
Flexion: 30°					1.9±2.0	2.1±2.4	1.7±1.8	1.5±1.7	2.4±2.2	2.6±2.8	3.5±3.5	1.7±1.9	3.1±3.6	2.8±3.7	2.4±2.5	2.3±2.5
Flexion: 60°					2.2±1.4	1.0±0.7	2.0±0.9	1.9±1.4	3.1±2.2	3.3±2.7	4.2±3.2	2.6±1.9	3.6±4.2	2.9±4.2	3.4±3.7	3.4±3.9
Flexion: 90°					3.6±2.0	2.5±1.4	2.9±1.8	2.9±2.2	4.8±2.0	4.8±2.1	5.3±3.1	3.9±2.4	4.3±5.0	3.5±4.6	3.7±4.2	3.5±4.3
Flexion: 110°					4.3±1.7	2.4±1.6	3.5±2.8	3.3±3.0	5.4±1.8	4.5±2.5	5.6±4.0	4.0±2.9	N/A	N/A	N/A	N/A

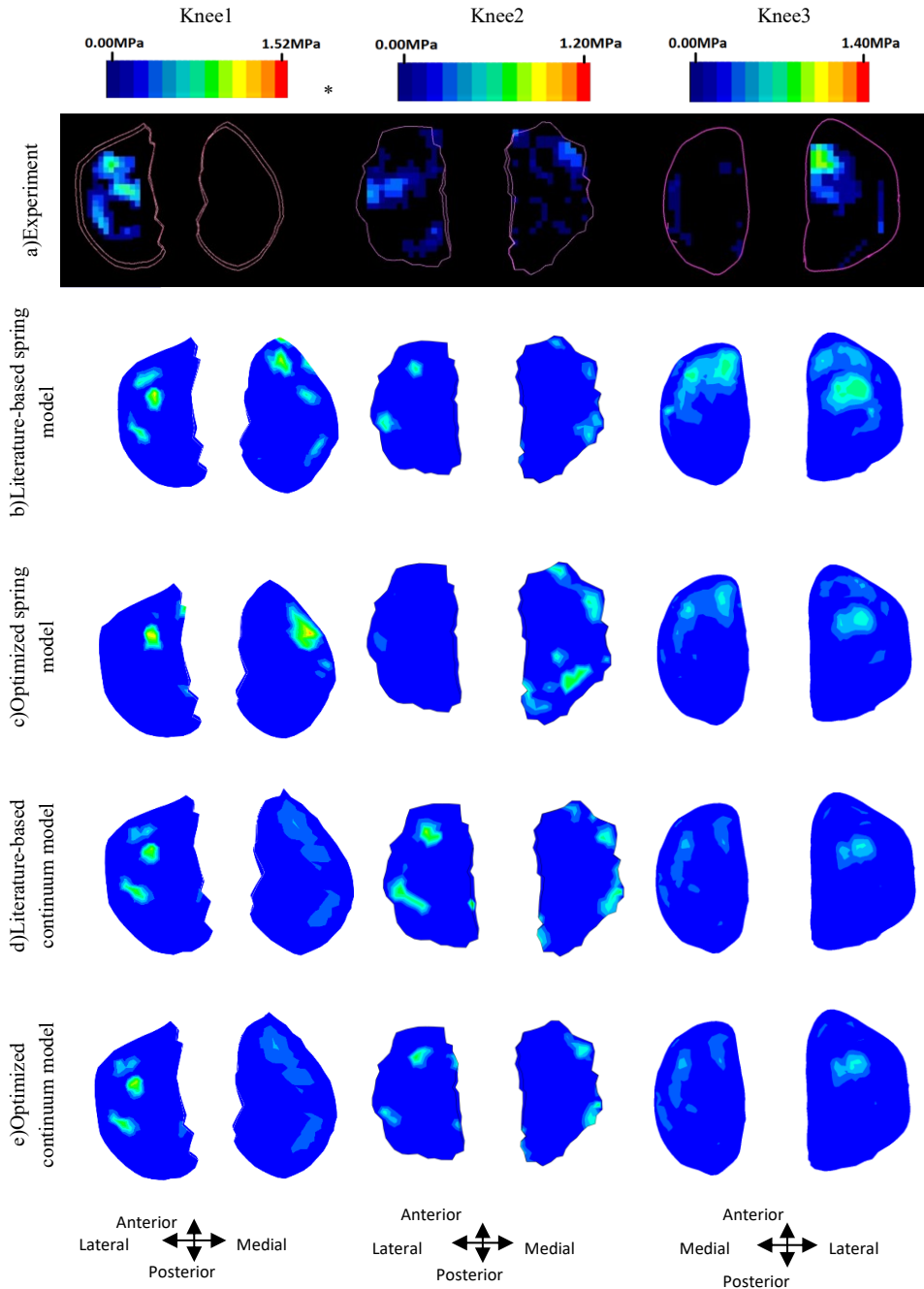


Figure A3: Contact pressure at medial and lateral tibial cartilages at a single flexion angle (0°) in tibia axially loaded high flexion case, for all three specimens, in: a) experiment, b) literature-based spring model, c) optimized spring model, d) literature-based continuum model, and e) optimized continuum model. (* Due to a technical problem in sensor reader, pressure map on medial plateau of the first knee was not recorded.)

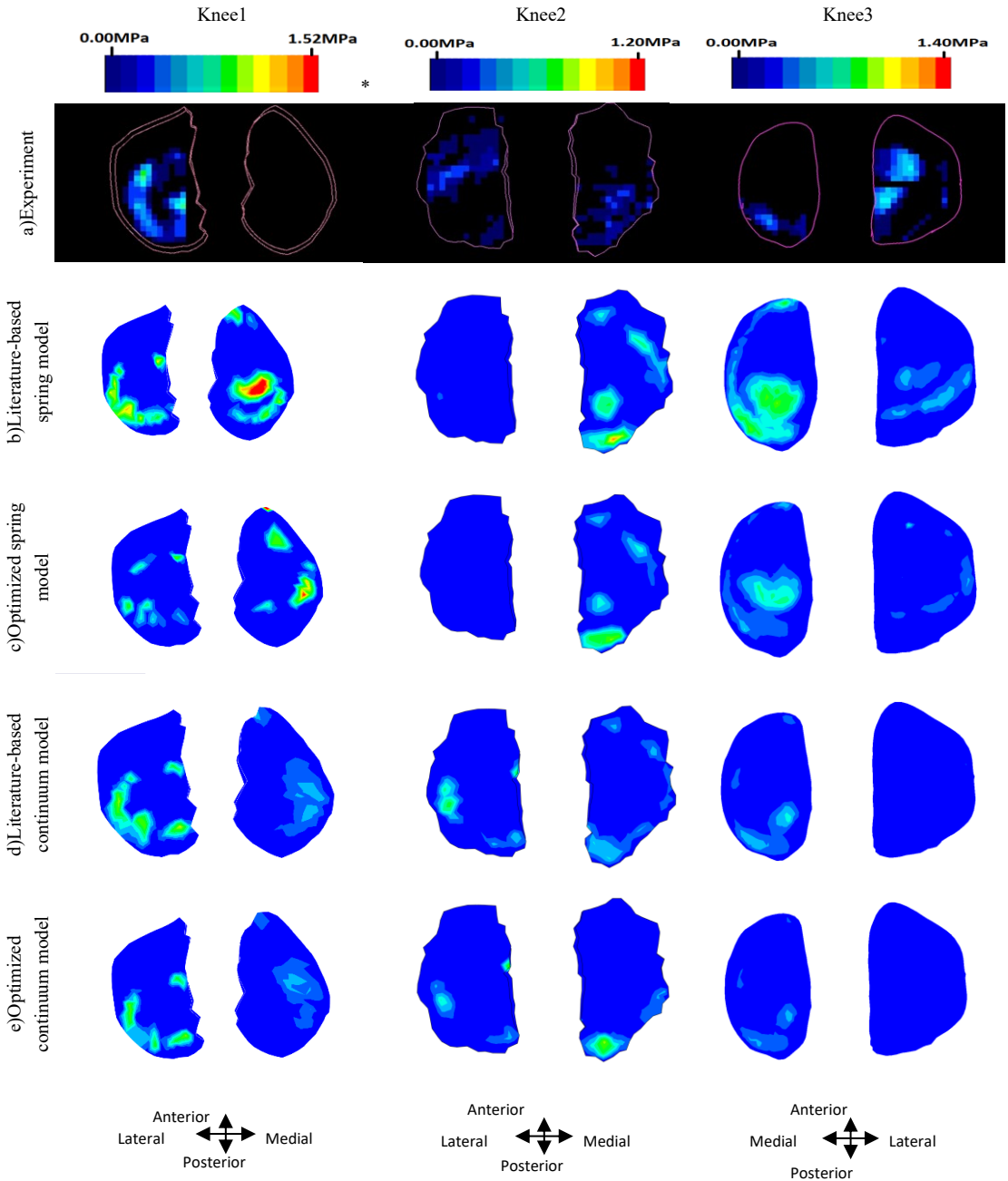


Figure A4: Contact pressure at medial and lateral tibial cartilages at a single flexion angle (30°) in tibia axially loaded high flexion case, for all three specimens, in: a) experiment, b) literature-based spring model, c) optimized spring model, d) literature-based continuum model, and e) optimized continuum model. (* Due to a technical problem in sensor reader, pressure map on medial plateau of the first knee was not recorded.)

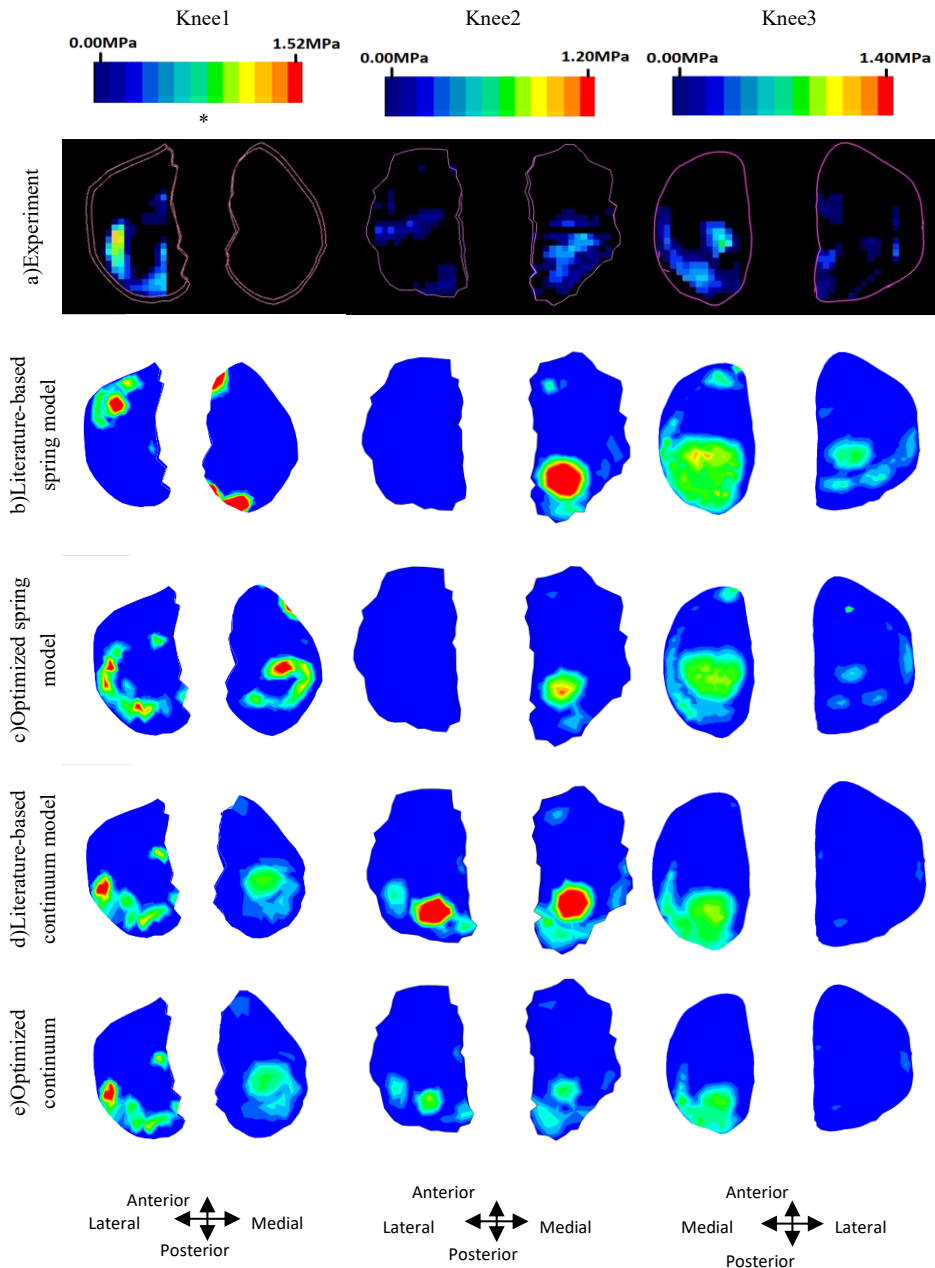


Figure A5: Contact pressure at medial and lateral tibial cartilages at a single flexion angle (60°) in tibia axially loaded high flexion case, for all three specimens, in: a) experiment, b) literature-based spring model, c) optimized spring model, d) literature-based continuum model, and e) optimized continuum model.

(* Due to a technical problem in sensor reader, pressure map on medial plateau of the first knee was not recorded.)

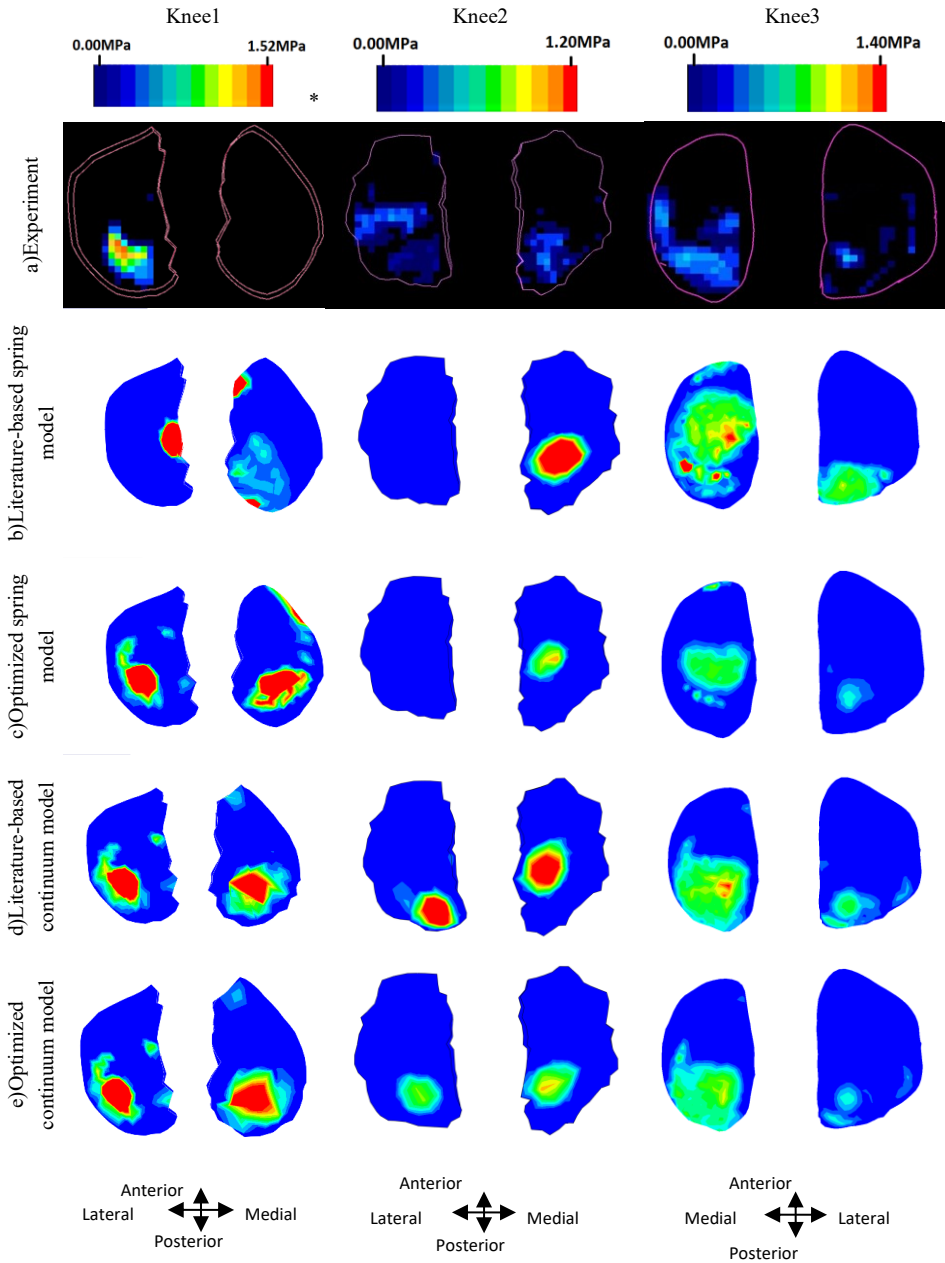


Figure A6: Contact pressure at medial and lateral tibial cartilages at a single flexion angle (110°) in tibia axially loaded high flexion case, for all three specimens, in: a) experiment, b) literature-based spring model, c) optimized spring model, d) literature-based continuum model, and e) optimized continuum model.

(* Due to a technical problem in sensor reader, pressure map on medial plateau of the first knee was not recorded.)

Appendix B

In order to check the geometrical symmetry of the contralateral knees used in chapter 7, the knees were scanned with proton density sequence, in a 3T Philips Ingenia MRI scanner (Philips Healthcare, Best, The Netherlands), with a slice thickness of 0.5mm. The knees were segmented using Mimics v18.0 (Materialise, Leuven, Belgium) to determine the bones and menisci. The bones geometry was then corrected based on the segmentation from CT data (Toshiba Aquilion ONE, Otawara, Japan). Total width of the medial meniscus (AP) and the width of the femur and tibial plateau were compared between the right and left knee.

To check the similarity in knee laxity, the left and right knee were prepared following a standard protocol and tested in a knee testing apparatus that allows for six degree of freedom motions [16-18]. Flexion-extension was applied to the femur, whereas the valgus-varus and internal-external rotations and anterior-posterior and medial-lateral translations were applied to the tibia. A series of laxity tests was applied to the knees while the position of the bony segments was recorded by an electromagnetic tracking system (3Space Fastrak, Polhemus Incorporated, VT, USA). In-house developed scripts (MATLAB R2013a, Natick, MA) were used to calculate the knee joint centre (similar to [1]), and to convert the raw tracking data to kinematics in the knee joint coordinate system [2], as described by Grood and Suntay [3].

Six different loading conditions were applied, at four different flexion angles (0, 30, 60 and 90°): an internal and external torque of 5.2 Nm, a varus and valgus moment of 12 Nm, and an anterior and posterior load of 100 N. These loads were based on literature values and provided sufficient laxity motion to characterize the knee ligaments without damaging the cadaveric specimens [4]–[7]. Each of the loading conditions was repeated three times to check the repeatability of the measurements. The joint laxity of the right and left knees were compared for the six loading regimes.

Symmetry results: The dimensional comparison of the contralateral knees confirmed their geometrical symmetry in, for instance, femoral epicondylar width (~90 mm), tibial plateau width (~80 mm) and AP distance of medial meniscus horns (~ 50 mm). The knees showed comparable laxity in all directions (Figure B1-a), with a maximum difference of 1.8 mm in anterior and 2.1 mm in posterior

translation (Figure B1-b), and 1.7° in valgus, 1.2° in varus (Figure B1-c), 2.7° in internal and 3.3° in external rotation (Figure B1-d).

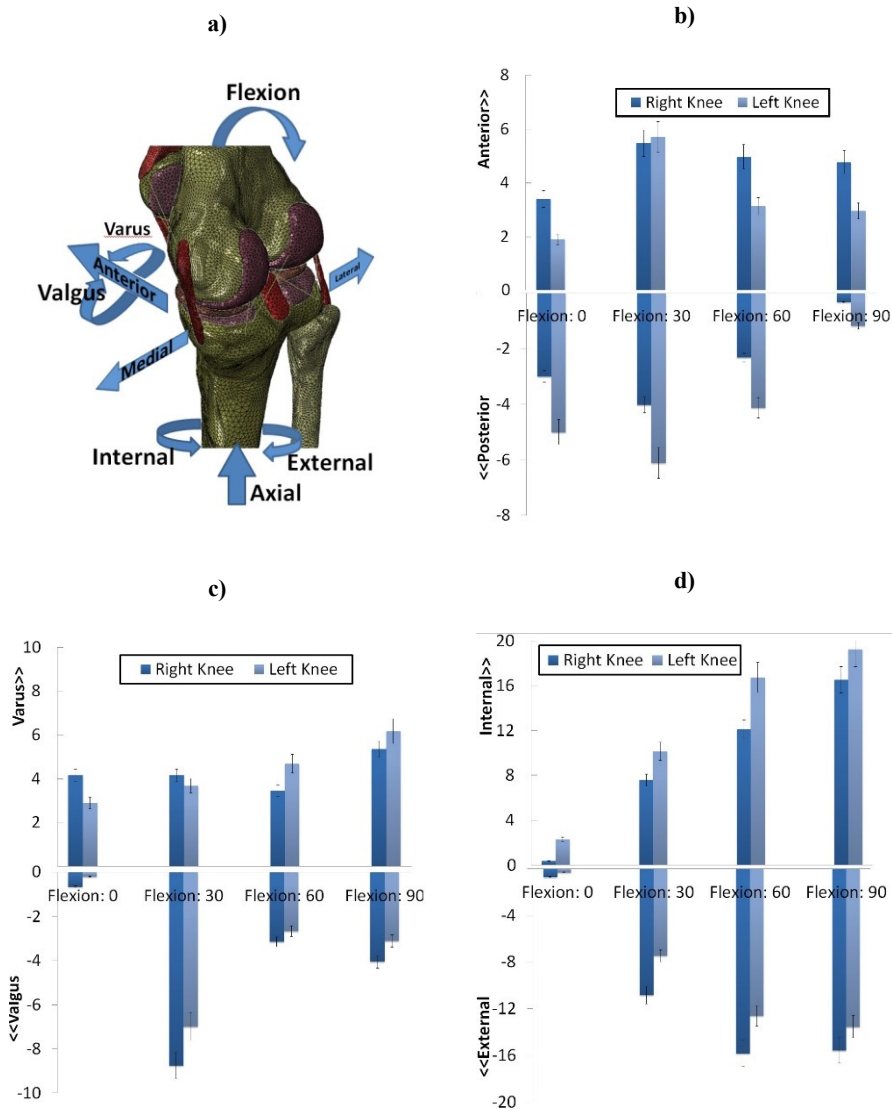
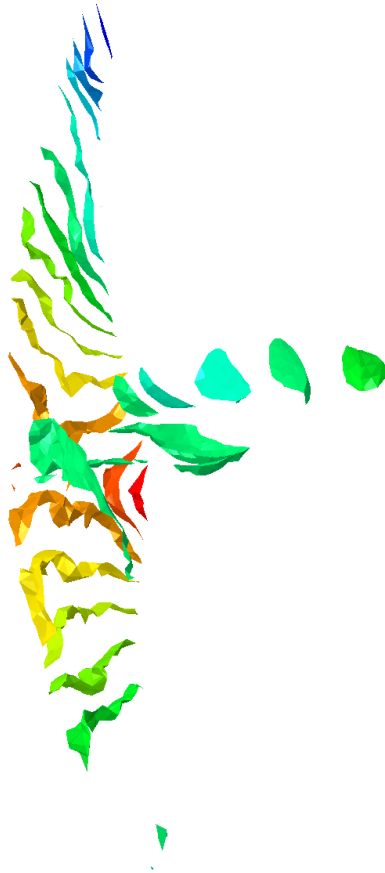


Figure B1: The results of the laxity comparison between the cadaveric right and left knee specimens in order to check their symmetry: a) different knee laxities indication in the FE model; b) anterior/posterior laxities against an anterior/posterior load of 100N; c) Valgus/varus rotational laxities while a valgus/varus moment of 12 N.m was applied; and d) Internal/external rotational laxities against an internal/external torque of 5.2 N.m.

References

- [1] D. L. Miranda, M. J. Rainbow, E. L. Leventhal, J. J. Crisco, and B. C. Fleming, “Automatic determination of anatomical coordinate systems for three-dimensional bone models of the isolated human knee,” *J. Biomchanics*, vol. 43, no. 8, pp. 1623–1626, 2010.
- [2] W. J. Zevenbergen, “Improved Anatomical Coordinate System of the Distal Femur Based on 3D Bone Geometry & Evaluation of the Inter- and Intra- Observer Variability of the Knee Ligament,” 2012.
- [3] W. J. Grood, E.S.; Suntay, “A joint coordinate system for the clinical description of three-dimensional motions applications to the knee,” *J. Biomech. Eng.*, vol. 105, no. 2, pp. 136–144, 1983.
- [4] D. L. Gollehon, P. A. Torzilli, and R. F. Warren, “The role of the posterolateral and cruciate ligaments in the stability of the human knee. A biomechanical study,” *J. Bone Joint Surg. Am.*, vol. 69, no. 2, pp. 233–42, 1987.
- [5] W. P. Seering, R. L. Piziali, D. A. Nagel, and D. J. Schurman, “The function of the primary ligaments of the knee in varus-valgus and axial rotation,” *J. Biomech.*, vol. 13, no. 9, pp. 785–794, 1980.
- [6] Keith L. Markolf, J. S. Mensch, and Harlan C. Amstutz, “Stiffness and laxity of the knee - the contributions of the supporting structures,” *J. bone Jt. Surg.*, vol. 58, no. 5, 1976.
- [7] M. a. Baldwin, C. W. Clary, C. K. Fitzpatrick, J. S. Deacy, L. P. Maletsky, and P. J. Rullkoetter, “Dynamic finite element knee simulation for evaluation of knee replacement mechanics,” *J. Biomech.*, vol. 45, no. 3, pp. 474–483, 2012.

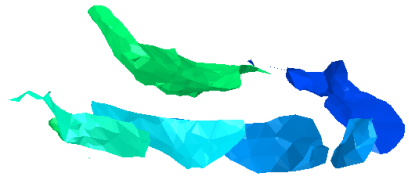


Acknowledgments

PhD portfolio

List of publications

Curriculum Vitae



Acknowledgments

PhD portfolio

List of publications

Journal papers

Naghibi Beidokhti, H., Janssen, D., Khoshgoftar, M., Sprengers, A., Perdahcioglu, E.S., Van den Boogaard, T., Verdonschot, N., 2016. A comparison between dynamic implicit and explicit finite element simulations of the native knee joint. *Med. Eng. Phys.* 38, 1123–1130.

Naghibi Beidokhti, H., Janssen, D., Groes, S. Van De, Hazrati, J., Boogaard, T. Van Den, Verdonschot, N., 2017a. The influence of ligament modelling strategies on the predictive capability of finite element models of the human knee joint. *J. Biomech.* 65, 1–11.

Naghibi Beidokhti, H., Janssen, D., Groes, S. Van De, Verdonschot, N., 2017b. The peripheral soft tissues should not be ignored in the finite element models of the human knee joint. *Med. Biol. Eng. Comput.* 2018, 56, 1189-1199.

Naghibi Beidokhti, H., Mazzoli, V., Gijsbertse, K., Hannik, G., Sprengers, A., Janssen, D., Van den Boogaard, T., Verdonschot, N., 2018. A Noninvasive MRI Based Approach to Estimate the Mechanical properties of Human Knee Ligaments. *J. Mech. Behav. Biomed. Mater.* *Under review.*

Naghibi beidokhti, H., Janssen, D., Van Tienen, T., Van de Groes, S., Van den Boogaard, T., Verdonschot, N., 2018. Optimal Graft Positioning and Tensioning in ACL Reconstructive Surgery Using Novel Finite Element Modeling Techniques. *Knee Surg. Sports Traumatol. Arthrosc.* *Under review.*

Naghibi beidokhti, H., Janssen, D., Van Minnen, B., Van den Boogaard, T., Van Tienen, T., Verdonschot, N., 2018. The Implications of Non-Anatomical Positioning of a Meniscus Prosthesis on Predicted Human Knee Joint Biomechanics. *Sci. Rep.*, *Under revision.*

Gijsbertse, K., Sprengers, A., **Naghibi Beidokhti, H.**, Nillesen M., de Korte C., Verdonschot, N., 2018. A Strain imaging of the lateral collateral ligament using high frequency and conventional ultrasound imaging: An ex-vivo comparison. *J. Biomech.* 73, 233-237.

Conferences (peer-reviewed)

H. Naghibi et al., “Can Material Composition Improve the Biomechanical Outcomes of a Medial Meniscus Implant?!”, 23rd Congress of the European Society of Biomechanics, Sevilla, Spain, 2017.

H. Naghibi et al., “The Impact of Shape and Material Integrity of Medial Meniscus Implant on Osteoarthritis Prevention”, 30th Annual Congress of the International Society for Technology in Arthroplasty, Seoul, South Korea, 2017.

H. Naghibi et al., “The Influence of ACL Reconstruction Surgical Technique on Knee Biomechanics: Single Versus Double Bundle”, 23rd Congress of the European Society of Biomechanics, Sevilla, Spain, 2017.

H. Naghibi et al., “Toward a Subject-specific Single Bundle ACL Reconstruction Based on Surgeon’s Graft Type Selection”, 23rd Congress of the European Society of Biomechanics, Sevilla, Spain, 2017.

H. Naghibi et al., “The Influence of Modeling Choices on the Predictive Capability of the Human Knee Joint Finite Element Models”, Orthopedic Research Society Annual Meeting, CA, USA, 2017.

H. Naghibi et al., “The Technical Aspects of Modeling Choices on the Predictive Capability of the Human Knee Joint Finite Element Models”, Science in the age of Experience, 4th Simulia global user conference, IL, USA, 2017.

H. Naghibi et al., “Subject-specific Knee Ligaments Modeling Approaches in Computational Finite Element Analysis: 1D and 3D”, 22nd Congress of the European Society of Biomechanics, Lyon, France, 2016.

H. Naghibi et al., “The Effect of Peripheral Soft Tissues on the Biomechanical Response of the Knee Joint”, 22nd Congress of the European Society of Biomechanics, Lyon, France, 2016.

H. Naghibi et al., “A Comparison between Dynamic Implicit and Explicit Finite Element Simulations of the Native Knee Joint”, 12th International Symposium on Computer Methods in Biomechanics and Biomedical Engineering, Amsterdam, The Netherlands, 2014.

(Second author), “Effects of Total Medial and Lateral Meniscectomies on the Knee Joint Biomechanics During Normal Gait - A Validated 3D Finite Element Method Study”, ANZORS 22nd Annual Scientific Meeting, Melbourne, Australia, 2016.

H. Naghibi et al., “A Novel Technique to Minimize the Biomechanical factors contribute in Osteoarthritis development in ACL-reconstructed human knees”, SIMULIA Benelux Regional User Meeting, Melbourne, Eindhoven, The Netherlands, 2017.

H. Naghibi et al., “Biomechanical Comparison between Two Common Subject-specific ACL-reconstruction Surgical Techniques: Is Double-bundle Reconstruction Worth It?!” , SIMULIA Benelux Regional User Meeting, Melbourne, Eindhoven, The Netherlands, 2017.

Curriculum Vitae

Hamid Naghibi was born on March 21st 1986 in Gonabad, Khorasan province, Iran. He obtained his diploma in Mathematics and Physics in 2003 in Mashad. In 2009, he finished his BSc studies in Mechanical engineering (Solid design), in Ferdowsi university of Mashad. As his BSc thesis, he worked on modeling of the complicated behavior of shape memory alloys in finite element and intelligent beam vibrations, under the supervision of Prof. Dr. Jalil Rezaeepazhand.

In 2009 he entered the top ranked technology university of Iran, Sharif university of technology, where he started his master studies in Mechanical engineering (applied design). He graduated in 2012 with his MSc thesis on minimization of loosening risk and wear in total knee prosthesis using functionally graded materials and shape memory alloys, under the supervision of Prof. Dr. Farzam Farahmand and Prof. Dr. M.T. Ahmadian.

In August, 2013 he moved to the Netherlands where he started his PhD project under the supervision of Prof. Dr. Nico Verdonschot, in Orthopedic Research Lab, Radboud University Medical Center. During his PhD studies, he worked on finite element modeling of human knee joint as a surgery pre-planning tool, as a part of BioMechTools project, funded by European Research Council, awarded to Prof. Nico Verdonschot.

In December, 2017, Hamid started working as a postdoctoral researcher at Robotics and Mechatronics group, University of Twente. He works in soft robotics project to contribute in improving the treatment of patients with liver cancer.

